UNIVERSIDADE DE LISBOA
FACULDADE DE CIÊNCIAS
DEPARTAMENTO DE FÍSICA

Comparison of 2D time-integrated, 3D time-integrated and 2D time-resolved portal dosimetry in detecting patient dose errors in external beam radiotherapy

Mariana Gomes Brás

Mestrado Integrado em Engenharia Biomédica e Biofísica
Perfil de Radiações em Diagnóstico e Terapia

Dissertação orientada por:

Prof. Dr. Frank Verhaegen, Head of Clinical Physics Research Department, MAASTRO Clinic, Maastricht, The Netherlands

Prof. Dr. Luís Peralta, Departamento de Física, Faculdade de Ciências da Universidade de Lisboa, Lisboa, Portugal

2016

"Trabalha como se tudo dependesse de ti; confia como se tudo dependesse de Deus."

"Work as if everything depended on you; trust as if everything depended on God."

Santo Inácio de Loyola

Acknowledgements

First of all, I would like to express my deep gratitude to my external supervisor, Prof. Dr. Frank Verhaegen, who gave me the opportunity to work with him and a top research team at MAASTRO. His expertise and guidance were crucial to achieve my goals in this project. Thank you for being always available to share your knowledge with me with patience and kindness.

The second person I want to thank is my internal supervisor, Prof. Dr. Luís Peralta, who shared with me his passion for Dosimetry. I can say that it was your subject in my Master that made me follow this path of dosimetry in medical physics. Thank you for being always available to help me.

A special thanks goes out to my second external supervisor, Mark Podesta, who was so patient and kind to teach me even thought he was busy with his work, he always found time for me. Your expertise and guidance made me to become a better researcher. Thank you for always supporting and encouraging me to believe in my potential. It was a pleasure work, have fun and run with you!

I would also like to express a special thanks to my third external supervisor, Lotte Schyns, who was always attentive to my work and available to help me no matter the circumstances. Thank you for your friendship and our coffee breaks!

I would also like to express my gratitude to the DGRT research group of MAASTRO. Our meetings were crucial to guide my project. I am also grateful for the help provided by the medical physicist Jonathan Martens during the CT acquisitions and the treatment planning insight provided by the medical physicist Chin Loon.

Special thanks goes out to the clinical physics research group for making me feel so welcome at MAASTRO. Thank you for always supporting me and show me the importance of friendship at work. It was amazing to share this experience almost every day with you. I will never forget our lunch times, coffee breaks and dinners out!

A ti, Verde, um sincero obrigado por partilhares esta experiência comigo. Embarcar nesta aventura não seria a mesma coisa sem ti! Obrigada pelo apoio incansável e por todos os momentos de diversão, não só nestes últimos sete meses, mas sobretudo ao longo destes fantásticos 5 anos de faculdade que criaram esta grande Amizade. Um obrigado especial também a ti, Robalo, pela Amizade, pelas palavras de carinho e encorajamento.

Um obrigado muito especial vai também para a Isabel e para o Gabriel. Ter-vos na MAASTRO foi uma sorte! Sorte não, pois acredito que nada acontece por acaso! Obrigada por todos os momentos divertidos (jantaradas, saídas, picnics, Carnaval…), por todos os conselhos, por todas as gargalhadas e por me terem feito sempre sentir tão bem acolhida. Obrigada pela vossa amizade! Obrigada também a ti, Sara, pela tua energia e alegria inesgotáveis que coloriam os nossos dias na MAASTRO! Um grande obrigado também a ti, Murillo, e a ti, Louise, pois apesar de não nos termos cruzado por muito tempo foi fantástico poder partilhar os últimos meses convosco.

I want also to thank to my lovely housemates Fedi and Evi. It was amazing to meet you and to share these months with you. Thank you for all the moments we shared. I have never thought I could do friendships like these in the Netherlands.

Other special thank goes out to my athletics team in Maastricht - Hub team. Thank you for providing me the opportunity to join you doing something we love, running! It was amazing to train with you on the track even with snow! A special thank goes also to my amazing French friend Solène for all the trainings, dinners and funny moments we shared.

Obrigada também ao João Carreira e ao Tiago Leonardo, pela vossa amizade e por me fazerem experienciar fins-de-semana bem diferentes do habitual nestes sete meses onde dominava sempre a comida típica portuguesa. A ti, Geraldes, obrigada pela alegria que vieste trazer a Maastricht neste último mês e meio! Obrigada pela amizade, por todos os momentos de diversão e por todos os picnics onde não faltavam as sandes com barulho. A vocês, André, Litos, Guimarães e Zé Nuno, obrigada por me fazerem sentir em Lisboa mesmo estando na Holanda durante as nossas trips.

Um grande obrigado também a vocês, Helena, Teresa, Marina, Sara, Rute, Gui, Bacalhau, Gustavo e restantes amigos tugas por me terem apoiado sempre não só ao longo destes sete meses, mas sobretudo ao longo destes 5 anos de faculdade!

Um obrigado muito especial à minha fantástica Equipa de Jovens de Nossa Senhora (incluindo o Samuel!) que mesmo estando em Portugal esteve sempre comigo no coração. Cada vez mais estou certa de que somos muito mais do que uma equipa o mês inteiro, o ano inteiro! Obrigada pela vossa amizade pura e verdadeira e por todas as reuniões via Skype!

Aos meus pais, Amélia e João Pedro, obrigada pelo vosso amor e apoio incondicional. Além de serem a razão de eu existir, tudo aquilo que sou é graças ao vosso exemplo e esta tese é por isso dedicada a vocês. Obrigada pelo esforço que sempre fizeram em prol da minha educação enquanto estudante em Lisboa, em Heidelberg e em Maastricht.

Ao meu irmão, à minha madrinha, à minha afilhada, aos meus avós e a toda a minha família um sincero obrigado pelo vosso amor e carinho que chegou sempre a Maastricht independentemente dos 2000 km de distância.

"Aqueles que passam por nós, não vão sós, não nos deixam sós.
Deixam um pouco de si, levam um pouco de nós."

"Those who pass us by, do not go alone, do not leave us alone.
They leave a little piece of themselves, take a little of us."

Anthóine de Sant-Exuperie

Abstract

In external photon beam radiotherapy, patient-related errors are common to occur during the treatment course of the patient. These errors, such as tumor regression or tumor shift, may result in discrepancies between the planned and the actually delivered dose distribution to the patient. In this way, it is vital to perform dose verification during the treatment course of the patient to detect these errors and ensure treatment quality. The Electronic Portal Imaging Device (EPID) has been used as a tool for performing both pre-treatment and in-treatment dose verification. Since the introduction of more complex beam delivering techniques, especially Volumetric Modulated Arc Therapy (VMAT), more complex dose verification methods based in EPID dosimetry have also been introduced such as 2D time-integrated portal dosimetry, 3D time-integrated portal dosimetry and, more recently, 2D time-resolved portal dosimetry.

The main goal of this project was to compare the performance of 2D time-integrated, 3D time-integrated and 2D time-resolved portal dosimetry in detecting dose discrepancies caused by simulated errors related to the patient's anatomy.

Multiple tumor shifts, tumor regressions and pleural effusion (excess fluid that accumulates in the pleural cavity) levels inside the lung were simulated in the planning CT-scan of six lung cancer patients treated with VMAT at MAASTRO clinic. Portal dose images were calculated in the original and manipulated planning-CT scans with the three portal dosimetry methods. For dose comparison 2D time-integrated, 2D-time resolved and 3D time-integrated gamma analyses were performed for each geometrical change and each patient employing five different gamma criteria. As main results, 3D time-integrated portal dosimetry demonstrated the highest performance (AUC = 0.85) in detecting tumor shifts and 2D time-resolved portal dosimetry revealed the highest performance in detecting tumor regressions (AUC = 0.93) and pleural effusion. A correlation between $D_{95\%}$ changes in the DVHs and gamma fail rates was found at individual patient level but not at the patient cohort level.

A phantom experiment was done to replicate the tumor shifts simulated in the patients. A set of simulations and measurements were performed following the same protocol. The dynamic thorax phantom was irradiated with VMAT for each tumor shift applied. The dose to the tumor was determined with film dosimetry and EPID images were collected during each irradiation. The results revealed that the phantom simulations and measurements follow the same behavior. The 2D time-resolved portal dosimetry showed to be able to detect more dose discrepancies caused by the tumor shifts than 2D time-integrated portal dosimetry.

As main conclusion, 2D time-resolved portal dosimetry was superior in general to 2D and 3D time-integrated portal dosimetry in detecting dose discrepancies caused by geometrical changes within the patients and the phantom. Time-resolved portal dosimetry is able to highlight discrepancies that are not shown when only the integrated portal dose images are compared.

Keywords: radiotherapy – EPID – VMAT – portal dosimetry – geometrical changes

Resumo

Em radioterapia externa com feixes de fotões é essencial que a distribuição de dose planeada seja entregue ao paciente com elevada precisão de modo a garantir a qualidade do tratamento. No entanto, existem certos tipos de erros que podem ocorrer durante as várias fracções de tratamento do paciente e prejudicar assim a qualidade do tratamento. Esses erros podem estar relacionados com o linac (acelerador linear) - posições incorrectas dos colimadores multi-folhas - ou com o paciente - erros de posicionamento do paciente ou alterações geométricas na anatomia do paciente. Os erros de posicionamento do paciente, como é o caso da translação ou rotação do paciente, podem fazer com que o feixe de radiação não atinja o tumor acabando por prejudicar o tecido saudável que se encontra à sua volta. No que diz respeito às alterações geométricas, as mais frequentes no decorrer do tratamento de radioterapia em pacientes com cancro no pulmão são o desvio do tumor, a regressão do tumor e a efusão pleural (excesso de fluido que se acumula na cavidade pleural). Estas alterações geométricas podem resultar numa discrepância entre a distribuição de dose planeada e a distribuição de dose que é realmente entregue ao paciente prejudicando assim a qualidade do tratamento. Deste modo, torna-se fundamental verificar a entrega da distribuição de dose quer antes quer durante o decorrer do tratamento do paciente de forma a detectar estes tipos de erros e garantir assim a qualidade do tratamento.

Outro factor que também tem contribuído para uma maior exigência das práticas de verificação de dose durante o tratamento do paciente é o aparecimento de novas técnicas de radioterapia externa mais complexas que envolvem mais graus de liberdade, como é o caso da técnica de VMAT (terapia de arco volumétrico). O aumento da complexidade destas técnicas aumenta também a complexidade do tratamento e leva por isso a uma maior exigência na validação e controlo de qualidade (QA) do tratamento.

Existem várias ferramentas de verificação de dose utilizadas em prática clínica para QA do tratamento e para detecção de discrepâncias de dose, como é o caso das câmaras de ionização, dos EPIDs (*electronic portal imaging devices*), dos filmes radiocrómicos, dos géis de polímeros ou outros detectores. O EPID tem sido o detector mais utilizado actualmente para a verificação de dose antes e durante o tratamento de radioterapia. Este detector obtém a distribuição de dose medida que depois é comparada com a distribuição de dose planeada (prevista). A análise gama é o método quantitativo mais utilizado para comparação de distribuições de dose. Este método utiliza em simultâneo dois critérios, a percentagem de diferença de dose (DD) e a distância de concordância (DTA), para o cálculo do índice gama pixel por pixel ou voxel por voxel. Ao aplicar um critério de aceitação (ex.: 3%, 3 mm), as discrepâncias entre as distribuições de dose de extensão geométrica e magnitude variável podem ser identificadas.

Esta tese centra-se em dosimetria portal de transmissão em que o paciente se encontra entre o feixe de radiação e o EPID que mede a distribuição de dose entregue ao paciente. O aparecimento de novas técnicas de radiação mais complexas, como IMRT (radioterapia de intensidade modulada) e VMAT também tem levado ao desenvolvimento de novos métodos de verificação de dose com base em EPID. O método de 2D *time-resolved portal dosimetry* foi introduzido recentemente para a

técnica VMAT. Este método diferencia-se pelo facto de o EPID ler a distribuição de dose para cada segmento (duração compreendida entre dois pontos de controlo consecutivos) do VMAT em vez de ler apenas a distribuição de dose cumulativa (*time-integrated portal dosimetry*).

O principal objectivo desta tese é a comparação do desempenho dos métodos 2D *time-integrated*, 3D *time-integrated* e 2D *time-resolved portal dosimetry* na detecção de discrepâncias de dose em pacientes com cancro no pulmão causadas pela simulação de alterações geométricas na anatomia do paciente.

Para tal foram simulados múltiplos desvios do tumor, múltiplas regressões do tumor e múltiplos níveis de efusão pleural (fluido que se acumula na cavidade pleural) em cada CT (Tomografia Computorizada) de planeamento de seis pacientes com cancro no pulmão que foram tratados com VMAT na MAASTRO Clinic. Também se procedeu ao cálculo de imagens de dose portal no CT de planeamento original e em cada CT manipulado (CT com a alteração geométrica já aplicada) recorrendo aos três métodos de dosimetria portal já referidos. De forma a comparar a dose planeada com a dose medida, foram feitas 2D *time-integrated*, 2D *time resolved* e 3D *time-integrated gamma analyses* para cada alteração geométrica simulada e para cada paciente utilizando cinco critérios gama diferentes.

Posteriormente, foi investigado o desempenho de cada um destes métodos através da construção de curvas ROC (*Receiver Operating Characteristic*) e da determinação dos valores da área sob a curva (AUC). Como principais resultados, 3D *time-integrated portal dosimetry* foi o método que demonstrou o melhor desempenho (AUC = 0.85) na detecção de desvios do tumor e 2D *time-resolved portal dosimetry* foi o método que revelou o melhor desempenho na detecção de regressões do tumor (AUC = 0.93) e de efusão pleural.

Além disso também foi estudada a correlação entre a variação da métrica $D_{95\%}$ do DVH (*Dose Volume Histogram*) calculado para cada paciente e as *gamma fail rates* obtidas para cada paciente e para cada tipo de alteração geométrica com cada método de dosimetria portal já referido. Esta correlação foi estudada tendo em consideração apenas um paciente, e tendo em consideração os seis pacientes como um grupo. Como resultado verificou-se que existe correlação a nível individual, mas não a nível colectivo. O facto de haver correlação a nível individual é bastante importante pois significa que no futuro será possível obter uma curva de regressão para cada simulação de um paciente e prever qual será a variação da métrica $D_{95\%}$ a partir das *gamma fail rates* medidas e decidir assim quando adaptar o plano de tratamento do paciente em causa.

Para além das simulações nos pacientes, também foi realizada uma experiência com um fantoma representativo do tórax humano (CIRS *dynamic thorax phantom*) com o intuito de replicar os desvios do tumor simulados nos pacientes. Foi feito um conjunto de simulações e medições experimentais seguindo o mesmo protocolo. No que diz respeito às medições experimentais, foi construído um mini-fantoma representativo do tumor (dois cilindros de PMMA - *polymethylmethacrylate*) com tecido pulmonar à volta (esponja) de forma a possibilitar a colocação de um filme radiocrómico entre os dois cilindros de PMMA. Nesta experiência foi feita uma irradiação com VMAT para cada desvio do tumor (mini-fantoma) aplicado no *dynamic thorax phantom* e a dose recebida no tumor foi medida em cada irradiação através de dosimetria com filme radiocrómico. Além disso, também foram adquiridas imagens portais do EPID durante cada irradiação. Os resultados deste estudo revelaram que as simulações e medições com o fantoma

seguem o mesmo comportamento. O método 2D *time-resolved portal dosimetry* demonstrou ter capacidade para detectar mais discrepâncias de dose causadas por desvios do tumor do que 2D *time-integrated portal dosimetry*.

Como principal conclusão, 2D *time-resolved portal dosimetry* demonstrou ser o melhor método na generalidade para detectar discrepâncias de dose causadas por alterações geométricas da anatomia dos pacientes e no fantoma. Este novo método de dosimetria portal foi capaz de identificar discrepâncias de dose que não são reveladas quando se comparam apenas *integrated portal dose images.*

Palavras-chave: radioterapia – alterações geométricas – VMAT – EPID – dosimetria portal

Contents

List of Figures

List of Tables

List of Abbreviations

ART	Adaptive Radiation Therapy
AUC	Area Under the Curve
CBCT	Cone Beam Computed Tomography
CP	Control Point
CT	Computed Tomography
CTV	Clinical Target Volume (= GTV + margin for subclinical disease)
DGRT	Dose Guided Radiation Therapy
DICOM	Digital Imaging and Communication in Medicine
DNA	Deoxyribonucleic acid
DPI	Dots Per inch
DTA	Distance To Agreement
DVH	Dose Volume Histogram
EBRT	External Beam Radiation Therapy
EPID	Electronic Portal Imaging Device
GTV	Gross Tumor Volume
HU	Hounsfield Unit
IGRT	Image Guided Radiation Therapy
IMRT	Intensity Modulated Radiation Therapy
linac	linear accelerator
MAASTRO	Maastricht Radiation Oncology
MLC	Multi Leaf Collimator
MRI	Magnetic Resonance Imaging
MU	Monitor Unit
MUMC+	University Hospital Maastricht
NSCLC	Non-Small Cell Lung Cancer
OAR	Organs At Risk
OD	Optical Density
PD	Percentage Difference
PDD	Percentage Depth Dose
PET	Positron Emission Tomography

PMMA	Polymethylmethacrylate
PTV	Planning Target Volume (= CTV + margin for geometrical uncertainties)
PV	Pixel Value
QA	Quality Assurance
ROC	Receiver Operating Characteristic
RT	Radiation Therapy
TIFF	Tagged Image File Format
TPS	Treatment Planning System
TTA	Time To Agreement
VMAT	Volumetric Modulated Arc Therapy
WHO	World Health Organization
ZON-PTC	South-East Netherlands Proton Therapy Centre

Preface

This project was carried out at the Clinical Physics Research department of MAASTRO (Maastricht Radiation Oncology) Clinic in Maastricht, The Netherlands. MAASTRO Clinic was founded in 1977 and is a radiotherapy institute that provides state-of-the-art radiation therapy for various types of cancer to approximately 4000 cancer patients each year in Limburg, south-east region of the Netherlands.

MAASTRO Clinic currently has six TrueBeam linear accelarators (linacs) from Varian, all equipped with EPID (electronic portal imaging device) and with CBCT (Cone Beam Computed Tomography). It also has 2 CT scanners and was the first center with a CT-PET scanner dedicated for radiotherapy, which now includes the possibility to acquire dynamic PET (Positron Emission Tomography) scans and 4D-CT-PET in lung cancer patients.

MAASTRO works closely with the radiotherapy department of the University Hospital Maastricht (MUMC+) and are developing together the South-East Netherlands Proton Therapy Center (ZON-PTC).

Currently, the Physics Research group has five research groups: dose-guided radiotherapy (DGRT), brachytherapy, proton therapy, advanced imaging and small animal radiotherapy. The project presented in this thesis was involved on the DGRT research group which focuses on performing accurate verification of the dose delivered to the patient.

The supervisor of this project was Prof. Dr. Frank Verhaegen, head of Clinical Physics Research department at MAASTRO, and the internal supervisor was Prof. Dr. Luís Peralta from the Physics department at Faculty of Sciences, University of Lisbon, Portugal. This project also had as associated supervisors Mark Podesta and Lotte Schyns, PhD students from the Clinical Physics Research department at MAASTRO.

Front view of MAASTRO Clinic.

1 Introduction

The development of more complex beam delivery techniques in external photon beam radiotherapy (EBRT), such as Intensity Modulated Radiotherapy (IMRT) and Volumetric Modulated Arc Therapy (VMAT), has increased the need for accurate verification of the dose delivery during patient treatment to ensure treatment quality.

Since VMAT uses many degrees of freedom during dose delivery, quality assurance (QA) is more difficult to perform for VMAT than for the conventional static radiation delivery techniques. Several verification devices specialized for arc trajectories have been used for performing VMAT QA, namely ArcCHECK (Sun Nuclear Corporation, Melbourne, FL), MatriXX (IBA, Schwarzenbruck, Germany) and Ocatvius (PTW, Freiburg, Germany) [1]. Apart from these devices, Electronic Portal Imaging Devices (EPIDs) have been used as an accurate tool for performing both pre-treatment and in-treatment dose delivery verification including time-integrated portal dosimetry and more recently, time-resolved portal dosimetry [2-4].

Pre-treatment QA is able to detect dose delivery changes caused by problems related to the linac, such as errors in the beam delivery. However, dose delivery deviations caused by changes in patient anatomy can only be detected on the day of the treatment or during treatment. This project has focused on dose delivery errors due to geometrical changes in patient anatomy that can frequently and rapidly occur over the course of fractionated EBRT. Tumor regression, tumor shift and pleural effusion in the lungs are examples of such geometrical changes [5]. If not detected, these changes may cause the actually delivered dose to deviate from the planned dose, thereby damaging the surrounding healthy tissues instead of the tumor.

In order to identify these dose delivery deviations in VMAT there are several EPID-based methods suitable for performing dose delivery verification. This project will focus on transit portal dosimetry in which EPIDs are used to obtain measured dose distributions behind the patient. Transit portal dosimetry is able to detect errors related to the beam delivery system itself and errors related to the patient [6]. Within transit portal dosimetry, 2D and 3D time-integrated portal dosimetry are currently employed in some radiotherapy centers [6-9]. Time-resolved portal dosimetry has been recently introduced for VMAT (Podesta et al. 2014 a) and has offered added value in assessing dynamic treatments. Instead of reading out the cumulative dose distribution to the EPID (time-integrated portal dosimetry), the dose distribution for each VMAT (time) segment is read out separately (time-resolved portal dosimetry) [2].

The main goal of this project is to compare the performance of three different transit portal dosimetry methods in detecting dose delivery deviations caused by patient anatomical changes: 2D time-integrated portal dosimetry, 3D time-integrated portal dosimetry (3D in vivo dosimetry) and 2D time-resolved portal dosimetry.

2 Background

2.1 Cancer

Cancer is characterized by the uncontrolled growth and spread of abnormal cells. If this spread is not controlled, it can result in serious illness and death. Cancer has become one of the greatest public health problems worldwide being one of the leading causes of morbidity and mortality. In 2008 there were 3.2 million new cases of cancer and 1.7 million deaths from cancer in Europe [10]. In the United States the estimated number of new cancer cases projected for 2015 was 1,658,370 and it was expected that about 589,430 Americans would die from cancer [11]. According to the World Health Organization (WHO), in twenty years from now the number of new cases of cancer will increase by 70% to more than 22 million cases [12].

2.1.1 Treatment options

Nowadays there are three main modalities for treating cancer: surgery, chemotherapy and radiotherapy. Surgery is usually done when the tumor is accessible or when organ preservation is not an essential requirement. Chemotherapy uses systemic agents (drugs) to kill the abnormal cells which are dividing rapidly. In this way, in several cases chemotherapy is used together with surgery and radiation therapy. Radiation therapy (radiotherapy) uses ionizing radiation to destroy the cancer cells. The most common types of ionizing radiation used are electrons, photons, protons and heavy ions (e.g.: carbon).

2.2 Radiotherapy

Radiotherapy is one of the main modalities for treating cancer next to surgery and chemotherapy. In order to destroy the tumor cells inside the human body, ionizing radiation is used in radiotherapy. Ionizing radiation may cause deletions, substitutions and/or actual breaks in the DNA (deoxyribonucleic acid) chain. The double strand breaks are more difficult to repair and therefore responsible for cell death. The reproductive death of the tumor cell occurs when the radiation damage is not repaired (correctly), causing abnormalities in the chromosomes.

The main goal of radiotherapy is to deliver a high dose to the tumor volume while minimizing the dose to the surrounding healthy tissue and nearby organs at risk (OAR) as much as possible. Since the surrounding normal tissues are also partially damaged by the radiation, a radiotherapy treatment is usually performed in a fractionated schedule, delivering the total dose in multiple treatments (fractions) to allow the normal tissues and nearby OAR to recover between fractions. In this way, an entire radiotherapy treatment typically consists of 30-40 fractions, 5 times per week, which takes approximately 6 or 7 weeks to deliver the total dose prescribed [13].

In radiotherapy, the radiation source can be located outside the patient (external beam radiotherapy), or within the tumor (brachytherapy). In brachytherapy a sealed radioactive source is introduced into or next to the area requiring treatment.

In EBRT the radiation is delivered from outside the patient by a linac. The radiation beams, mostly megavoltage x-rays (MV photon beams), electrons and protons, are focused on the tumor target and by using multiple beams in an optimum beam angle configuration is possible to limit the dose to the surrounding healthy tissues.

2.2.1 External Mega Voltage Photon Beam Radiotherapy

External Mega Voltage photon beam radiotherapy is the most common form of EBRT applied. This technique is implemented using linear accelerators that generate and accelerate electrons to energies ranging from 4 to 20 MeV (Figure 2.1). When these electrons collide with the tungsten target, high-energy MV X-rays or photons are produced. These high energy x-rays are shaped as they exit the linac to conform to the shape of the patient's tumor and the customized photon beam is directed to the patient's tumor. The beam may be shaped either by moulded blocks that are placed in the head of the linac (jaws) or by a multileaf collimator (MLC) that is incorporated into the head of the linac. The MLC typically consists of a series of 80 to 160 movable metallic leaves arranged in pairs. By changing their individual position, these leaves can block some fractions of the radiation beam thereby shaping the beam aperture according to the tumor shape [14].

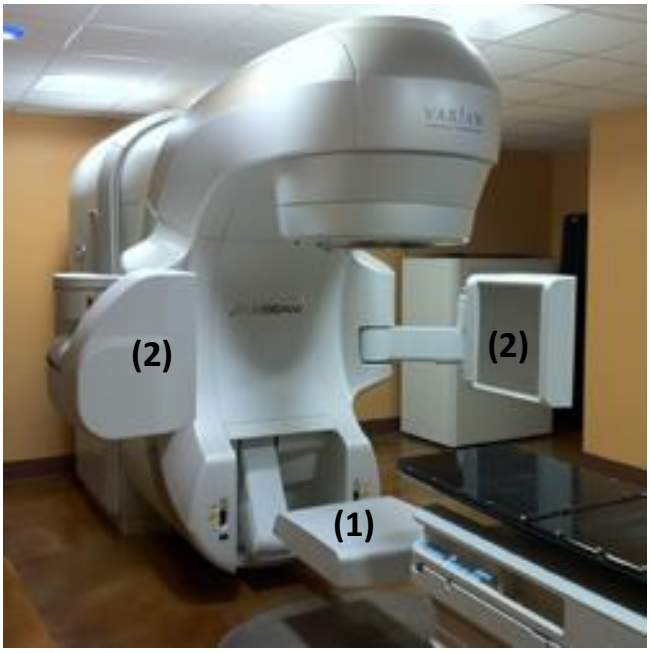

Figure 2.1 – TrueBeam Varian High Energy linac equipped with (1) an electronic portal imaging device (EPID) which acquires MV images of the treatment beam and (2) a kilo Volt (kV) imaging system [15].

2.2.2 Radiotherapy workflow

The external photon beam radiotherapy process involves several steps until directing the dose to the proper locations of the patient. These steps can be divided into two different phases: preparation and treatment delivery (Figure 2.2).

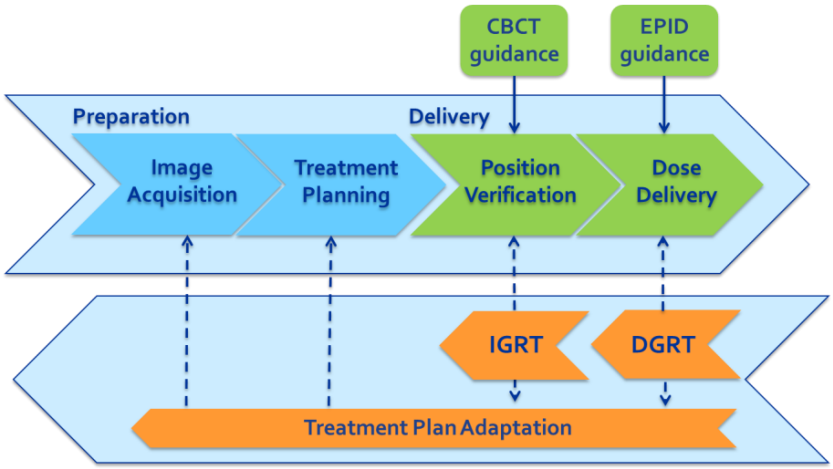

Figure 2.2 – Schematic overview of the external photon beam radiotherapy workflow. The feedback loop which involves treatment adaptation is also called adaptive radiotherapy.

2.2.2.1 Preparation

The preparation phase starts after the tumor diagnosis of the patient with the acquisition of the patient's anatomical information. Generally the anatomical information is acquired with a CT scanner, typically one week prior to the start of the treatment. However, the anatomical information can also be acquired with other imaging modalities, such as Magnetic Resonance Imaging (MRI). In order to avoid the tumor growth between the CT-scan acquisition and the treatment start, the time between the acquisition of the CT and the first treatment should be as short as possible. The CT-scan is then transferred to the treatment planning system (TPS). This is one of the most important steps where the radiation oncologist delineates the target volumes on this initial CT, also called planning CT. The main target volumes to be considered in a treatment plan are the following: 1) Gross Tumor Volume (GTV) which is the gross palpable or visible extent and location of tumor; Clinical Target Volume (CTV) which is the GTV plus a certain margin to account for microscopic disease spread, and 3) Planning Target Volume (PTV) which is the CTV plus a certain margin to account for the effect of delivery uncertainties, such as patient set-up and intra-treatment variations (e.g. organ motion) [16]. Besides the target volumes delineation, the OAR near the tumor site also have to be delineated in order to minimize the prescribed dose to them.

Based on the anatomical information of the planning CT, the delineated structures and the dose prescription, the plan is generated and a 3D (planned) dose distribution is calculated. As a result, a

3D treatment plan is obtained which consist of dose information over a 3D matrix of points over the patient anatomy.

The Dose Volume Histogram (DVH) summarizes the information contained in the 3D planned dose distribution and is the most common tool used for quantitative evaluation of treatment plans. A DVH is a histogram relating the radiation dose delivered to a tissue volume. Two types of DVH are possible: the differential DVH which shows the (relative) volume receiving a specified dose and the cumulative DVH which is the integral form and shows the (relative) volume receiving a specified dose or more. The most common one is the cumulative DVH. For a perfect treatment plan, the ideal cumulative DVH for a target volume would appear as a horizontal line at the top of the graph (100%), with a vertical drop at the prescribed dose indicating that 100% of the tumor volume receives the prescribed dose (Figure 2.3 (b)). In the case of a critical structure (OAR), the ideal cumulative DVH would appear as a horizontal line at the bottom of the graph and a vertical line at 0 Gy, indicating that 100% of the critical structure receives 0 Gy (Figure 2.3 (b)). A drawback of the DVH methodology is the lack of spatial information [17].

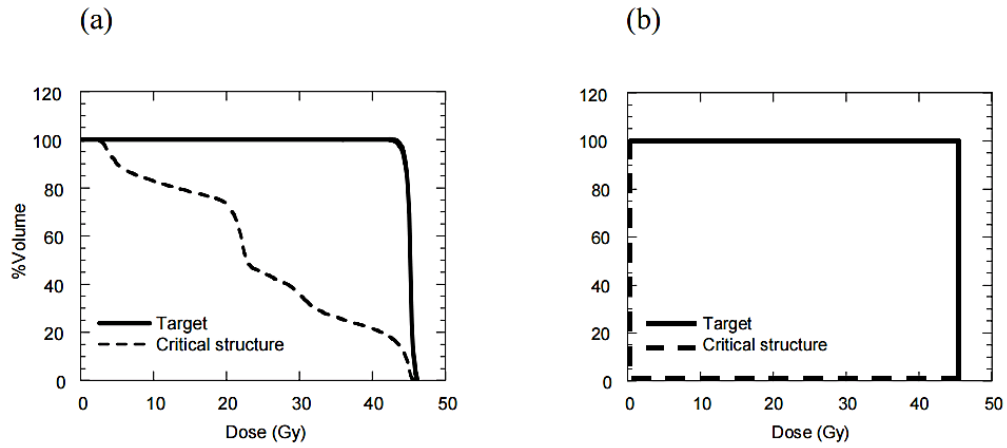

Figure 2.3 – Representation of cumulative DVHs. The ideal cumulative DVHs are represented on the right (b) for a target structure (prostate) and a critical structure (bladder) [17].

The treatment plan is finalized by selecting the number of beams, the beam angles and corresponding weights, the beam energy and by defining the beam shapes. In this way, it is possible to achieve a homogeneous dose in the tumor and simultaneously spare the surrounding normal tissue structures by modulating the beam shape according to the tumor shape to fit the profile of the target.

2.2.2.2 Treatment Delivery

The need to reduce the dose to normal tissue and OAR while directing a high dose to the tumor volume has led to the development of newer modalities for treatment delivery: dynamic Intensity Modulated Radiation Therapy (IMRT) and Volumetric Modulated Arc Therapy (VMAT).

2.2.2.2.1 IMRT

In dynamic IMRT the fluence distributions are adapted to the treatment constraints of the patient and each radiation beam is modulated by continuously moving the leaves of the MLC which is a computer-controlled mechanical beam shaping device placed inside the linac head. For each beam direction, the optimised fluence distribution is achieved by sequential delivering several subfields with optimised shapes and weights. With these dynamically shaped fields, the dose distribution can be delivered more conformal to the tumor.

2.2.2.2.2 VMAT

More recently, there has been some interest in improving dynamic IMRT into a treatment modality where also the beam angle is continuously varied. This treatment modality is called VMAT and was first introduced in 2008 by Karl Otto [18]. VMAT can deliver highly conformal dose distributions by continuously and simultaneously varying gantry angle, field shape and dose rate during treatment [19]. The most important benefit of VMAT compared to the conventional IMRT techniques is the possibility of treating the whole target volume in a 360 degree-rotation therefore providing shorter treatment times, typically less than 2 minutes (Figure 2.4).

The TPS (Eclipse, Varian Medical Systems) for VMAT uses control points (CPs) to optimise arc delivery treatment plans. The CPs consist of static configurations that the linac (MLC, gantry, etc.) should correspond and conform to during smaller arc sections in order to deliver the planned treatment. The term 'CP' is defined as the instantaneous configuration at a point in time while the term 'segment' is defined as the duration between two consecutive CPs [20]. In this way, N CPs correspond to N-1 segments.

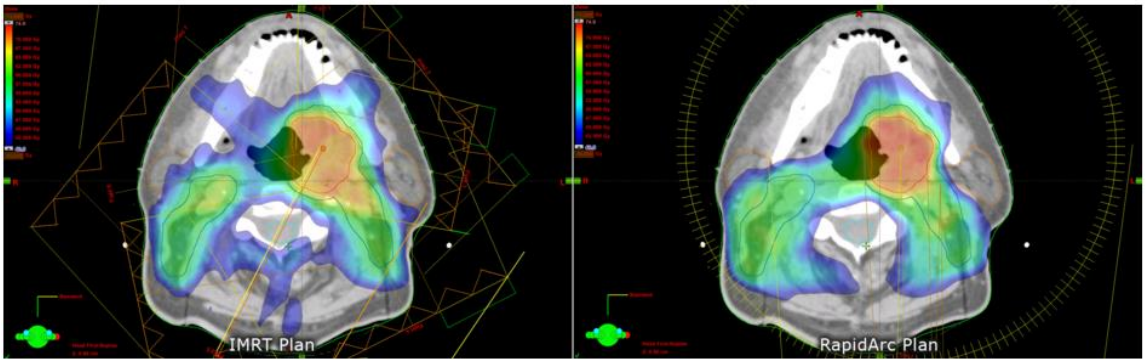

Figure 2.4 – Comparison between an IMRT (left) and a VMAT (right) plan. The VMAT plan was obtained with the RapidArc system commercialized by Varian Medical Systems. The VMAT plan shows a more conformed dose distribution [21].

2.2.2.3 Treatment verification

2.2.2.3.1 Position verification

The advanced developments of more complex delivery techniques like IMRT and VMAT have increased the need for accurate verification of patient positioning during treatment to ensure that the treatment is delivered as planned. As a result, modern linacs are equipped with two types of imaging detectors – EPID and kilo Voltage (kV) imaging system – to verify patient positioning during treatment (Figure 2.1). The EPID is used to image the MV treatment beam and therefore verify patient positioning, but it has been replaced over time by the kV-imaging system which acquires high quality online images and is able to reconstruct the 3D anatomical information of the patient into Cone Beam Computed Tomography (CBCT) images [22, 23].

2.2.2.3.2 Dose verification (portal dosimetry)

Besides their application as imaging detectors, the EPIDs can also be used as planar dose detectors. The most common type of EPID available today is the amorphous-silicon (a-Si) EPID which consists of an X-ray converter that converts X-ray photons to visible light, an array of light detectors and an electronic acquisition system for receiving and processing the resulting digital image [6]. A more detailed characterization of this EPID will be presented in section 2.3.1.

EPID measurements can be performed with minimum set-up requirements and a 2D delivered dose conversion can be done immediately using the digital images acquired. Although an EPID image contains 2D and not 3D information, it is still possible to reconstruct the 3D dose distribution inside a patient or more recently, time-resolved or 4D dose distributions [6]. In this way, EPID dosimetry allows dose verification in: 1) a point; 2) a plane (2D); 3) 3D, and 4) 4D or time-resolved. Due to these capabilities, EPIDs can perform both pre-treatment (prior to the treatment) and in-treatment (during treatment) dose verification, also called portal dosimetry.

To perform both pre-treatment and in-treatment portal dosimetry several steps are required. The first step is to acquire the planned dose and data from the TPS (e.g. planning CT) which will be then compared to the measured dose. Based on the planned dose and TPS data, point dose, planar dose (2D) or the 3D or 4D planned dose distributions are calculated with a prediction model. In a second step, when the treatment is being delivered the EPID images acquired need to be converted into portal dose images [2, 23]. Then, these 2D portal dose images can be used to reconstruct 3D or 4D dose distributions. Finally, it is necessary to do a quantitative comparison between the measured dose distribution and the planned (predicted) dose distribution using a dose comparison method. The most commonly used quantitative dose comparison method is the gamma evaluation [24].

2.2.2.3.2.1 Gamma evaluation method

The gamma evaluation method is a tool by which the predicted and measured dose distributions can be compared in a quantitative manner in the dose and spatial domains [2, 24]. The method uses two criteria simultaneously, a geometrical distance to agreement (DTA) and a percentage dose difference (DD), to calculate the gamma value for each pixel/voxel in an image/volume. Each

reference point p_r in the predicted dose distribution is compared to all evaluated points p_e in the measured dose distribution. The points search in the measured distribution is limited to a search box $\dot{v}$ within which the points are evaluated, therefore allowing a shorter calculation time. The geometry of this search box can be a circle (2D gamma analysis) or a sphere (3D gamma analysis) having a radius that is defined as the region of interest [20, 25]. The gamma value $|\gamma(p_r)|$ is defined as the minimum distance between the reference point and the distribution of evaluated points, as described in the following equation.

$$|\gamma(p_r)| = \min\left\{\sqrt{\left(\frac{\Delta D(p_r,p_e)}{DD}\right)^2 + \left(\frac{\Delta d(p_r,p_e)}{DTA}\right)^2}\right\} \forall \{p_e \in \dot{v}\} \quad (2.1)$$

Where $\Delta D(p_r,p_e)$ and $\Delta d(p_r,p_e)$ are the dose difference and geometrical distance between points p_r and p_e, respectively. DD and DTA represent the dose difference and distance to agreement selected for the gamma analysis, respectively. The dose difference and geometrical distance are normalized using acceptance criteria: percentage dose difference (DD) and distance to agreement (DTA), respectively. The most common used acceptance (gamma) criterion is [3%, 3 mm] [26].

The calculated gamma value $|\gamma|$ is then multiplied by the sign (+ or -) of the dose difference ΔD. In this way, positive gamma values represent a dose increase (hotspot) in the measured dose distribution compared to the planned dose distribution whereas negative gamma values represent a dose decrease (cold spot) in the measured dose distribution compared to the planned dose distribution (Figure 2.5) [25].

As a final step, the acceptance criteria are applied. The pixels or voxels for which $|\gamma| \leq 1$ meet the acceptance criteria and are considered to pass the gamma analysis. The pixels or voxels for which $|\gamma| \geq 1$ do not meet the acceptance criteria and are considered to fail the gamma analysis [20].

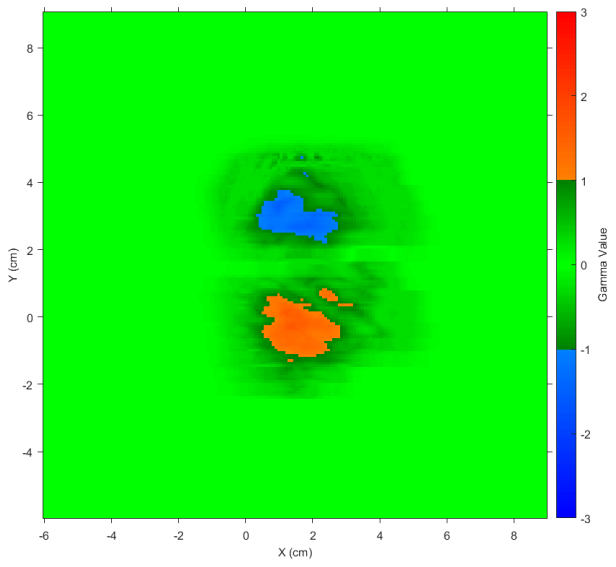

Figure 2.5 – Example of a time-integrated gamma analysis. The hot spot shown in red represents an over-dosage whereas the cold spot shown in blue represents an under-dosage.

The recent introduction of time-resolved portal dosimetry for VMAT (Podesta et al., 2014) led to the development of a time-resolved gamma analysis (Podesta et al., 2014) which allows a dose comparison in a time-dependent manner [2, 20].

Despite time-resolved gamma analysis being similar to time-integrated gamma analysis, some parameters had to be added to the previous gamma function. The time dimension (Δt) was introduced in the gamma function in addition to the already existing dose and spatial distance dimensions. A new acceptance criteria, time to agreement (TTA), was also introduced in addition to the percentage dose difference and distance to agreement. Besides, the search box υ was extended by a time of interest.

$$|\gamma(p_r, t_r)| = \min\left\{\sqrt{\left(\frac{\Delta D(p_r,p_e)}{DD}\right)^2 + \left(\frac{\Delta d(p_r,p_e)}{DTA}\right)^2 \left(\frac{\Delta t(p_r,p_e)}{TTA}\right)^2}\right\} \forall \{p_e \in \dot{\upsilon}\} \qquad (2.2)$$

The time-resolved gamma analysis produces multiple (time) frames - one frame for each VMAT segment while the time-integrated gamma analysis only produces one single frame for each beam. With time-resolved gamma analysis the predicted and measured portal dose images are compared for each VMAT segment [25].

2.2.2.4 Adaptive radiotherapy

Currently, it is possible to detect patient anatomical changes during treatment delivery by monitoring treatments with kV imaging systems or with portal dosimetry. In order to figure out when the corresponding patient treatment plan needs to be adapted due to such anatomical changes, a new concept emerged in radiotherapy workflow: adaptive radiotherapy (ART). ART is a feedback loop that incorporates the information collected during the treatment course and enables a continuous adaptation of the patient treatment plan during the radiotherapy course to account for temporal changes in the anatomy of the patient [27, 28].

Nowadays, ART is mainly performed based on image-guided radiotherapy (IGRT) by monitoring the kV CBCT data. However, these IGRT methods are qualitative and do not allow to quantify dose differences. To overcome this limitation, a few radiotherapy centers started taking into account the quantitative dose differences generated by portal dosimetry [29, 30]. This is also called dose-guided radiotherapy (DGRT).

2.3 State-of-the-art of EPID dosimetry

Electronic portal imaging devices were originally developed for verification of patient positioning during treatment and to replace film that was previously used [31]. The images of the megavoltage treatment beam acquired by the EPID, also called portal images, have been used to identify errors in the patient set-up or errors of the radiation field placement prior or during field delivery.

Shortly after their introduction in clinical practice as a tool for set-up verification measurements of the patient position, it was realized that EPID images also contained dose information [31]. Since then, several research groups started investigating the dosimetric characteristics of different types of EPIDs and different methods based on EPID dosimetry [6].

In most of the radiotherapy departments, EPIDs are already fixed to the linac due to its previous application as imaging detector for patient positioning verification. Consequently, it has become more advantageous for those departments also use EPID for dose verification without the need for additional hardware when compared to the other dosimetry devices.

Several types of EPIDs have been developed and can be categorized according to their technical design. The first EPID being commercially available was the liquid-filled ionization chamber EPID (Li-Fi EPID), followed by the camera-based EPID (CC-based EPID) and, more recently, the amorphous-silicon EPID (a-Si EPID) which currently is the most used. [6].

2.3.1 a-Si EPID

In 1995, Antonuk et al. described the amorphous-silicon EPID (a-Si EPID) for the first time [32]. The device consists of an X-ray converter, a light detector and an electronic acquisition system for receiving and processing the resulting digital image [6, 32].

An example of an a-Si EPID commonly used nowadays is the aS1000 EPID from Varian Medical Systems (Figure 2.6). It is a flat panel imager composed by arrays of light sensitive amorphous-Si photodiodes arranged in a total 40 x 30 cm^2 active detector area. Each frame is a scan of the detector elements and this EPID has a maximum frame rate of 9.574 fps. The aS1000 has in total 1024 x 768 pixels; each pixel (picture element) consisting of a light sensitive photodiode and a thin film transistor to enable readout [34]. The picture elements register the amount of radiation that falls on them and convert that amount into the corresponding number of electrons. The electrons are then converted into electrical signals which are further processed by the imaging device or a computer resulting in the final digital image (portal image).

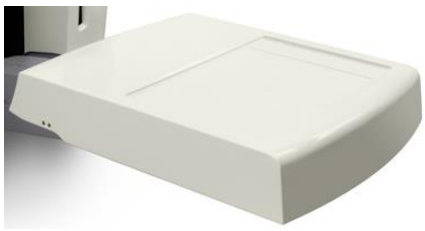

Figure 2.6 – aSi 1000 EPID from Varian Medical Systems.

2.3.2 Methods based on EPID dosimetry

In EPID dosimetry, also called portal dosimetry, two types of dose verification can be applied: pre-treatment (performed prior to the treatment) and in-treatment (performed during treatment) dosimetry.

In pre-treatment dose verification a comparison is done between the planned dose distribution (obtained from the TPS) and the measured dose distribution when the radiation beams are delivered outside patient treatment time, i.e. with open fields or a phantom. These measurements can be used e.g. to check the pre-treatment conditions and to determine the dose delivered to the EPID or to the phantom.

In the case of in-treatment dosimetry a comparison is done between the planned dose distribution and the measured dose distribution when the radiation beams are delivered during patient treatment time. These measurements can be used to determine the dose delivered to the EPID or to the patient.

There are different EPID-based dosimetry methods that can be categorized depending on whether or not radiation beams have been transmitted through an attenuating medium (a phantom or patient) between the source and the EPID (non-transit dosimetry and transit dosimetry, respectively) or whether the dose is reconstructed inside a phantom or a patient. There are also different arrangements for EPID dosimetry and different locations where the delivered dose distribution can be determined (at the EPID level or inside the patient/phantom), as represented at Figure 2.7 [6].

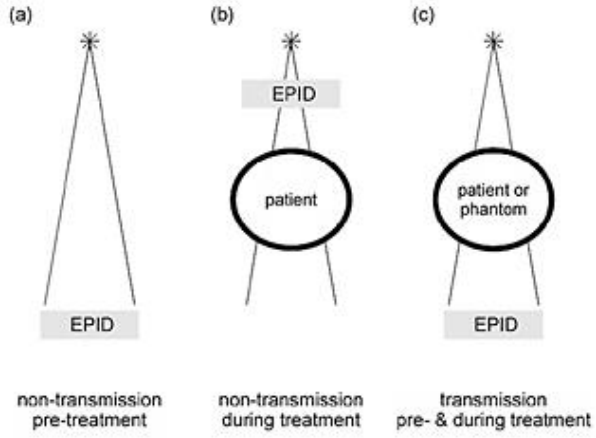

Figure 2.7 – Representation of the different arrangements for EPID dosimetry, each one with the possibility to verify a dose distribution at the EPID level or inside the patient or phantom. Adapted from [6].

2.3.2.1 Transit portal dosimetry

In order to ensure the quality of the radiotherapy treatment, it becomes vital to verify that the patient is receiving the correct dose during treatment. To this end, it has become important to determine the actually delivered dose from transit EPID images, based on the radiation beam passing through the patient, as described in Figure 2.7c. In this way, the dose verification can be

performed either at the level of the EPID or by reconstructing the dose inside a digital representation of the patient.

Transit portal dosimetry can be classified by point-dose verification, 2D portal dose prediction models, 3D dose reconstruction models and, more recently, 4D (time-resolved) dose reconstruction models.

2.3.2.2 2D Transit portal dosimetry

The 2D transit portal dose verification method consists of predicting the portal dose at the level of the EPID behind a patient or phantom. With this method, a 2D dose distribution can be measured behind a patient, thus allowing dosimetric treatment verification.

Several research groups have proposed different 2D dose prediction models. These models calculate the planned portal dose at the position of the EPID, which can then be compared with the measured portal dose during treatment. If the predicted and measured portal dose distributions are equal, then the actual delivered dose to the patient is assumed to be the same as the planned dose. However, if there are discrepancies between the two dose distributions errors may have occurred during the patient treatment.

Since the model developed by van Elmpt et al. (2005) is currently implemented at MAASTRO Clinic and will be used for the purpose of this project, it will be reviewed in this section [35]. This 2D portal dose prediction model describes the relation between three sets of data: two portal dose images, one with and a second without the patient between the beam source and the EPID, and the radiological thickness of the path crossed by the photons in the patient. In this way, the model is able to predict a 2D portal dose image behind a patient, based on a portal dose image without the patient in the beam in combination with the radiological thickness of the patient extracted from the planning CT scan. This model is therefore a tool that allows 2D verification of patient treatments by comparing predicted and measured portal dose images.

2.3.2.3 3D (in vivo) portal dosimetry

The 2D dose prediction models referred above allow the comparison between the planned and measured portal dose at the EPID level. However, if there are discrepancies between these two dose distributions it may be difficult to interpret the differences in terms of patient dose. In order to overcome this limitation, several methods have been developed to reconstruct the delivered dose distribution inside the patient from the EPID and then compare with the planned dose distribution obtained from the TPS [36-41]. In 3D portal dosimetry, the comparison between the two dose distributions is not done at the EPID level but at the patient level instead. One of those reconstruction models, which was used in this thesis, is the 3D dose reconstruction model developed by van Elmpt et al. (2006), which allows a full three-dimensional reconstruction of the dose actually delivered to the patient [36].

This reconstruction model is based on measured EPID images without the patient placed in the beam and an independent dose calculation algorithm based on a Monte Carlo dose engine. The

model involves four steps until the final dose calculation (Figure 2.8). As a first step, a portal image is measured under the same conditions as the actual treatment and is converted into a portal dose image using a global calibration model for a-Si EPIDs (Nijsten S. et al.) [23]. The second step is to extract from this portal dose image the energy fluence exiting the linac. As a third step, a phase space distribution is sampled from the energy fluence. In the final step, the reconstructed phase space distribution is the starting point for the dose calculation. The 3D dose calculation is performed inside the patient or phantom geometry (planning CT or CBCT scan) based on the Monte Carlo XVMC code [42]

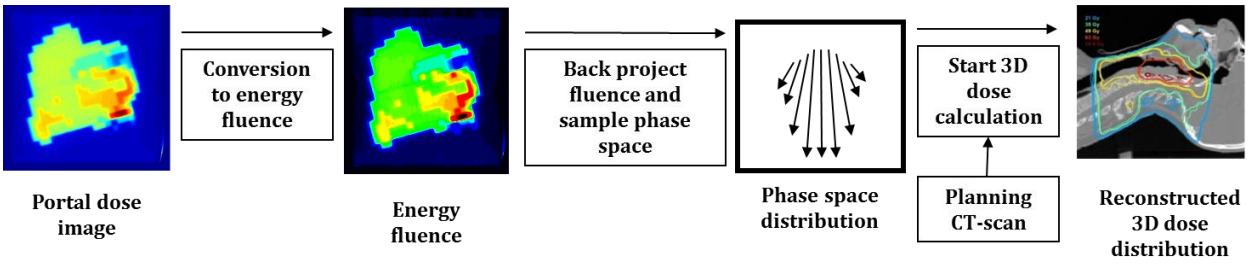

Figure 2.8 - Schematic representation of the several steps involved in the model used for 3D in vivo dosimetry developed by van Elmpt et al. (2006). In a first step the 2D open-field portal dose images acquired by the EPID from all beam directions are converted to energy fluence. This energy fluence is then back-projected to level of the linac. Based on this new energy fluence distribution, a forward Monte Carlo 3D dose calculation is done inside the patient's planning CT or CBCT scan. As a result, a reconstructed 3D dose distribution in the planning CT or CBCT scan is obtained.

Several research groups have investigated the use of dose reconstruction models for performing verification of the dose delivered to the patient in three dimensions [6]. van Elmpt et al. (2009) presented and validated a model used for 3D in vivo dose verification based on information gathered during treatment, i.e. the patient anatomy using CBCT and the 2D transit EPID images. The dose information in these images was back-projected through the CBCT scan and used for Monte Carlo simulation of the dose distribution inside the CBCT scan, as represented in Figure 2.8 (van Elmpt et al., 2006). With this study it was possible to verify the dose delivered to the patient by combining in-room imaging with the transit dose measured during treatment [43].

2.3.2.4 Time-integrated and time-resolved portal dosimetry for VMAT

Due to the introduction of dynamic radiation delivery techniques where the fields are not static, like IMRT with dynamic MLC and VMAT, the concepts '2D transit time-integrated' and '3D time-integrated' portal dosimetry appeared because in these dynamic techniques the images acquired by the EPID are time dependent. The EPID acquires a series of portal images during treatment delivery that are integrated over time at the end.

Currently, to detect dose delivery changes in VMAT, 2D time-integrated or 3D time-integrated portal dosimetry are employed in some radiotherapy institutes. With these methods the doses in all VMAT segments over time are summed up. However, due to the integral nature of these methods,

there are also some dose deviations that will average out based on the arc trajectory resulting in minor or no indication of dose delivery deviation [5, 44].

Recently, time-resolved portal dosimetry was introduced for VMAT at MAASTRO Clinic [2, 20, 45]. With this novel method the comparison between the transit portal dose images acquired during treatment and the predicted transit portal dose images based on the planning CT of the patient is done separately for each VMAT segment during the arc trajectory.

2.3.2.4.1 Clinical approaches

As a consequence of the appearance of time-dependent radiation delivery techniques (dynamic IMRT and VMAT) in EBRT, several EPID-based methods for dose verification have been developed and improved in order to follow this technological development. In this section recent clinical approaches to time-integrated and time-resolved portal dosimetry for VMAT are reviewed.

2.3.2.4.1.1 2D Time-integrated portal dosimetry

Persoon et al. (2015) and Podesta et al. (2015) investigated if 2D time-integrated portal dosimetry for VMAT could detect dose differences caused by anatomical changes throughout the treatment course in a cohort of lung cancer patients [5]. These patients were treated with VMAT following daily CBCT-based images which were visually inspected for anatomical changes (e.g. tumor regression). When relevant geometrical differences were observed in the daily CBCT images compared to the original planning CT, it was decided to acquire a new planning CT. 2D time-integrated portal dosimetry was performed to compare the planned dose distribution with the delivered dose distribution at the level of the EPID with the patient placed in the beam. The validated prediction model developed by van Elmpt et al. (2005) was used to simulate both the planned and delivered 2D portal dose images based on the patient geometries described by the planning CT and the new planning CT [35]. This study demonstrated that 2D time-integrated portal dosimetry could detect most geometrical changes caused by atelectasis (i.e. collapse or closure of parts of the lung). However, for other causes the method was not sensitive enough to identify the geometrical changes. This study concluded that 2D time-integrated portal dosimetry seems to hide certain dose delivery changes and therefore a time-resolved dose verification technique seems to be essential to verify VMAT dose distributions, which should be able to capture the dynamic and timed nature of VMAT.

2.3.2.4.1.2 3D Time-integrated portal dosimetry (3D in vivo dosimetry)

In order to investigate the exact cause of the dose discrepancies found with 2D transit portal dosimetry, it is mandatory to perform 3D portal dosimetry which allows a meaningful analysis of the delivered dose distribution in target volumes or OAR [6, 46].

Persoon et al. (2013) presented the first clinical results of adaptive radiotherapy based on 3D time-integrated portal dosimetry for a group of five lung cancer patients treated with VMAT [29]. To

achieve that, they developed a method for 3D portal dose measurement (PDM), also called 3D time-integrated portal dosimetry, combined with kV-CBCT imaging which can be seen in Figure 2.9. The 2D EPID images were acquired during treatment and were automatically converted to 2D portal dose images [23]. These 2D portal dose images were then used as input for a 3D portal dose reconstruction algorithm to calculate the actually delivered 3D dose distribution of the day from the kV-CBCT image acquired prior to the treatment [47]. The dosimetric effect of the patient anatomical changes was quantified based on the 3D portal dose measurement. At the end a comparison was done between the measured and planned 3D portal dose distributions using the gamma evaluation and DVH analysis. The decision of re-planning the treatment plan of each patient was based on both quantitative dose analysis (gamma and DVH metrics analysis) and visual inspection of the kV-CBCT image.

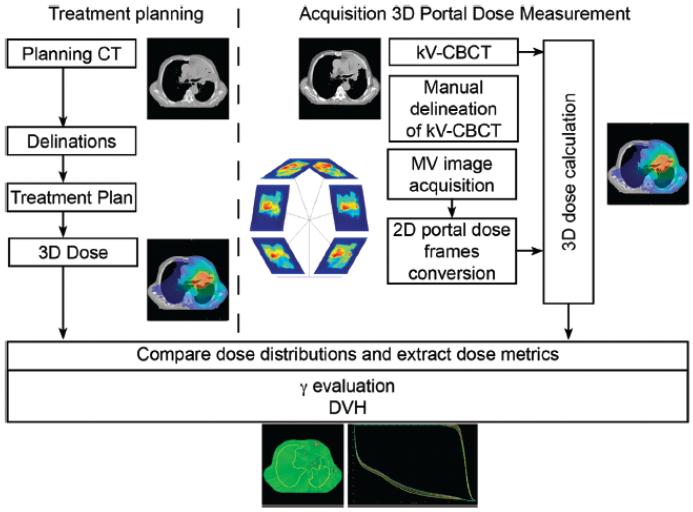

Figure 2.9 - Workflow of the 3D portal dose measurement acquisition and extraction of dose metrics from the DVH and gamma evaluations. On the left side a typical treatment planning process is depicted. On the right side the treatment process is depicted, the acquisition of the PDM. Adapted from [29].

This study showed that in four out of five patient cases, the treatment plan had to be adapted based on 3D time-integrated portal dosimetry and confirmed with a visual inspection of the kV-CBCT due to changes in atelectasis that induced shifts of the tumors and consequently a decrease of their dose coverage. It was demonstrated that 3D time-integrated portal dosimetry can play an important role in informed decision-making when adapting the treatment plan of a patient and is a promising method for detecting dose deviations over time for lung cancer patients.

2.3.2.4.1.3 2D Time-resolved portal dosimetry

Since 2D time-integrated portal dosimetry for VMAT seems to hide certain dose delivery changes caused by patient anatomical changes as shown by Persoon et al. (2015) and Podesta et al. (2015), a time-resolved dose verification method has become essential to verify VMAT dose distributions [5]. In order to overcome those limitations revealed by 2D time-integrated portal dosimetry, 2D time-

resolved portal dosimetry for VMAT has been recently introduced at MAASTRO Clinic as a method for verifying the dosimetric information at the various time control points of the VMAT beam delivery. Instead of reading out the cumulative dose distribution to the EPID (time-integrated portal dosimetry), the dose distribution for each VMAT time segment is read out separately (time-resolved portal dosimetry) [2, 25].

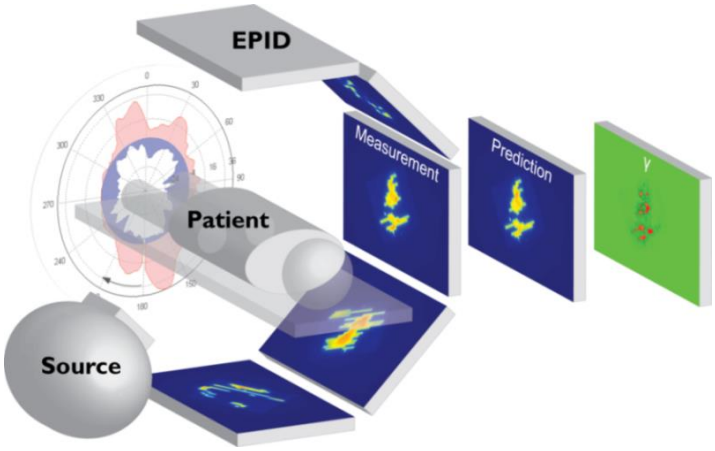

Figure 2.10 – Schematic overview of 2D time-resolved portal dosimetry (time-resolved transit planar dosimetry) for VMAT. The measured transit planar portal dose images per CP during treatment are compared to the predicted transit portal dose images per CP. A time-resolved gamma evaluation is used for dose comparison. The gamma evaluation results can be expressed by a gamma map or by a polar plot as function of the gantry angle where the red region represents an over-dosage and the blue region represents an under-dosage. Adapted from [45].

Persoon et al. (2015) and Podesta et al. (2015) presented a proof of principle in order to demonstrate that time-resolved transit planar dosimetry (2D time-resolved portal dosimetry) does not suffer from the same geometrical shortcomings of integrated methods and offers added value in detecting dose delivery changes caused by patient anatomical changes [45]. They studied a cohort of four patients, each showing a geometrical change during the course of the treatment: pleural effusion, rectal gas pockets and tumor regression. For time-integrated portal dosimetry, the portal doses in all CPs were summed over time. For time-resolved portal dosimetry the model used to convert the portal images into portal dose images was adapted such that a portal dose image per CP was generated (Figure 2.10). A comparison between the planned dose and the simulated delivered dose of VMAT beams was done per CP and calculated using the planning CT and the kV-CBCT of the day. The dose evaluation was performed with a static gamma evaluation for time-integrated portal dosimetry and with a time-resolved gamma evaluation for time-resolved portal dosimetry.

This study demonstrated that for the four patient cases studied, time-resolved portal dosimetry was superior to time-integrated portal dosimetry. Time-resolved portal dosimetry was able to detect the geometrical changes of the patients while time-integrated portal dosimetry did not identify discrepancies in the dose delivery.

3 Materials & Methods

3.1 Materials

3.1.1 Clinical equipment and software

At MAASTRO Clinic all patients are planned with Varian's treatment planning system Eclipse v11 using the Acuros dose algorithm. After treatment planning, patients are treated with VMAT which is delivered by a Varian TrueBeam linear accelerator. The linac can deliver photon beams of 6 and 10 MV and is equipped with the a-Si EPID (the Varian aS1000) to acquire portal images and with a kV-CBCT imager to acquire CBCT images during several treatment fractions. Portal images are acquired with Varian's iTools, a software package to capture all individual image frames during the VMAT delivery.

3.1.2 Research software

For clinical research, the patient data are collected from the clinical database. Patient data consists of the treatment plans of the patients including the planning CT-scan acquired before treatment (typically one week before), the DICOM (Digital Imaging and Communication in Medicine) RTSTRUCT which contains information about the delineated structures and the DICOM RTPLAN that contains information related to the treatment itself (e.g. number of beams, beams energy and MLC positions). After patient data collection, these data can be loaded into the research software.

In this thesis two in-house developed research software were used to perform portal dose calculations (*TARDIS* and Transformation GUI). Both of them are developed in MATLAB and are able to perform portal dose calculations for 2D and 3D time-integrated portal dosimetry and more recently, time-resolved (4D) portal dosimetry. These software are also able to generate DVH curves based on 3D dose distributions and to perform 2D, 3D and 4D gamma analyses (Figure 3.1).

One of the software (Transformation GUI) also allows the simulation of different manipulations in the planning CT such as patient rotation, structure shifts and structure deformations. In this thesis this software was used to simulate geometrical changes within the patient by manipulating the patient's planning CT.

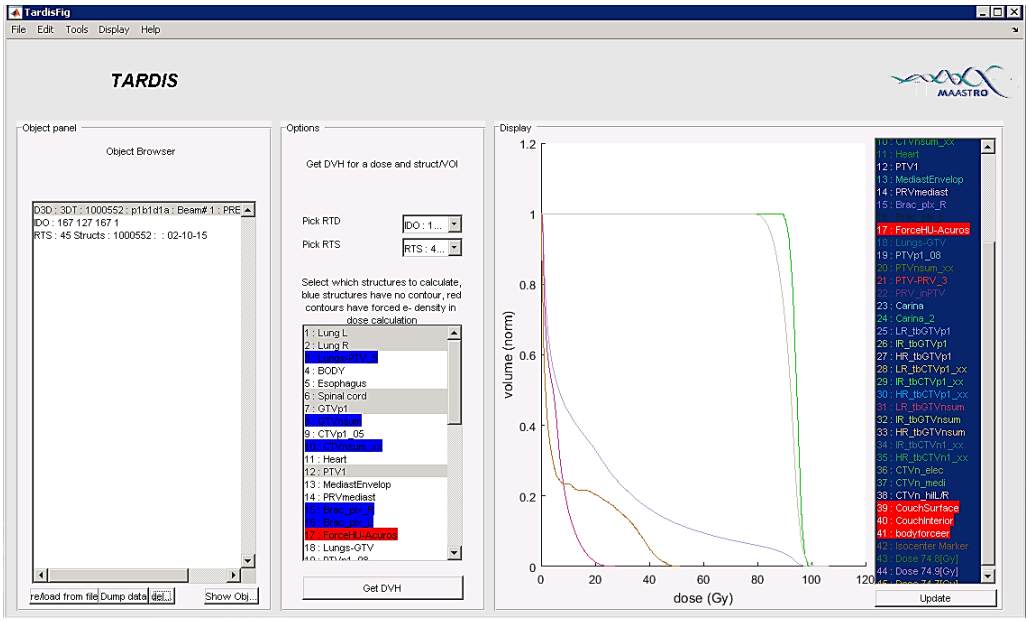

Figure 3.1 – Snapshot of the *TARDIS* software with the DVH sharpness.

3.2 Methods

3.2.1 Patient simulations

In order to investigate the impact of geometrical changes within a patient on the delivered dose distribution, a cohort of 6 Non-Small Cell Lung Cancer (NSCLC) patients from the clinical data base was used for analysis. All patients were treated at MAASTRO Clinic using VMAT, applying the dose in one or two-half arcs, using 6 or 10 MV photon beam quality delivered with a Varian True Beam Accelerator.

During the course of a radiotherapy treatment of lung cancer patients, tumor shift, tumor regression and pleural effusion (fluid accumulated in the pleural cavity) are some of the most common geometrical changes that can occur within the patient between treatment fractions. Therefore, these three types of geometrical changes were simulated by manipulating the planning CT of each patient. Since a patient's CT contains information about the photon attenuation (the linear attenuation coefficient can be obtained from the HU - Hounsfield Unit - values in each voxel), the dose calculations are performed on the CT image after converting the HU values into electron densities.

3.2.1.1 Tumor shift

Tumor shift was simulated by changing the absolute position of the tumor's bitmask (GTV structure) and updating the corresponding HU values of the CT image. The voxels where the tumor used to be before being shifted are replaced by the HU values of the lung tissue (-750 HU which is

the standard HU value for lung tissue). The shifts were simulated along the Y axis because this was the one that induced more discrepancies in the resultant dose distributions. Figure 3.2 shows the directions of each axis and was used as reference for this thesis.

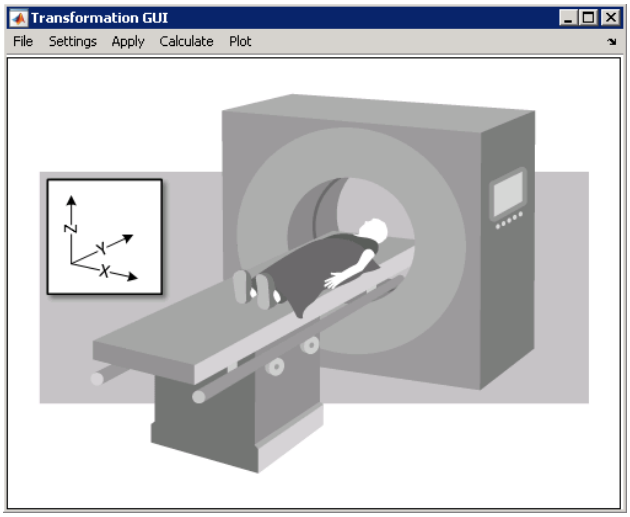

Figure 3.2 – Snapshot of the Transformation GUI software. The representation of the X, Y and Z axis was used as reference for this thesis.

Since the resolution of the CT image in the Y axis is 0.3 cm, multiple shifts of 0.3 cm were applied to the tumor to avoid image artifacts. The range of shifts applied goes from 0.3 cm until 3.9 cm in steps of 0.3 cm. The direction of the shifts applied along Y axis was chosen according to the tumor position inside the lung of each patient.

Figure 3.3 shows an example of 5 multiple tumor shifts of 0.5 cm along the positive direction of Y axis in one of the patients case.

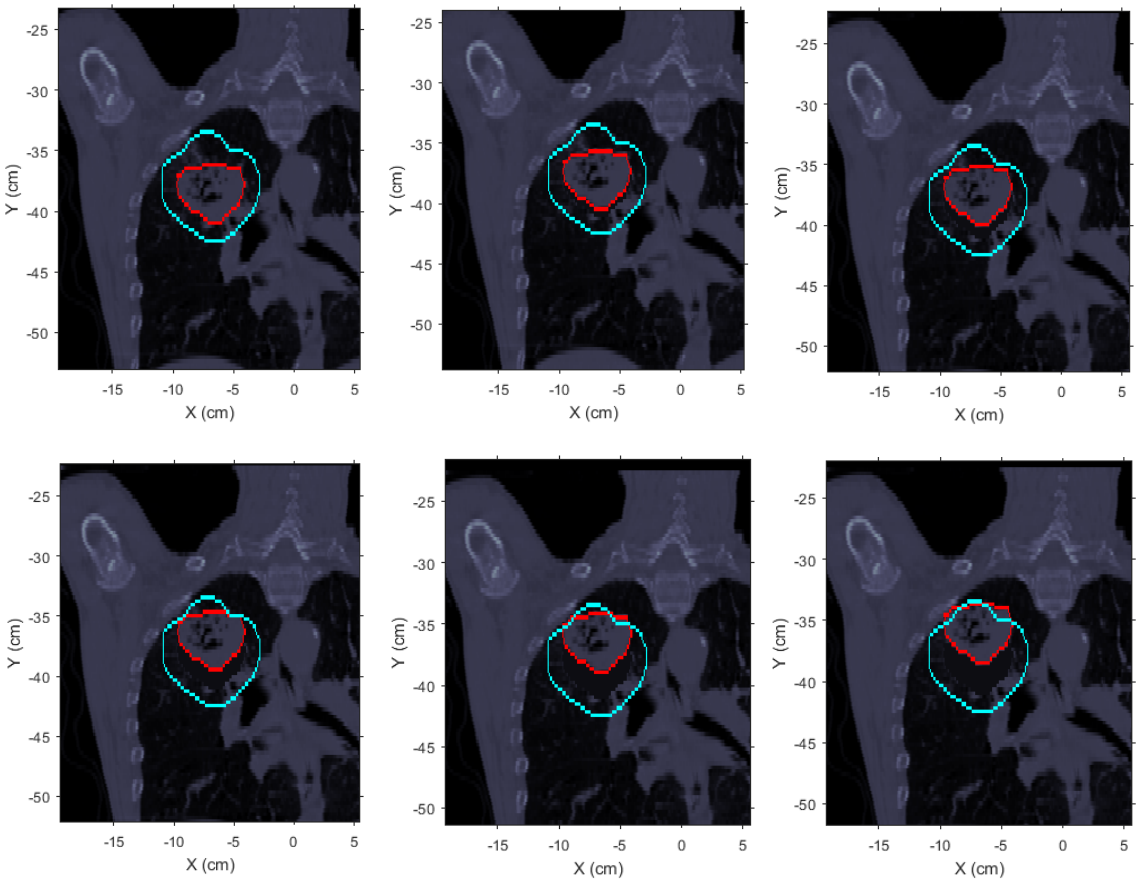

Figure 3.3 – Example of simulated tumor shifts of different magnitudes along the positive direction of Y axis. The blue contour represents the original PTV and the red contour represents the GTV (tumor structure). Top left: original CT (without tumor shift). Top center: 0.5 cm tumor shift. Top right: 1.0 cm tumor shift. Bottom left: 1.5 cm tumor shift. Bottom center: 2.0 cm tumor shift. Bottom right: 2.5 cm tumor shift.

3.2.1.2 Tumor regression

Tumor regression was simulated by applying a centroid-based deformation to the tumor structure. The magnitude of the regression was changed by multiplying the deformation vectors with a scaling factor. Before the deformation is applied to the tumor, the HU values of the voxels in the volume where the original tumor used to be were forced to -750 (standard HU value for lung tissue). Regressions between 10% and 90% were applied to the original tumor volume in steps of 10%.

Figure 3.4 shows an example of simulated tumor regressions of different magnitudes.

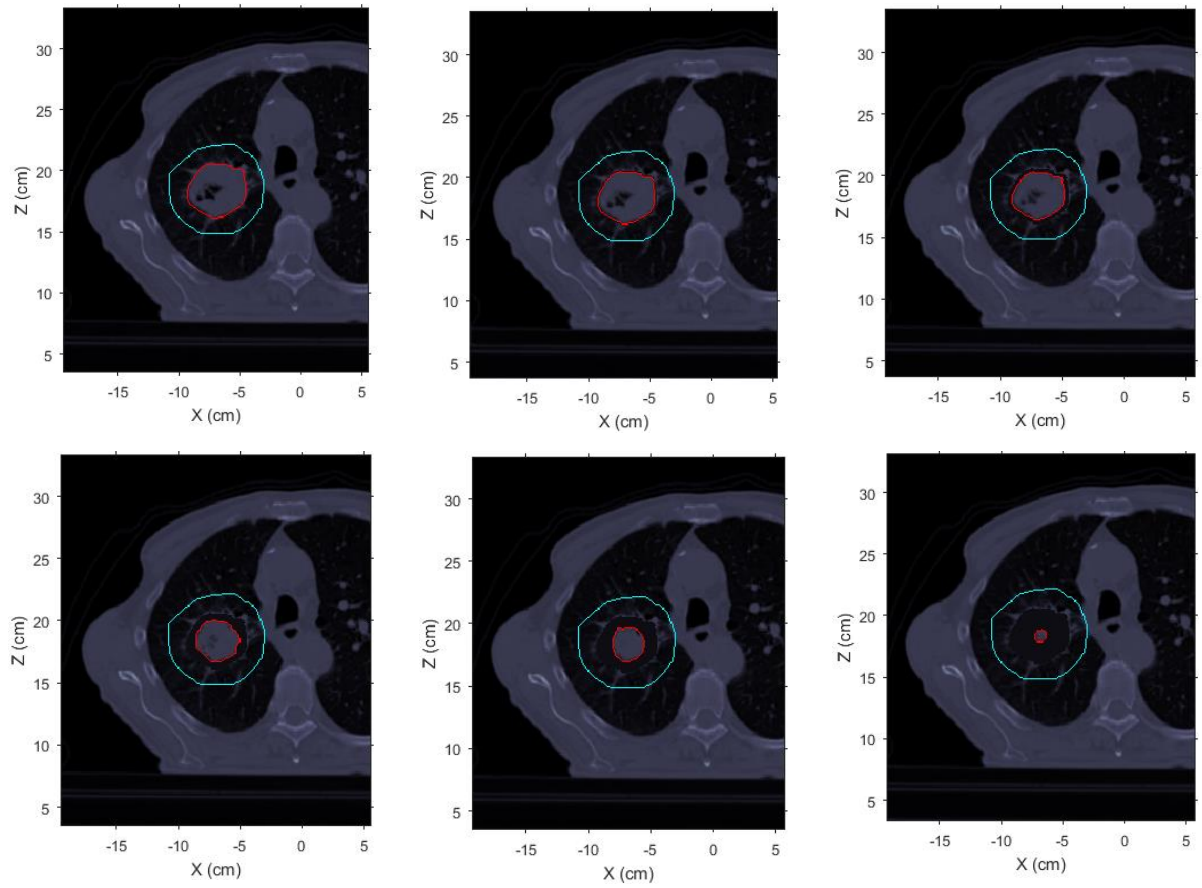

Figure 3.4 – Example of simulated tumor regressions of different magnitudes. The blue contour represents the original PTV and the red contour represents the GTV (tumor structure). Top left: original CT (without tumor regression). Top center: 10% of tumor regression. Top right: 30% of tumor regression. Bottom left: 50% of tumor regression. Bottom center: 70% of tumor regression. Bottom right: 90% of tumor regression.

3.2.1.3 Pleural effusion

Pleural effusion is caused by fluid accumulation in the pleural cavity. Since the patient is in the supine position during treatment, gravity will cause the fluid to accumulate on the dorsal side of the pleural cavity. According to the MAASTRO clinical protocol, the extent of pleural effusion is the fluid level (in cm) in the sagittal slice (YZ plane) of the CT which contains the tumor centroid.

Pleural effusion was simulated by forcing the HU values of the pleural effusion volume to be the HU value for water which is 0. In a first step, the absolute position of the tumor centroid is calculated and the sagittal slice which contains the tumor centroid is selected. In a second step, the absolute position of the first lung VOI voxel along the z axis is calculated (z_{min}). Finally, a pleural effusion bitmask that consists of all lung VOI voxels that have a z-coordinate such that $z\text{-}z_{min}$ <= fluid level is created. The HU values of all CT voxels inside the pleural effusion bitmask were forced to 0 as referred above.

For patients where the tumor was positioned at the bottom of the lung, fluid levels were simulated between 0.1 cm and 1.0 cm in steps of 0.1 cm. Otherwise fluid levels were simulated between 0.5 cm and 4.0 cm in steps of 0.5 cm.

Figure 3.5 shows an example of simulated pleural effusion of different magnitudes inside the lung which contains the tumor.

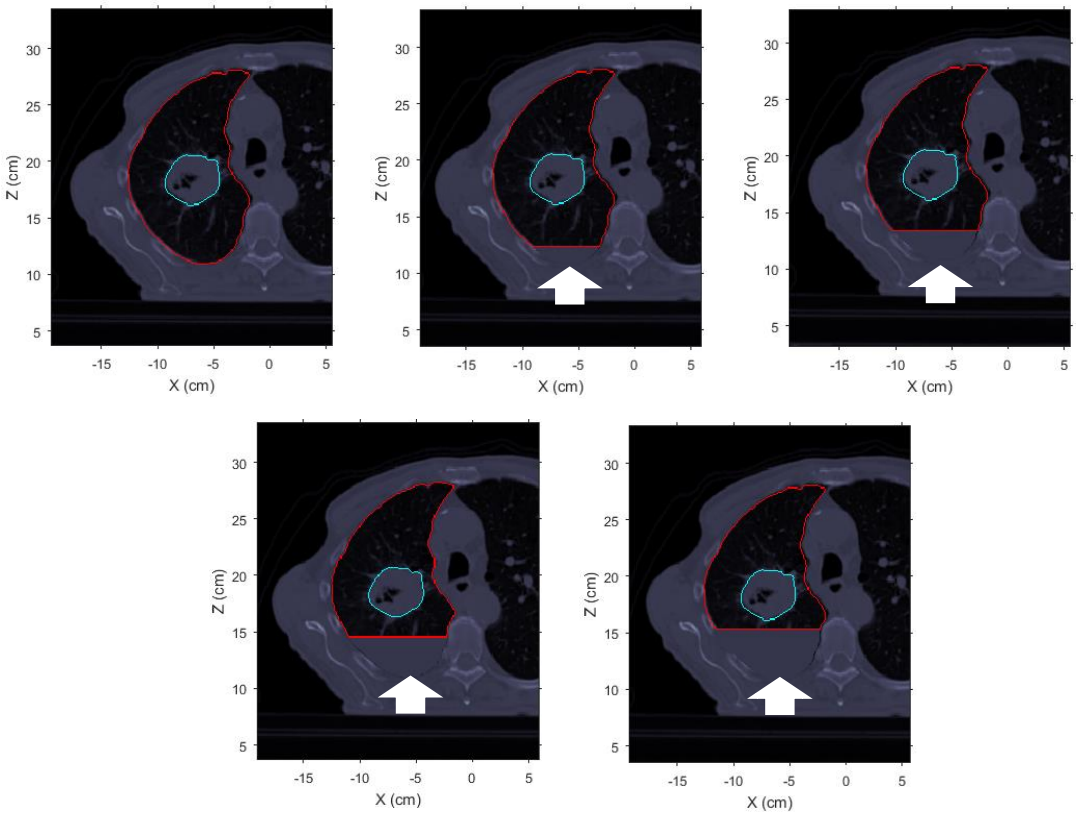

Figure 3.5 – Example of simulated pleural effusion of different magnitudes inside the left lung. The blue contour represents the GTV (tumor structure) and the red contour represents the right lung which contains the tumor. Top left: original CT (without pleural effusion). Top center: 1 cm of fluid level. Top right: 2 cm of fluid level. Bottom left: 3 cm of fluid level. Bottom right: 4 cm of fluid level.

3.2.2 Dose evaluation

After simulating the three types of geometrical changes of different magnitudes in the planning CT of each patient, portal dose images were simulated: one for the initial planning CT and one for each manipulated CT [35]. All simulations were performed using the initial unadapted treatment plan.

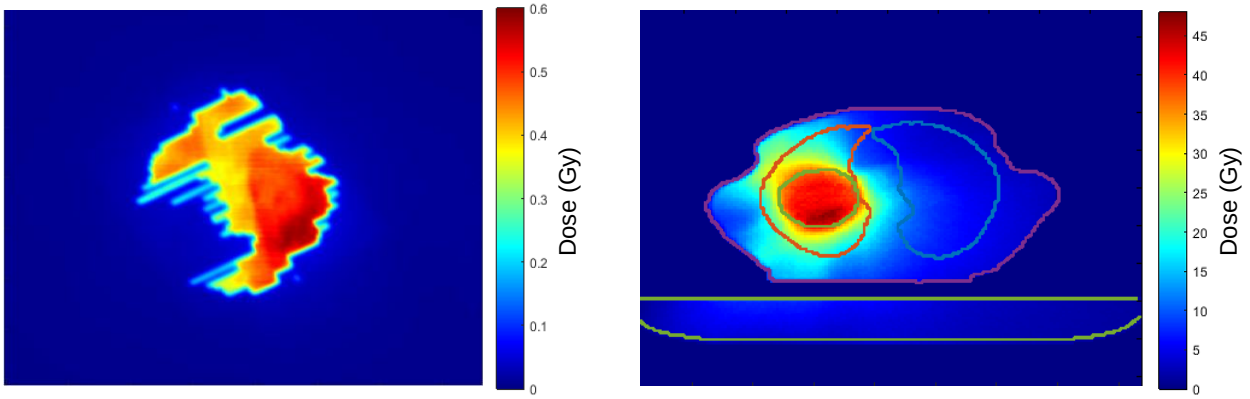

Figure 3.6 - Example of 2D and 3D dose distributions. Left: portal dose image at the EPID level. The shape of the dose distribution is caused by the position of the MLCs. Right: portal dose image reconstructed in 3D at the patient level. The couch is represented in the bottom (light green contour) and the body structure is represented in the center (XZ plane). The tumor (green contour) is inside the left lung (red contour).

The comparison between the planned and simulated dose distributions (portal dose images) was performed at the patient level (3D time-integrated portal dosimetry) and at the EPID level (2D time-integrated and 2D time-resolved portal dosimetry). Figure 3.6 shows an example of a dose distribution simulated at the EPID level and at the patient level. The 3D dose distributions inside the patients were obtained using a Monte Carlo based three-dimensional dose reconstruction method derived from the portal dose images [36].

The portal dose images obtained with each portal dosimetry method for each transformation were compared with the original one (without transformation) using a global 2D gamma analysis in the case of 2D time-integrated and 2D time-resolved portal dosimetry and a global 3D gamma analysis in the case of 3D time-integrated portal dosimetry. In all gamma analyses five gamma criteria for global dose difference (%) and distance to agreement (mm) were employed: [1%, 1 mm], [1.5%, 1.5 mm], [2%, 2 mm], [2.5%, 2.5 mm] and [3%, 3 mm]. Despite the [3%, 3 mm] gamma criterion being used at MAASTRO Clinic for clinical decision protocols and being the most commonly used for published studies (Low et al., 2013), there was interest in exploring other gamma criteria that could be more suitable than the [3%, 3 mm] [26]. In fact, published studies have indicated that this gamma criterion is not clinically relevant recommending stricter gamma criteria instead [48-50].

For the 3D time-integrated gamma analysis the results were expressed in terms of percentage of failing voxels and volume of failing voxels inside the GTV structure. For 2D time-integrated and time-resolved gamma analysis the results were expressed in terms of percentage of failing pixels inside the field mask, absolute area of failing pixels inside the field mask and absolute area of failing pixels inside the field mask per beam (2D time-integrated) and per segment (2D time-resolved).

In the case of 3D time-integrated portal dosimetry, DVH curves were generated for each planning CT and for each manipulated CT based on the calculated 3D dose distributions and the $D_{95\%}$ metric (dose to 95% of the volume) of the transformed GTV was extracted. The percentage of change of this metric inside each transformed GTV in comparison to the original GTV was determined according to the following formula:

$$\Delta D_{95\%} = \frac{D_{95\%}(\text{Transformed GTV}) - D_{95\%}(\text{Original GTV})}{D_{95\%}(\text{Original GTV})} \times 100\ (\%) \quad (3.1)$$

3.2.3 Correlation analysis between gamma results and differences in $D_{95\%}$ metric

To define decision support protocols for adaptive radiotherapy and prevent subjective decision-making, portal dosimetry metrics should be linked to relevant changes in DVH metrics. Therefore, correlations between DVH metric (difference in $D_{95\%}$ metric inside the transformed GTV) and 2D time-integrated, 2D time-resolved and 3D time-integrated portal dosimetry were investigated for all the five gamma criteria.

The correlation analysis (Pearson's R^2) was performed in MATLAB for each patient separately and for the six patients as a group in order to investigate if there was a correlation not only within a patient but also between the 6 patients.

3.2.4 Sensitivity and specificity of the gamma analysis

The DVH analysis is the gold standard method used by physicians to look at dose discrepancies in clinical practice. However, it is known that the gamma analysis can detect dose discrepancies that sometimes are not detected by the DVH analysis [5].

According to MAASTRO clinical practice, a difference between the planned and delivered dose is considered significant (gamma positive) when the [3%, 3mm] gamma fail rate exceeds the threshold of 10% in the in-field region of the 2D portal dose image for at least one beam. Regarding the DVH analysis, the delivered dose is considered to be deviating significantly from the planned dose (DVH positive) when one of the DVH metrics shows a difference higher than 4%.

The same MAASTRO current action levels were used as reference to investigate the sensitivity and specificity of the gamma analysis methods. The difference of the $D_{95\%}$ metric inside the transformed GTV calculated for each patient and each simulated geometrical change was used for DVH analysis. In the same way, the gamma fail rate inside the GTV calculated for each patient and each simulated geometrical change was used for gamma analysis.

The DVH analysis was considered as the gold standard method and each gamma analysis method was considered as the diagnostic test. For all the five gamma criteria and each type of geometrical change, three ROC (Receiver Operating Characteristic) curves (Kumar and Indrayan, 2011) were generated: one for 2D time-integrated, one for 2D time-resolved and one for 3D time-integrated gamma analysis [51].

ROC curve is the plot that displays the trade-off between the sensitivity and (1-specificity) across a series of cut-off points. The validity of a diagnostic test compared with the gold standard is determined by the sensitivity and specificity. In order to quantify the performance of each gamma analysis method, the total area under the curve (AUC) was calculated for each ROC curve. The optimal threshold for each gamma analysis method and gamma criteria was obtained as the point on the ROC curve closest to the (0, 1) point [51].

3.2.5 Phantom simulations and measurements

In order to replicate one of the geometrical changes simulated in the patients, a dynamic thorax phantom was used to mimic the simulation of tumor shifts inside the lung. A set of simulations and measurements of tumor shifts was performed with this phantom using the initial treatment plan.

3.2.5.1 Phantom characteristics

The CIRS Dynamic Thorax Phantom is a precision instrument for investigating the impact of tumor motion inside the lung (Figure 3.7) [52].

The phantom body represents an average human thorax in shape, proportion and composition. A lung equivalent rod containing an air gap to insert a target and or various detectors is inserted into the lung equivalent lobe of the phantom. The phantom body is connected to a motion actuator box that induces 3D target motion through linear translation and rotation of the lung equivalent rod. Motion of the rod itself is radiographically invisible due to its matching density with the surrounding material. The target and its motion, given its density difference, can be resolved. The center of the target is positioned off central axis of the rod.

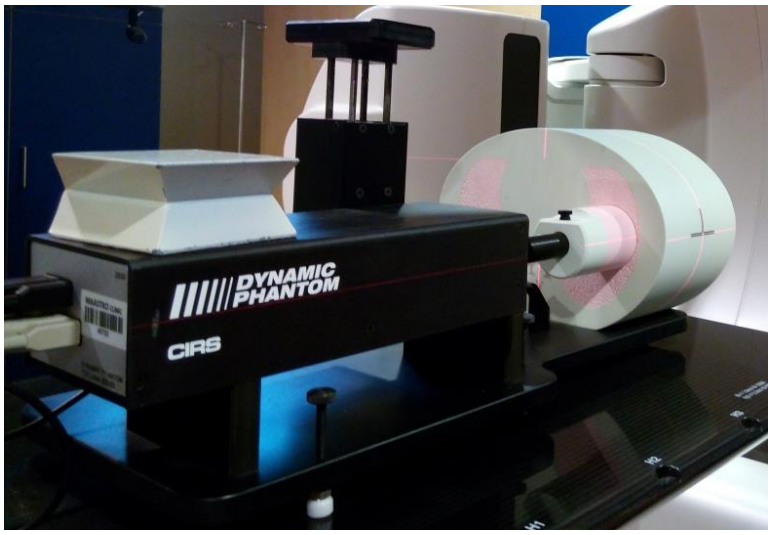

Figure 3.7 – CIRS Dynamic Thorax Phantom.

The phantom is composed by four different materials: plastic water (body), lung equivalent material (two lungs) and cortical and trabecular bone equivalent material (spine).

A new insert representative of the tumor with lung tissue around was created in order to allow the placement of a Gafchromic EBT3 film piece within the tumor for dose verification. The PMMA (polymethylmethacrylate) cylinder insert, representing the tumor (approximately 120 HU), is placed inside a larger sponge cylinder (approximately -820 HU), representing the surrounding lung tissue (Figure 3.8). The insert can be separated in two in order to place the film and can be introduced into the air gap of the lung equivalent rod (Figure 3.9). The PMMA cylinder has a 2.5 cm

diameter and a 2.0 cm height in total. The sponge is dry, viscous and made of 100% vegetable material.

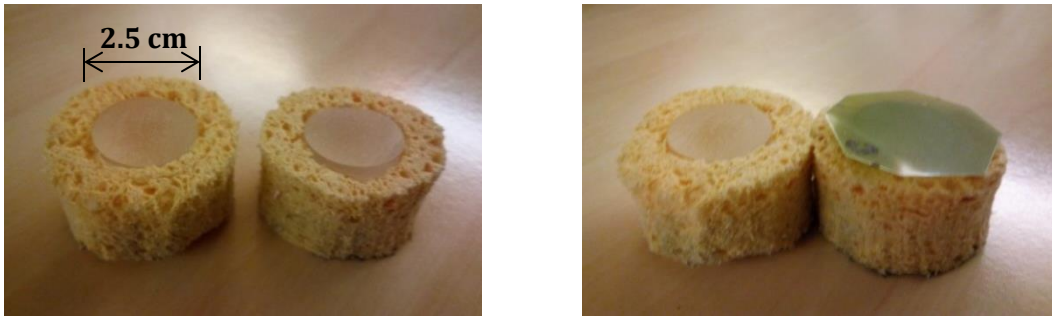

Figure 3.8 – Representation of the two parts of the insert composed by sponge and PMMA without the film piece (left) and with the film piece (right).

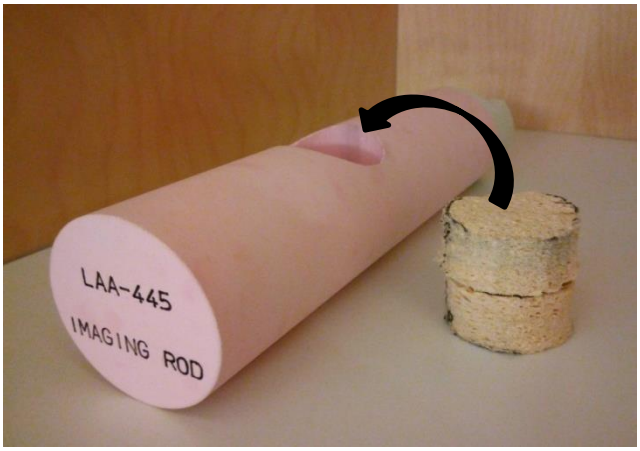

Figure 3.9 – Representation of the lung equivalent rod of the phantom with the air gap on the top to introduce the whole insert.

3.2.5.2 Phantom treatment plan

A CT scan of the phantom with the new insert containing a film piece inside was acquired and a treatment plan was designed with ARIA research software (Varian Medical Systems) based on this planning CT. The phantom was planned to be irradiated using VMAT with a 6 MV photon beam at a Varian TrueBeam linear accelerator (Varian Medical Systems). The dose was planned to be delivered in two half-arcs as usual in many treatment plans of lung cancer patients. The dose per fraction was 2 Gy and the treatment consisted of 35 fractions in total. Figure 3.10 shows an axial slice of the CT of the phantom and figure 3.11 shows the treatment plan of the phantom.

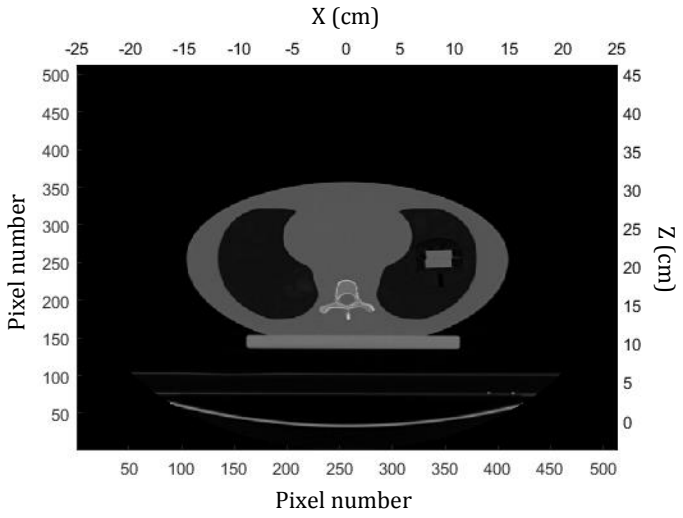

Figure 3.10 - Axial slice of the CT image of the phantom with the new tumor model insert inside the left lung.

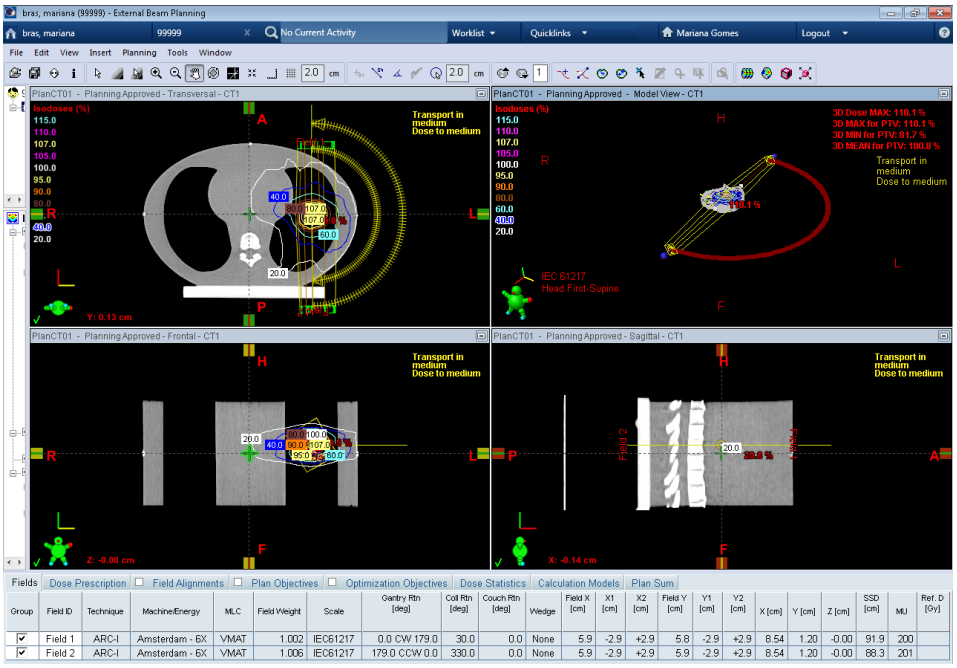

Figure 3.11 – Representation of the treatment plan of the phantom in ARIA research software (Varian Medical Systems).

3.2.5.3 Phantom simulations

In the same way as in the patient simulations, tumor shifts were simulated on the planning CT of the phantom. A range of shifts between 0.3 cm and 3.3 cm in steps of 0.3 cm was applied to the CTV structure along the negative direction of the Y axis. The reason to shift the CTV and not the GTV was to ensure that all tumor tissue including the edges was being shifted.

After applying the tumor shifts, 3D portal dose images were simulated: one for the initial planning CT and one for each transformed CT. All simulations were performed using the initial unadapted treatment plan.

A mask in the center of the tumor where the film piece is placed was created on the original CT image and on each transformed CT image. The mask consists of a circular area with a 0.5 cm radius in the XZ plane that covers 2 slices in Y axis. After interpolating each mask with the corresponding 3D dose distribution, the mean dose inside the mask was determined.

3.2.5.4 Phantom measurements

In the same way as in the phantom simulations, the phantom was irradiated with the initial treatment plan. The same range of shifts was applied to the tumor along the negative direction of the Y axis using the CIRS Motion Control Software that enables to shift the lung equivalent rod which contains the tumor. For each tumor shift applied a new film piece was placed within the tumor insert, a new irradiation was performed and portal images were collected using the on-board EPID during irradiation (Figure 3.12). Afterwards, the portal images were converted to portal dose images [23].

Figure 3.12 – Setup of the phantom measurements. The phantom is positioned at the isocenter of the linac and the on-board EPID is under the couch.

The portal dose images from each tumor shift were then compared with the portal dose images obtained from the original tumor position using a global 2D gamma analysis that employs the five

gamma criteria already mentioned in section 3.2.2. Time-integrated and time-resolved gamma analyses were performed for each tumor shift.

The film dose of each irradiation was determined using a red channel analysis and a calibration curve. Details regarding the film calibration and the measurement film analysis can be found in the appendix of this thesis.

3.2.5.5 Comparison between phantom simulations and measurements

A comparison between the phantom simulations and measurements was performed. For the simulation analysis, the mean dose inside the tumor mask where the film was placed was plotted as function of the tumor shifts. For the measurement analysis, the mean dose inside the central circular area of the measurement films was also plotted as function of the tumor shifts.

3.2.6 Supplementary study

In this study a cohort of 460 lung cancer patients described in a previous study (Persoon et al., 2015) was used for analysis [5]. These patients were treated with VMAT following daily CBCT and were visually inspected for geometrical changes on a daily basis. Forty-six patients were subject to changes and had a re-CT with re-delineated contours and an adaptive treatment plan. The reasons for adaptation were: change in atelectasis (n = 18), tumor regression (n = 9), change in pleural effusion (n = 8) or other causes (n=11).

Two portal dose images (one for the initial planning CT and other for the re-CT) were simulated for each patient [35]. In both simulations the patient was irradiated with the initial unadapted treatment plan. The portal dose images were compared using a global 2D gamma analysis and employing seven gamma criteria [1%, 1 mm], [2%, 2 mm], [3%, 2 mm], [3%, 3 mm], [4%, 4 mm], [5%, 3 mm] and [10%, 10 mm]. Both 2D time-integrated and 2D time-resolved gamma analyses were performed. The results were expressed in terms of fail rates, absolute fail area and absolute fail area per beam (2D time-integrated) and per segment (2D time-resolved).

The main purpose of this study was to investigate the quantitative relationship between the gamma analysis results and the tumor volume as well as between the gamma analysis results and the survival of the patients. For the tumor volume analysis, 8 patients from the 46 patients cohort were excluded due to absence of GTV (n = 2), undefined contour sequence of the GTV (n = 2) or existence of more than one GTV (n = 4). In the case of survival analysis, 21 patients from the 46 patients cohort were excluded due to the fact that they were still alive on the day of patient data collection. The tumor volume was calculated for each patient based on the planning-CT and the DICOM RTSTRUCT by determining the sum of the voxels volume inside the GTV structure whereas the survival of each patient was calculated as the difference between the death date and the first treatment date of the patient.

A correlation analysis (Pearson's R^2) was performed in MATLAB between the tumor volume and the gamma analysis results as well as between the days of survival and the gamma analysis results.

4 Results

4.1 Patient simulations – a single patient

Multiple DVH and gamma analyses were performed for each patient and each category of geometrical change (tumor shift, tumor regression and pleural effusion). Therefore, only the results relative to one patient and each geometrical change are shown in this section.

For the 2D time-integrated and 2D time-resolved gamma analyses the gamma failure was calculated as fail rate (percentage of failing pixels), absolute fail area (cm^2) and absolute fail area per beam (2D time-integrated) or absolute fail area per segment (2D time-resolved). In the case of 3D time-integrated gamma analysis, the gamma failure was calculated as fail rate (percentage of failing voxels) and fail volume (volume of failing voxels). In this section only the results expressed as gamma fail rates are shown since this is the most common way of present the gamma failure in the literature.

4.1.1 Tumor shift

Based on the simulated 3D dose distributions, a DVH curve of the GTV was generated for each tumor shift applied. Figure 4.1 shows the DVH curves resultant from these simulations. The different line colors represent the different tumor shifts. It can be seen that the DVH curves are shifted to the left as a result of the tumor shift increase. The reason behind this is that when a shift is applied to the GTV, the GTV gets away from the highest dose region. By consequence, the volume receiving the planned dose decreases.

The $D_{95\%}$ metric inside the GTV was extracted from the previous DVH curves for each tumor shift. Figure 4.2 represents the percentage change of this metric as function of the tumor shift. There are negative values due to the fact that the differences of this metric were not calculated as absolute values. It can also be seen that for a tumor shift larger than 1.2 cm the difference in this metric starts decreasing.

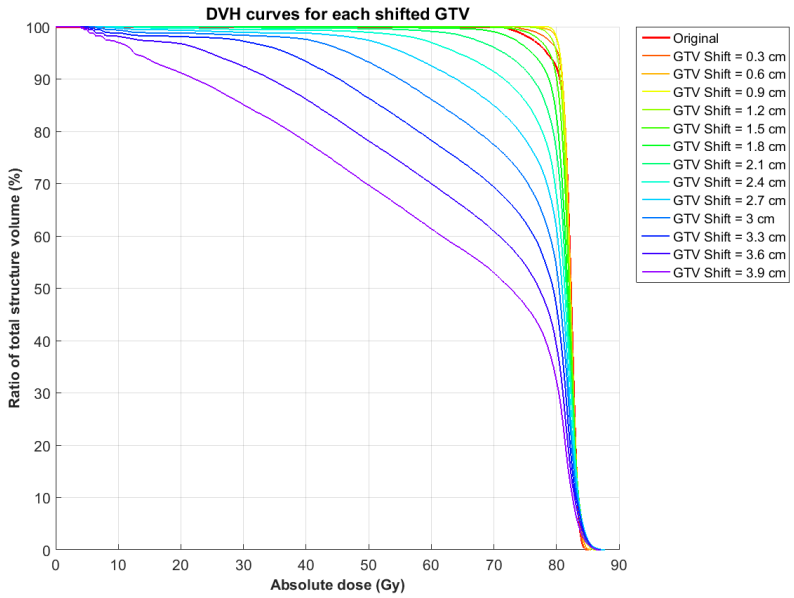

Figure 4.1 – DVH curves for the original GTV and each shifted GTV. The red line represents the DVH of the original GTV and the other colors represent the DVH of each shifted GTV.

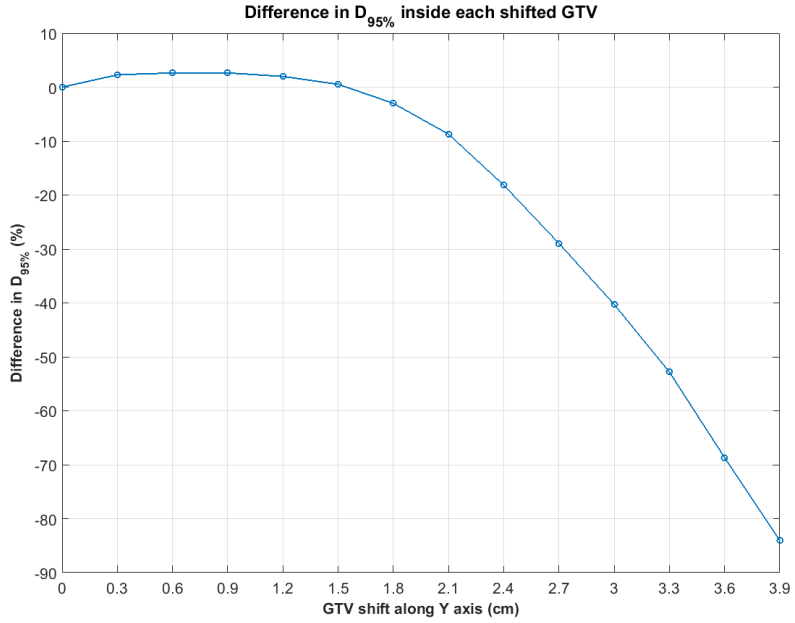

Figure 4.2 – Difference in $D_{95\%}$ metric of the GTV DVH as function of the GTV shift along the Y axis.

2D time-integrated, 2D time-resolved and 3D time-integrated gamma analyses were performed for each tumor shift and gamma criterion. Figures 4.3, 4.4 and 4.5 show the gamma fail rates resultant from the tumor shift simulations obtained with these three gamma analysis methods and the five

gamma criteria. By comparing the three figures it can be seen that 2D time-integrated and 2D time-resolved portal dosimetry are more able to detect smaller tumor shifts than 3D time-integrated portal dosimetry. For a [3%, 3 mm] gamma criterion the 3D time-integrated portal dosimetry only starts detecting dose discrepancies for a tumor shift equal or larger than 1.2 cm whereas 2D time-integrated and 2D time-resolved portal dosimetry are capable of detecting a 0.6 cm tumor shift.

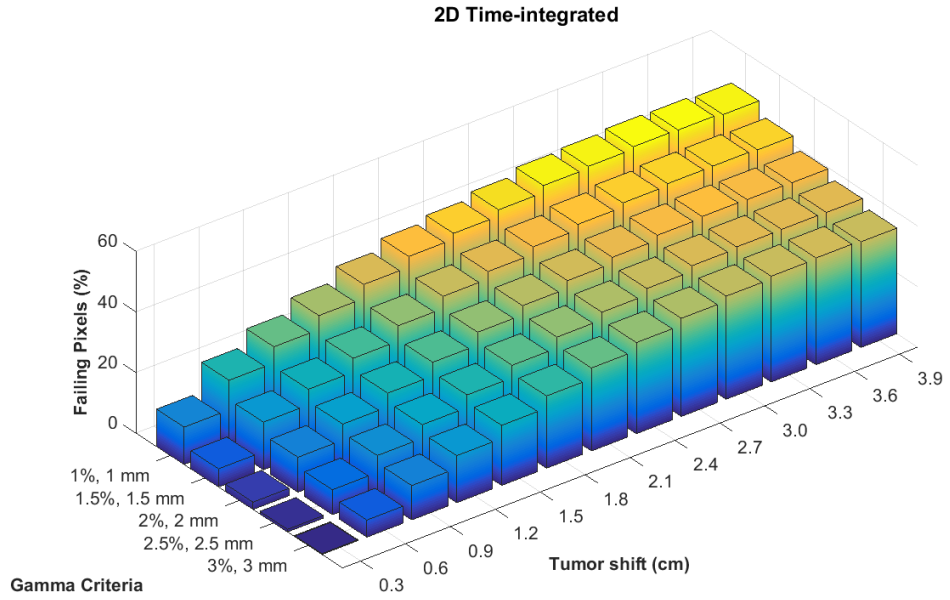

Figure 4.3 – Gamma fail rates (percentage of failing pixels) for the tumor shift simulations obtained with 2D time-integrated portal dosimetry.

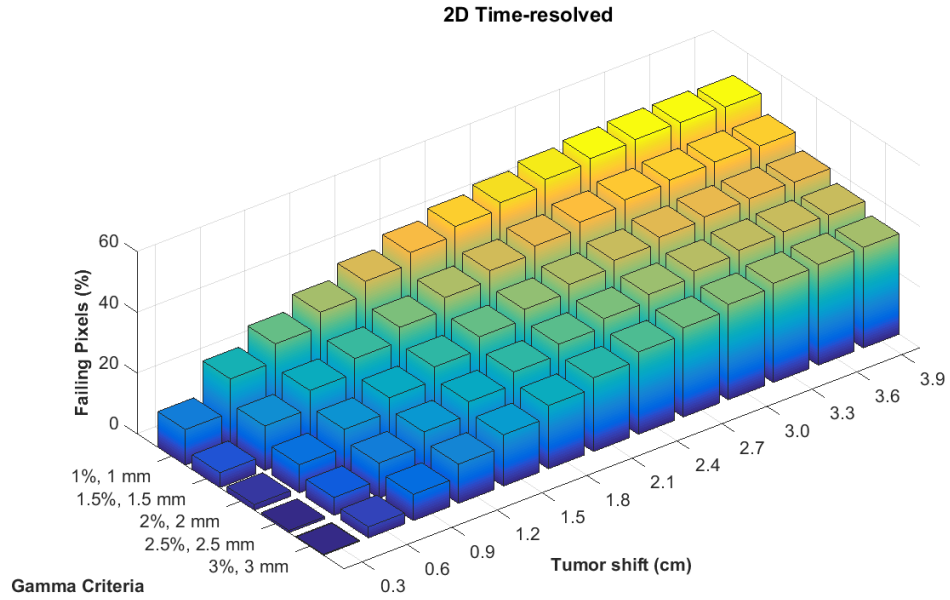

Figure 4.4 - Gamma fail rates (percentage of failing pixels) for the tumor shift simulations obtained with 2D time-resolved portal dosimetry.

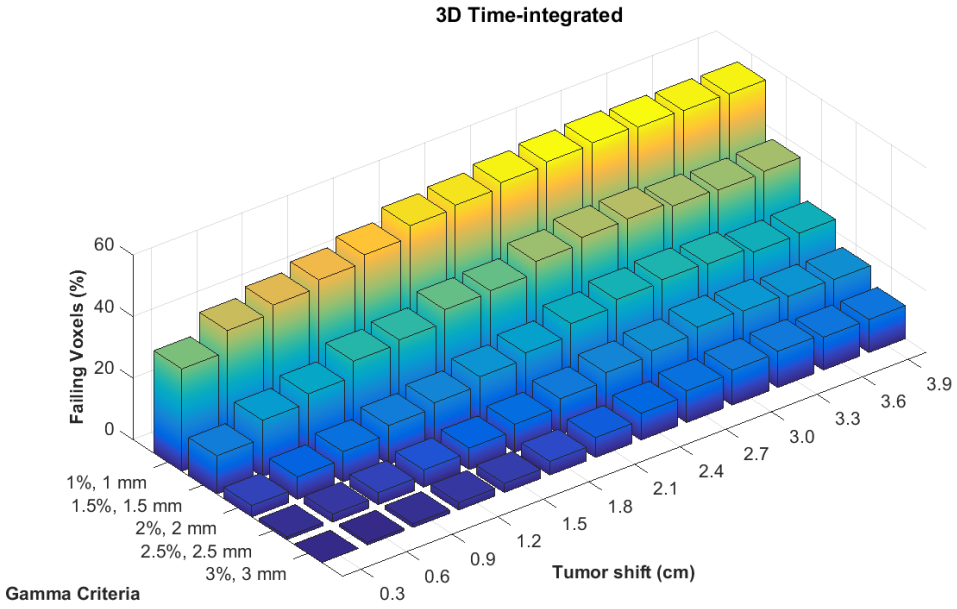

Figure 4.5 - Gamma fail rates (percentage of failing voxels) for the tumor shift simulations obtained with 3D time-integrated portal dosimetry.

4.1.2 Tumor regression

For the tumor regression simulations DVH curves were generated based on the calculated 3D dose distributions. Figure 4.6 shows the DVH curves of the GTV as function of the tumor regression where the different line colors represent the different tumor regressions. The GTV DVH curves are shifted to the right as a result of the tumor regression increase. In fact when the GTV shrinks uniformly, the shrunken GTV gets more dose than the original one because now a smaller volume is receiving dose in the highest dose region (center of the radiation field).

The $D_{95\%}$ metric inside the shrunken GTV was extracted from each DVH curve. In figure 4.7 the difference in this metric is shown as function of the tumor regression. Despite the percentage change is small (the maximum is between 5% and 6%), it increases as the tumor regression increases.

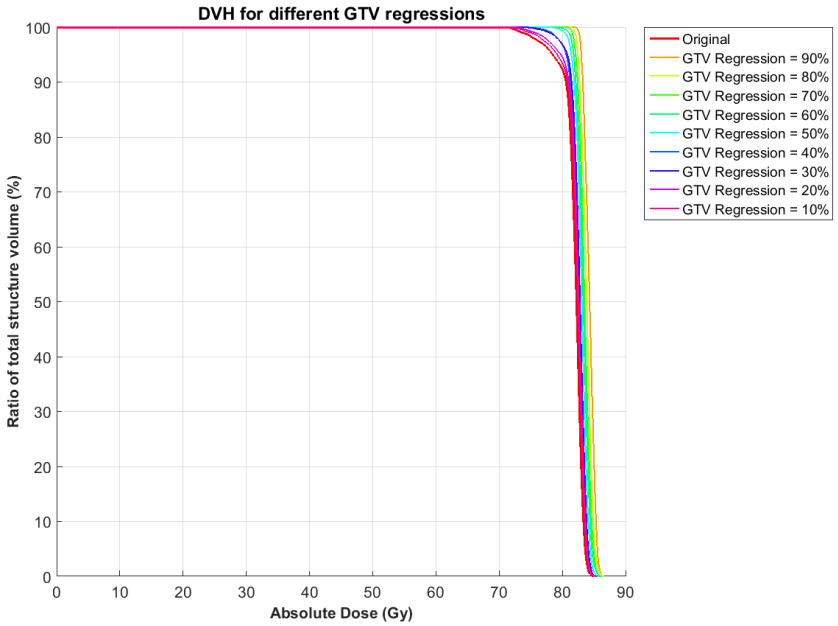

Figure 4.6 – DVH curves for the original GTV and each transformed GTV. The different color lines represent different tumor regressions. The DVH for the original GTV is represented in red.

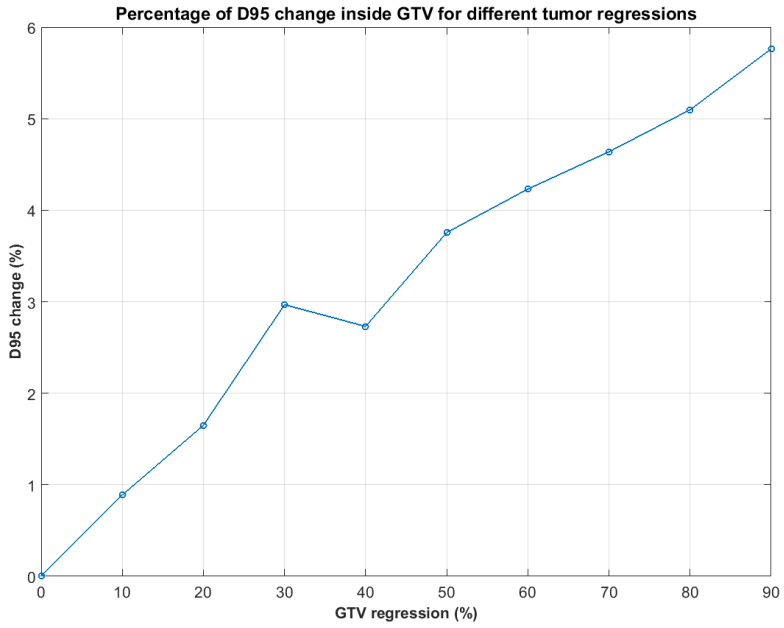

Figure 4.7 - Difference in $D_{95\%}$ metric of the GTV DVH as function of the GTV regression.

As a result of the 2D time-integrated, 2D time-resolved and 3D time-integrated gamma analyses, the gamma fail rates were plotted as function of each new tumor volume resultant from the tumor regression and the gamma criterion as represented in figures 4.8, 4.9 and 4.10. The first new tumor

volume (68.7 cm^3) corresponds to a tumor regression of 10% of the original tumor volume whereas the last one (6.0 cm^3) corresponds to a tumor regression of 90%. The results reveal that 2D time-integrated and 2D time-resolved portal dosimetry are able to detect smaller tumor regressions than 3D time-integrated portal dosimetry. It can be seen that when employing a [3%, 3 mm] gamma criterion 3D time-integrated portal dosimetry can only detect a tumor regression larger than 50% (new tumor volume = 37.5 cm^3) while 2D time-integrated and 2D time resolved portal dosimetry can detect a 30% tumor regression which corresponds to a new tumor volume of 51.5 cm^3.

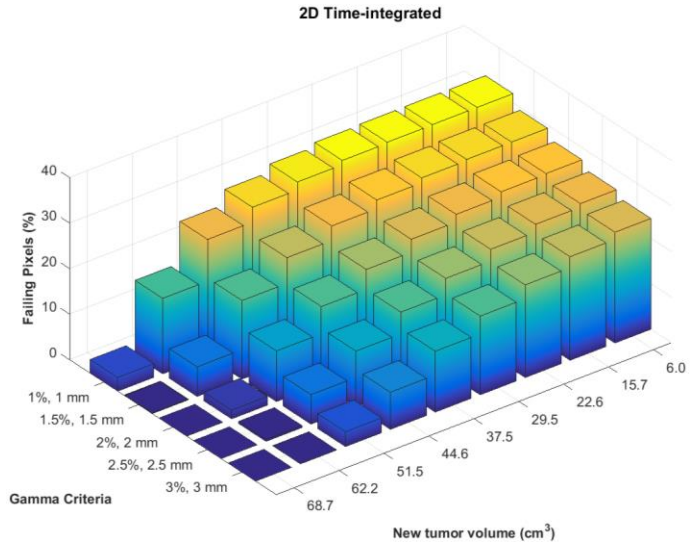

Figure 4.8 – Gamma fail rates (percentage of failing pixels) obtained with 2D time-integrated portal dosimetry as function of the new tumor volume and the gamma criteria.

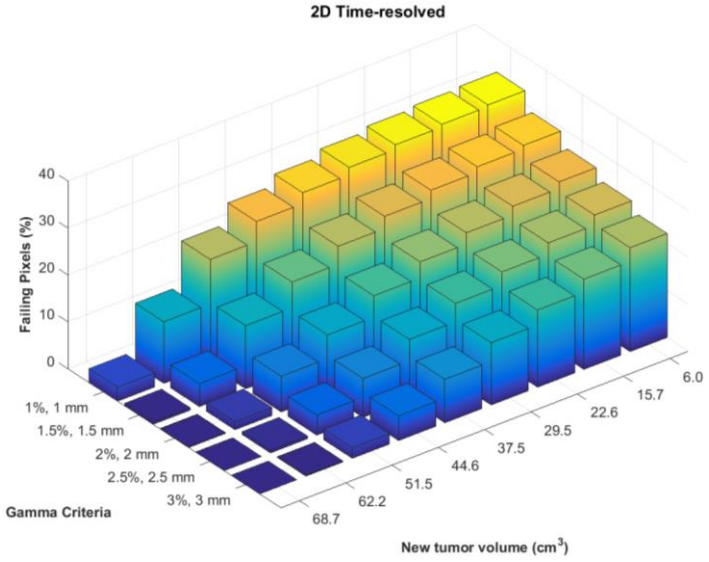

Figure 4.9 - Gamma fail rates (percentage of failing pixels) obtained with 2D time-resolved portal dosimetry as function of the new tumor volume and the gamma criteria.

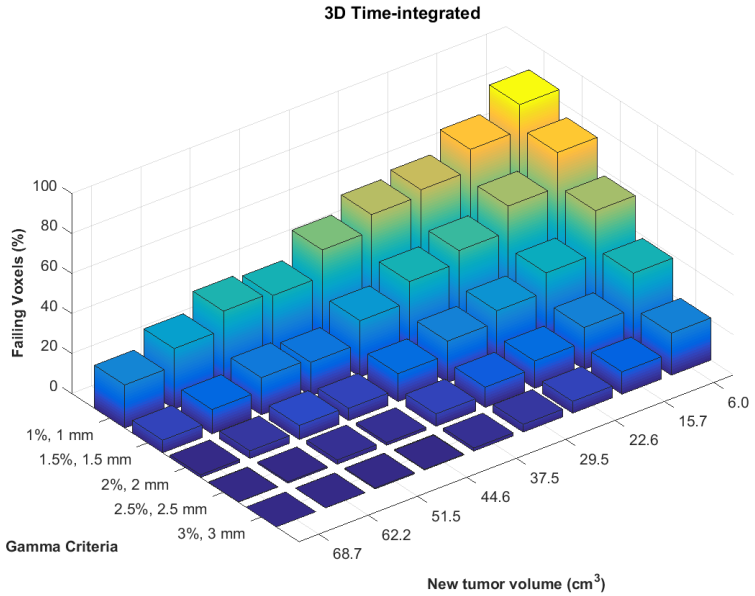

Figure 4.10 - Gamma fail rates (percentage of failing voxels) obtained with 3D time-integrated portal dosimetry as function of the new tumor volume and the gamma criteria.

4.1.3 Pleural effusion

DVH curves of the GTV were generated based on the 3D dose distributions for each level of pleural effusion in the lung which contains the tumor. Figure 4.11 shows the DVH curves according to each simulated level of pleural effusion where the different line colors represent the different levels of pleural effusion. As a result of pleural effusion, the DVH curves are shifted to the left due to the presence of fluid inside the lung that attenuates the radiation dose and the volume receiving the planned dose decreases.

In figure 4.12 a relationship can be seen between the difference of $D_{95\%}$ metric extracted from the DVH curves and the different levels of pleural effusion. There are negative values due to the fact that the differences of this metric were not calculated as absolute values. The results reveal that pleural effusion causes a small change of the $D_{95\%}$ metric (the maximum change is between -1.8 % and -2%). According to MAASTRO clinic current levels, a DVH is considered to be deviating significantly when a difference of the $D_{95\%}$ metric is higher than 4%. In this way we can say that the pleural effusion simulations did not cause a significant change in the DVH of the GTV when obtained with 3D time-integrated portal dosimetry.

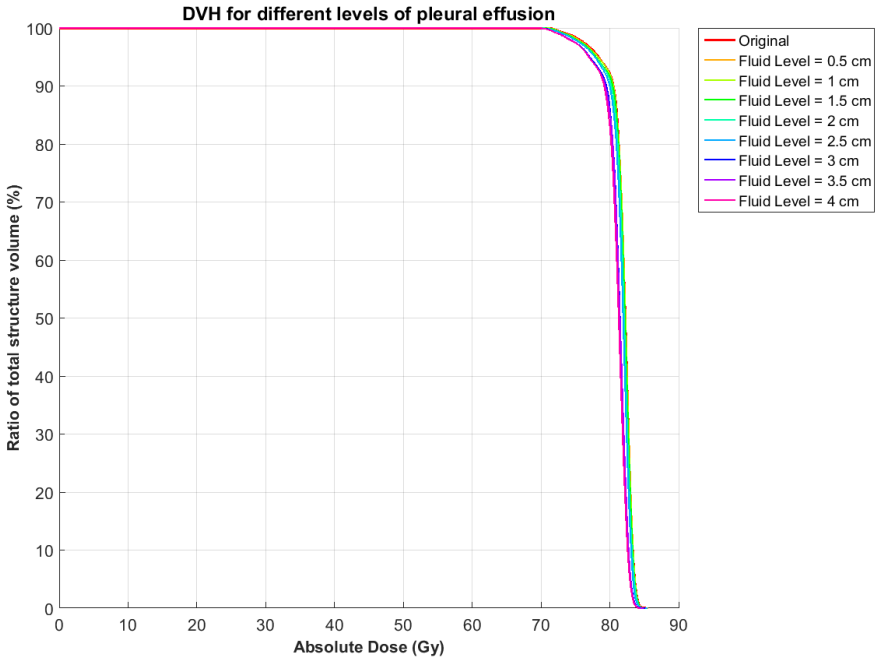

Figure 4.11 – DVH curves for the GTV after the simulation of different levels of pleural effusion in the lung which contains the tumor. The red line represents the original GTV without the presence of fluid volume in the lung.

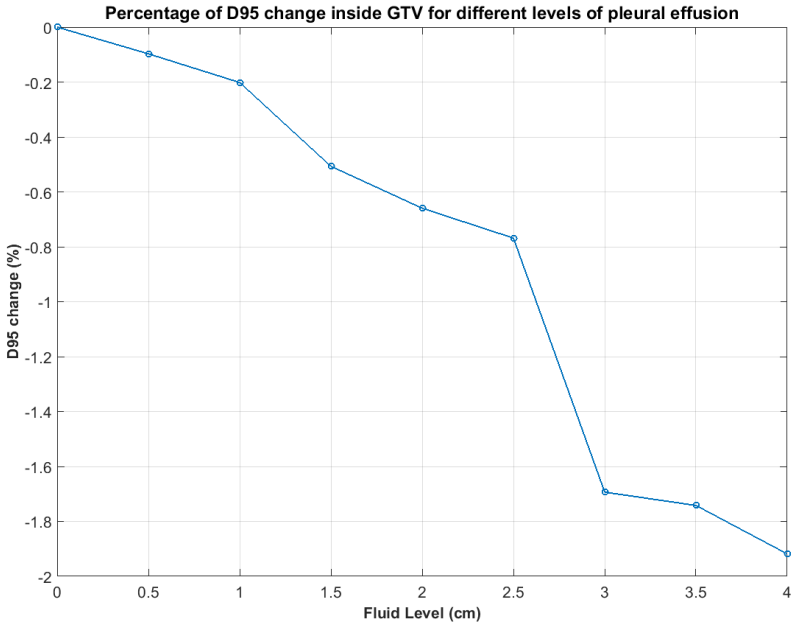

Figure 4.12 - Difference in $D_{95\%}$ metric of the GTV DVH as function of the level of pleural effusion in the lung which contains the tumor.

The gamma fail rates resultant from 2D time-integrated, 2D time-resolved and 3D time-integrated gamma analyses are shown in figures 4.13, 4.14 and 4.15, respectively, as function of the fluid volume in the lung and the gamma criterion. The 3D time-integrated gamma analysis results produced lower gamma failures than 2D time-integrated and time-resolved especially for [2.5%, 2.5 mm] and [3%, 3 mm] gamma criteria. When comparing the three figures, it can also be seen that time-resolved gamma analysis is able to detect a smaller fluid volume (201.2 cm^3) than 2D and 3D time-integrated gamma analyses when using the largest gamma criteria ([2%, 2 mm], [2.5%, 2.5 mm] and [3%, 3 mm]).

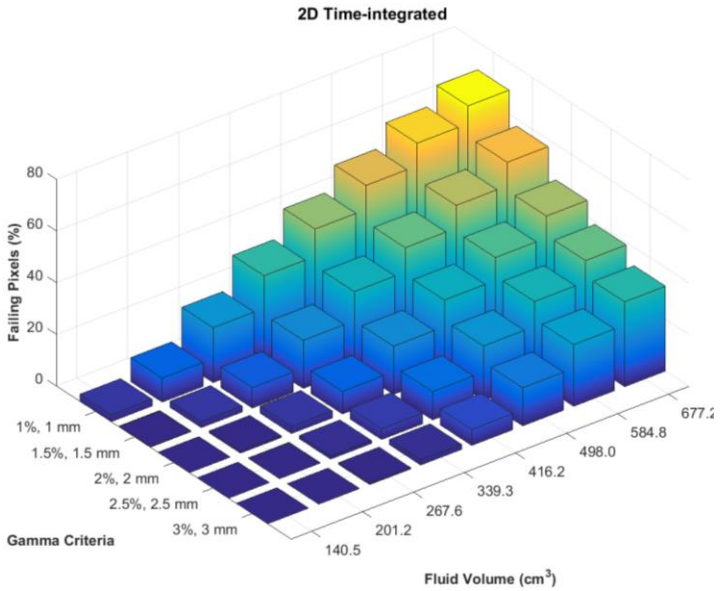

Figure 4.13 - Gamma fail rates (percentage of failing pixels) obtained with 2D time-integrated portal dosimetry as function of the fluid volume in the lung which contains the tumor and the gamma criteria.

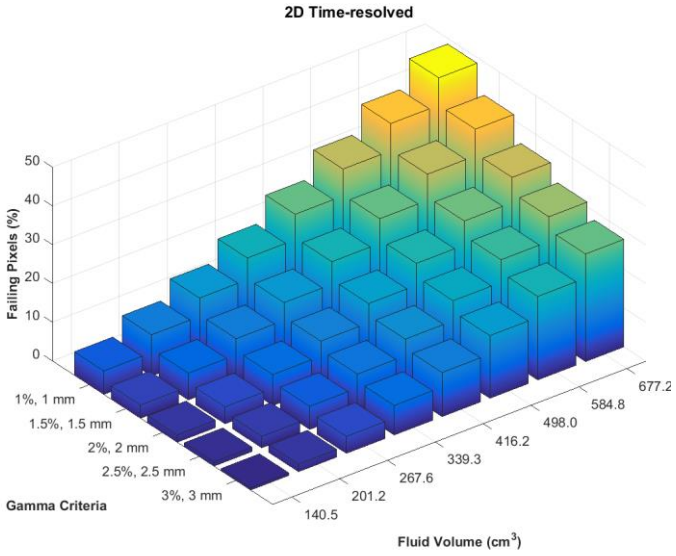

Figure 4.14 - Gamma fail rates (percentage of failing pixels) obtained with 2D time-resolved portal dosimetry as function of the fluid volume in the lung which contains the tumor and the gamma criteria.

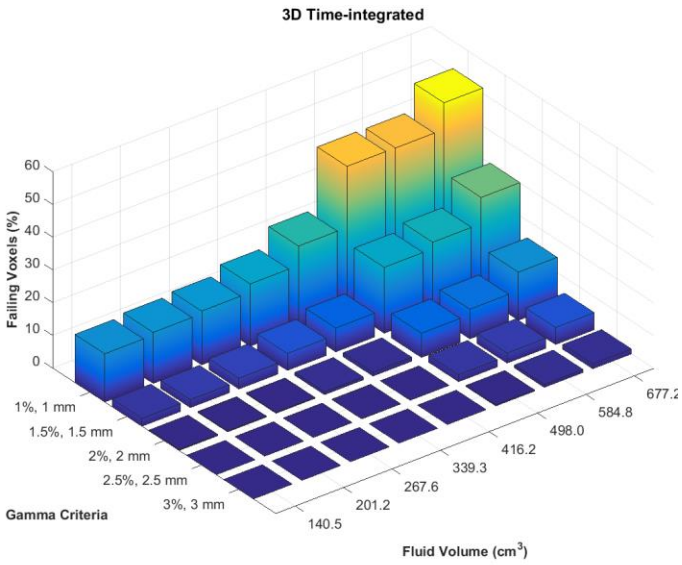

Figure 4.15 - Gamma fail rates (percentage of failing voxels) obtained with 3D time-integrated portal dosimetry as function of the fluid volume in the lung which contains the tumor and the gamma criteria.

For all categories of geometrical changes it was shown that the [3%, 3 mm] gamma criterion was too lax to detect some of the dose discrepancies specially when performing 3D time-integrated portal dosimetry. By contrast the [1%, 1 mm] gamma criterion was too sensitive always detecting much more gamma failure than the other gamma criteria. Since it is very restricted it also detects noise and therefore more gamma failure.

Pleural effusion was the geometrical change that produced more differences between 2D time-integrated and 2D time-resolved gamma analyses. Table 4.1 shows both gamma analyses for each level of pleural effusion using the [3%, 3 mm] gamma criterion. The time-resolved gamma analyses are represented by their 104^{th} (time) frames since these were one of the frames that show more differences when comparing with the time-integrated gamma analyses.

Since the fluid volume has a higher electron density than the lung tissue, the radiation beam is more attenuated by the fluid volume (at the patient level) and the EPID gets lower dose as consequence. This under-dosage is represented in blue. It can be seen that the time-integrated gamma analysis only shows an under-dosage (blue region) for a fluid level equal or higher than 2.0 cm which corresponds to a fluid volume of 339.3 cm^3. By contrast the time-resolved gamma analysis already shows an under-dosage for a fluid level of 0.5 cm (Table 4.1).

Since time-resolved gamma analysis allows a dose comparison for each VMAT (time) segment along the arc trajectory, it is able to detect more dose discrepancies than 2D time-integrated gamma analysis which just compares the cumulative dose distribution.

Table 4.1 – 2D Time-integrated and 2D time-resolved gamma analyses (3%, 3 mm) for the simulated levels of pleural effusion in the lung which contains the tumor.

Fluid level	2D Time-integrated	2D Time-resolved
0.5 cm ($140.5\ cm^3$)	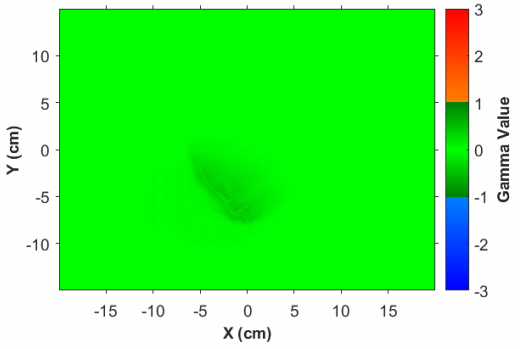	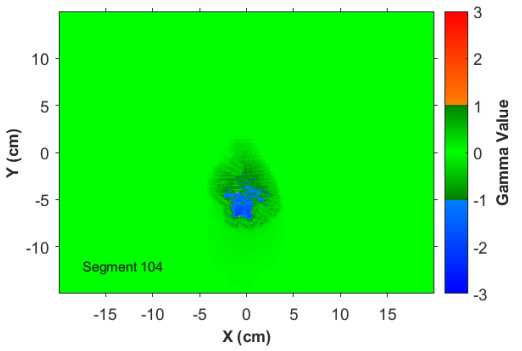
1.0 cm ($201.2\ cm^3$)	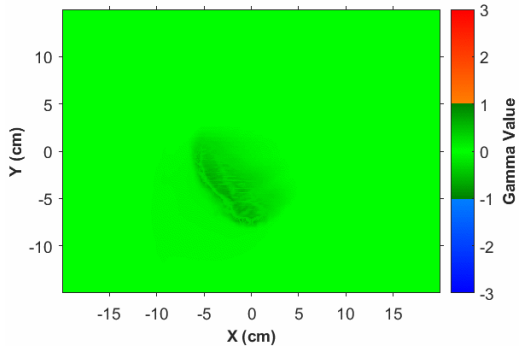	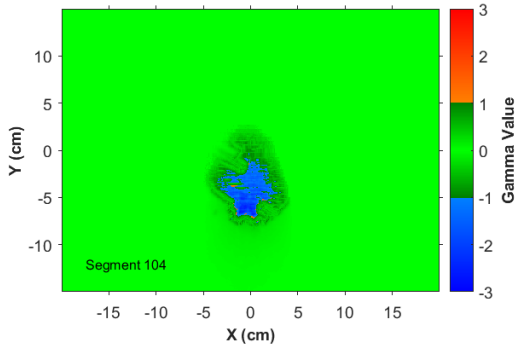
1.5 cm ($267.6\ cm^3$)	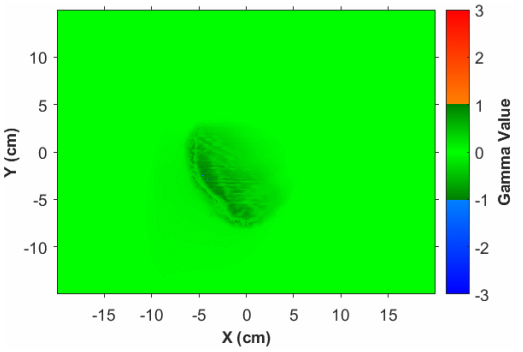	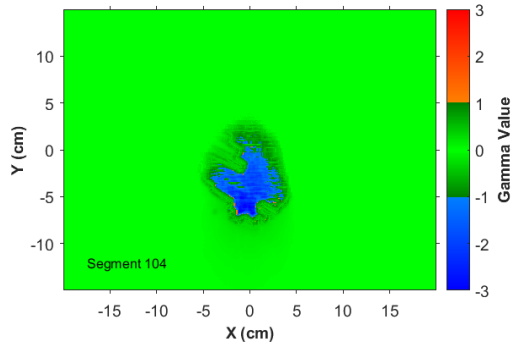
2.0 cm ($339.3\ cm^3$)	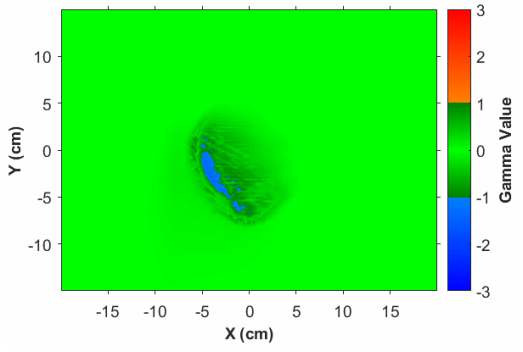	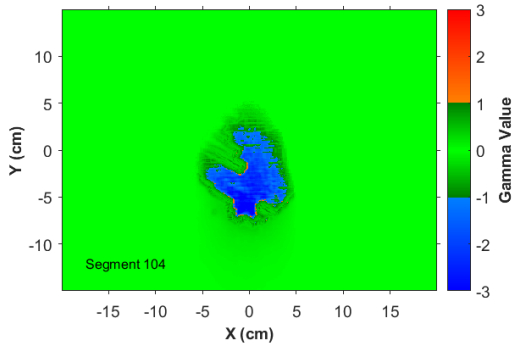

2.5 cm (416.2 cm³)	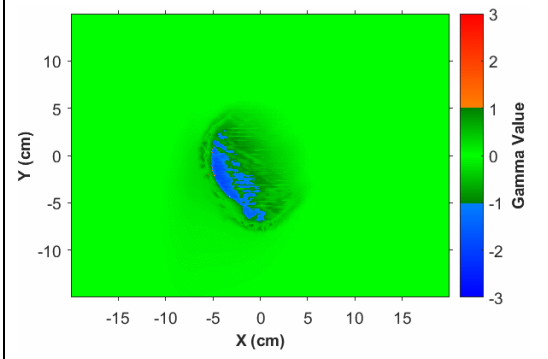	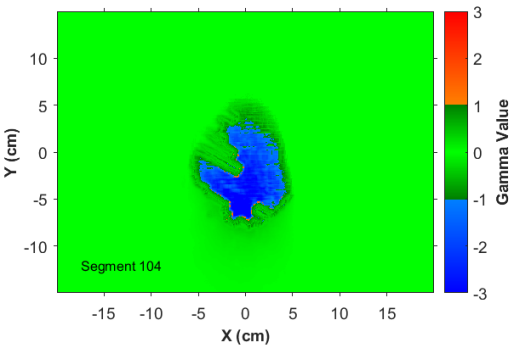
3.0 cm (496.0 cm³)	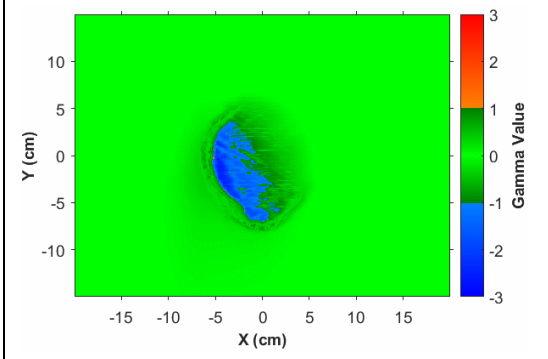	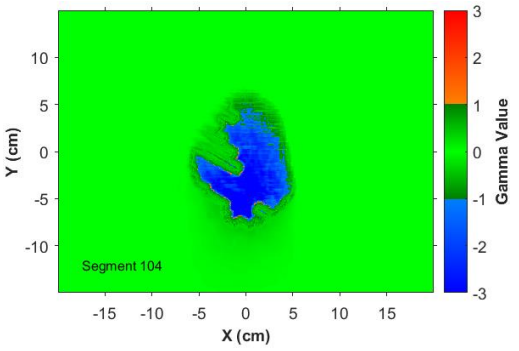
3.5 cm (584.8 cm³)	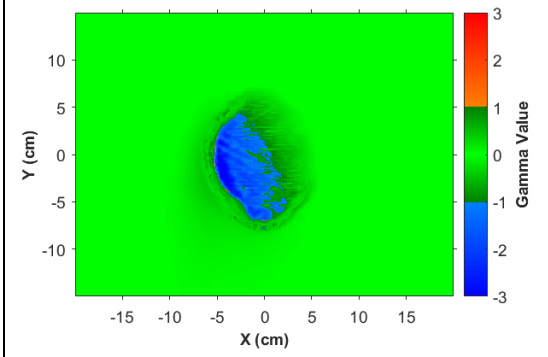	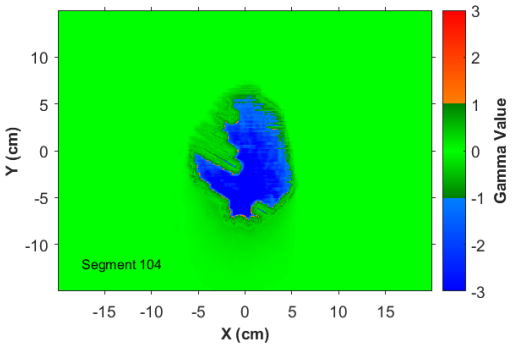
4.0 cm (677.2 cm³)	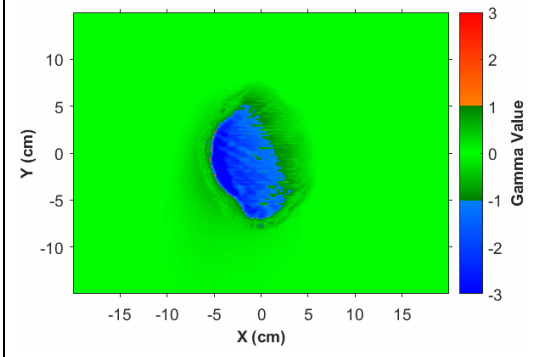	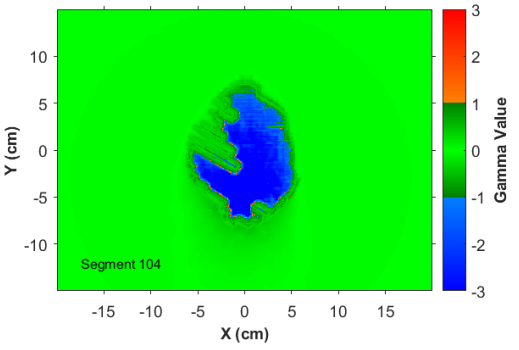

4.2 Correlation analysis

To define decision support protocols for adaptive radiotherapy and prevent subjective decision-making, gamma analysis metrics should be correlated to relevant changes in DVH metrics. Several research groups have been trying to find a correlation between gamma analysis and DVH metrics. Some published studies have found a correlation, but the majority could not find it [5, 53-56]. A correlation analysis between the difference in $D_{95\%}$ metric and the gamma failure inside the GTV was performed in this study for the three categories of geometrical changes taking into account a single patient (the same patient as in section 4.1) and also the six patients as a group. The results expressed as fail rates for the [2%, 2 mm] gamma criterion are shown as example.

4.2.1 Correlation analysis in a single patient

In this section the correlation analysis results relative to the same patient whose results were shown in section 4.1 are presented. Figures 4.16, 4.17 and 4.18 show the correlation between the difference in $D_{95\%}$ metric and the gamma fail rates resultant from the tumor shift, tumor regression and pleural effusion simulations, respectively. The gamma fail rates inside the GTV were obtained with 2D time-integrated (graph on the left), 2D time-resolved (graph in the middle) and 3D time-integrated (graph on the right) gamma analyses. Each point of the graphs represents the result corresponding to one simulated geometrical change (eg. one tumor shift) and the straight line is the linear fit to the data.

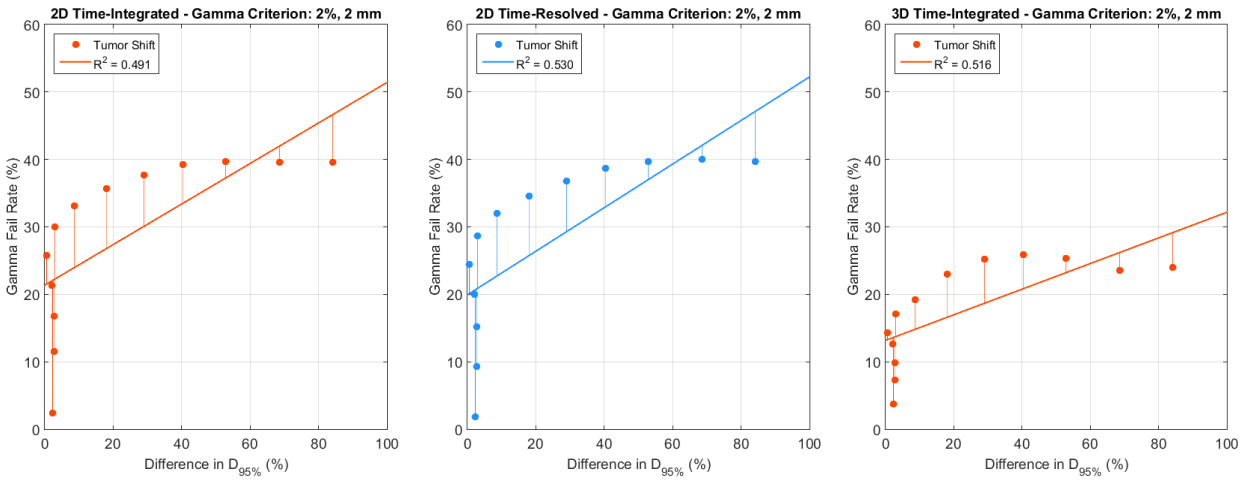

Figure 4.16 - Correlation between the difference in $D_{95\%}$ and the gamma fail rate obtained with 2D time-integrated (left), 2D time-resolved (middle) and 3D time-integrated (right) gamma analyses resultant from the tumor shifts simulations in one patient case.

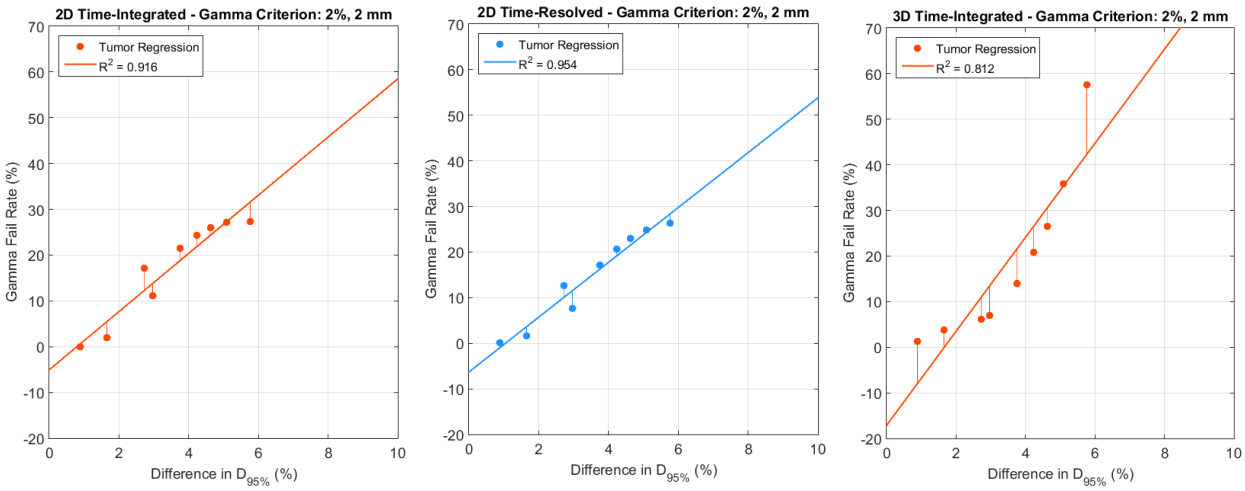

Figure 4.17 - Correlation between the difference in $D_{95\%}$ and the gamma fail rate obtained with 2D time-integrated (left), 2D time-resolved (middle) and 3D time-integrated (right) gamma analyses resultant from tumor regression simulations for one patient case.

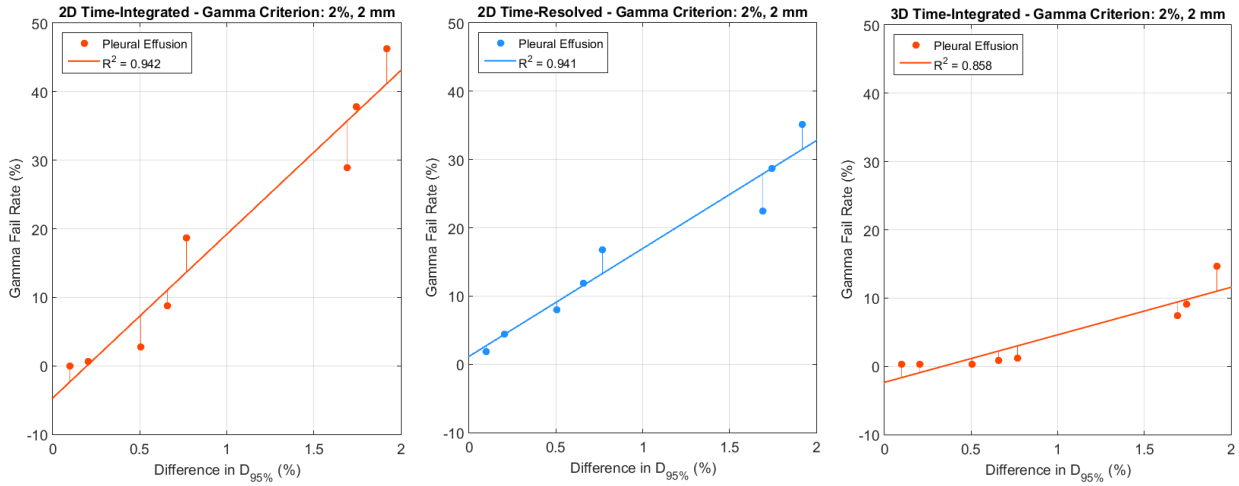

Figure 4.18 - Correlation between the difference in $D_{95\%}$ and the gamma fail rate obtained with 2D time-integrated (left), 2D time-resolved (middle) and 3D time-integrated (right) gamma analyses resultant from pleural effusion simulations for one patient case.

There is a linear relationship between the difference in $D_{95\%}$ metric and the gamma fail rates in a single patient especially for tumor regression and pleural effusion. For tumor shift, the data could be fitted to another function but the purpose was to use the same fit for all geometrical changes. The correlation coefficients do not vary considerably between the different gamma analysis methods. Even so, for tumor regression and pleural effusion 2D time-integrated and 2D time-resolved gamma analyses showed a better correlation with the DVH metric than 3D time-integrated gamma analysis. The same was verified for the other gamma criteria apart from the [2%, 2 mm].

4.2.2 Correlation analysis in six patients

A correlation analysis was also performed for the three types of geometrical changes taking into account the results from the six patients as a group. Figures 4.19, 4.20 and 4.21 show the correlation between the difference in $D_{95\%}$ metric and the gamma fail rates resultant from the tumor shift, tumor regression and pleural effusion simulations in the patients, respectively. The gamma fail rates inside the GTV were obtained with 2D time-integrated (graph on the left), 2D time-resolved (graph in the center) and 3D time-integrated (graph on the right) gamma analyses. Each point of the graphs represents the result correspondent to one simulated geometrical change in one patient and the straight line represents the linear fit to the data.

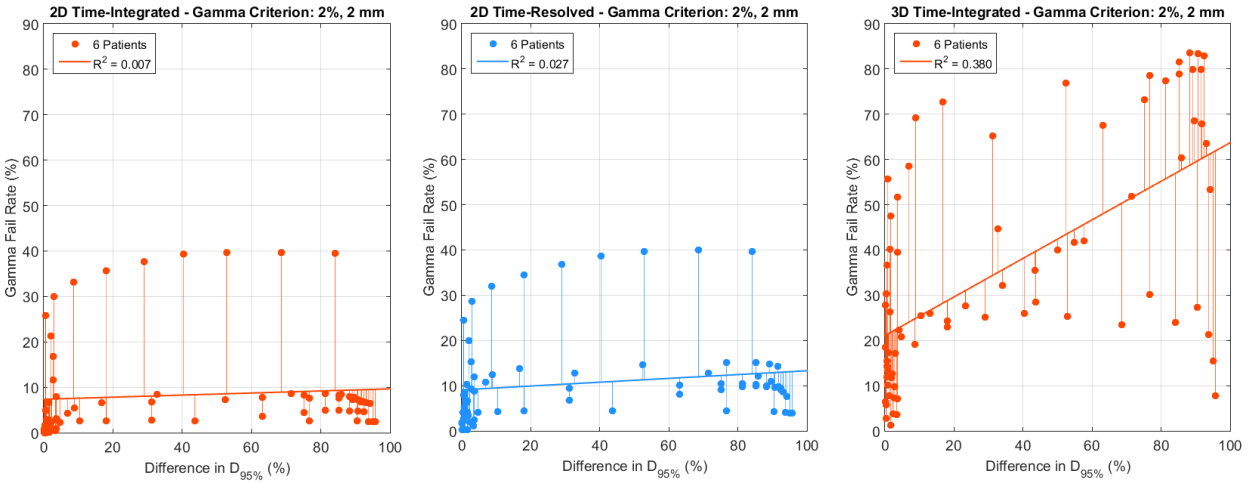

Figure 4.19 - Correlation between the difference in $D_{95\%}$ and the gamma fail rate obtained with 2D time-integrated (left), 2D time-resolved (middle) and 3D time-integrated (right) gamma analyses resultant from the tumor shifts simulations in six patients.

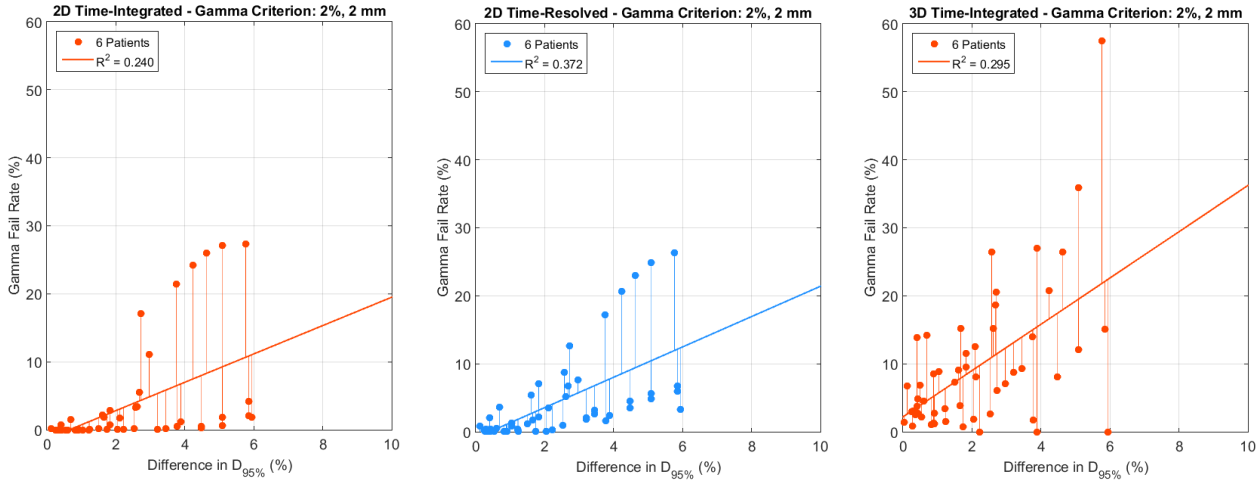

Figure 4.20 - Correlation between the difference in $D_{95\%}$ and the gamma fail rate obtained with 2D time-integrated (left), 2D time-resolved (middle) and 3D time-integrated (right) gamma analyses resultant from the tumor shrinkage simulations in six patients.

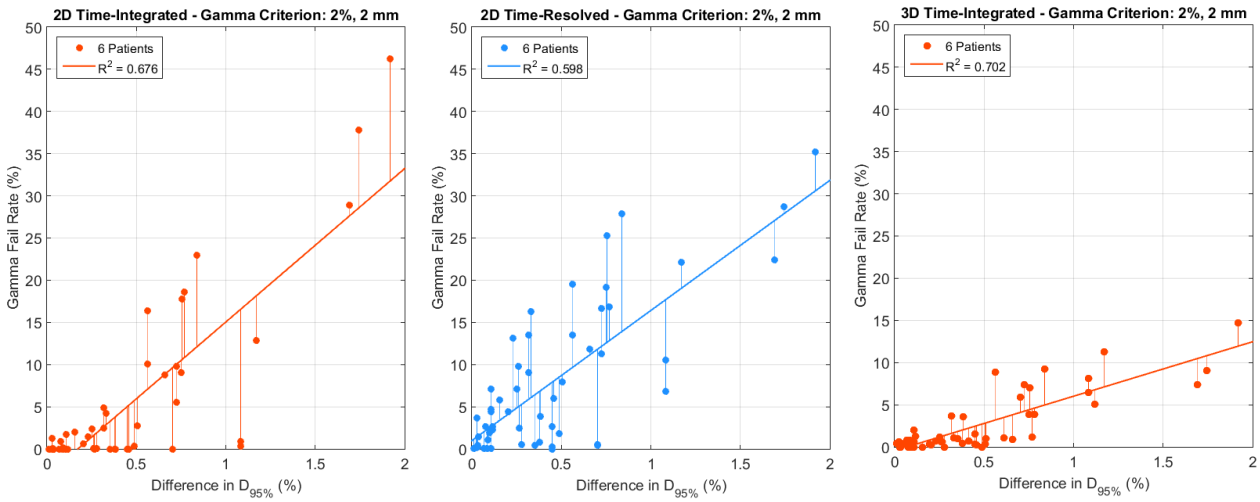

Figure 4.21 - Correlation between the difference in $D_{95\%}$ and the gamma fail rate obtained with 2D time-integrated (left), 2D time-resolved (middle) and 3D time-integrated (right) gamma analyses resultant from the pleural effusion simulations in six patients.

Unlike the correlation analysis in a single patient, there is no correlation when involving the six patients as a group. Only pleural effusion revealed correlation coefficients larger than 0.5.

4.3 Sensitivity and specificity of the gamma analysis

The sensitivity and specificity of the different gamma analysis methods were determined for the tumor shift and tumor regression simulations based on ROC curves taking into account the results from all six patients. It was not possible to generate ROC curves for the pleural effusion simulations due to the absence of positive DVHs (DVHs where the difference in $D_{95\%}$ metric was lower than 4%). The performance of the gamma analysis methods was quantified based on the AUC values.

4.3.1 Tumor shift

Figure 4.22 shows the ROC curves obtained for the tumor shift simulations for 2D time-integrated and 2D time-resolved gamma analyses whereas Figure 4.23 shows the ROC curves for 3D time-integrated gamma analysis. The reference line indicates that the tested methods have 50% of probability in detecting the forced error (tumor shift). The curves were generated for all the five gamma criteria and the circle represented in each ROC curve indicates the optimal threshold point for that gamma analysis method (Table 4.2).

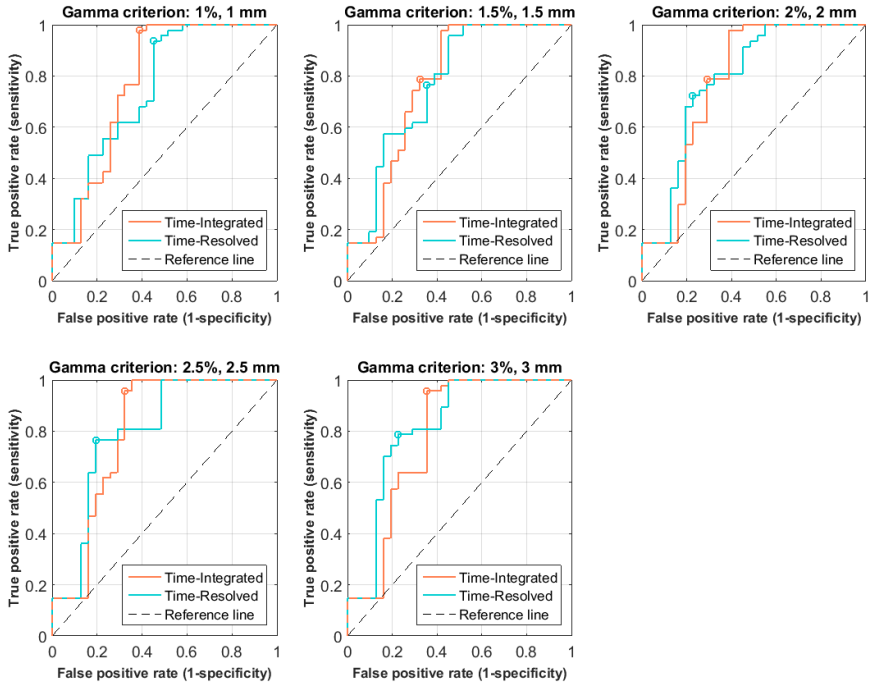

Figure 4.22 – ROC curves resultant from the tumor shift simulations for 2D time-integrated and 2D time-resolved gamma analyses and for all the five gamma criteria used.

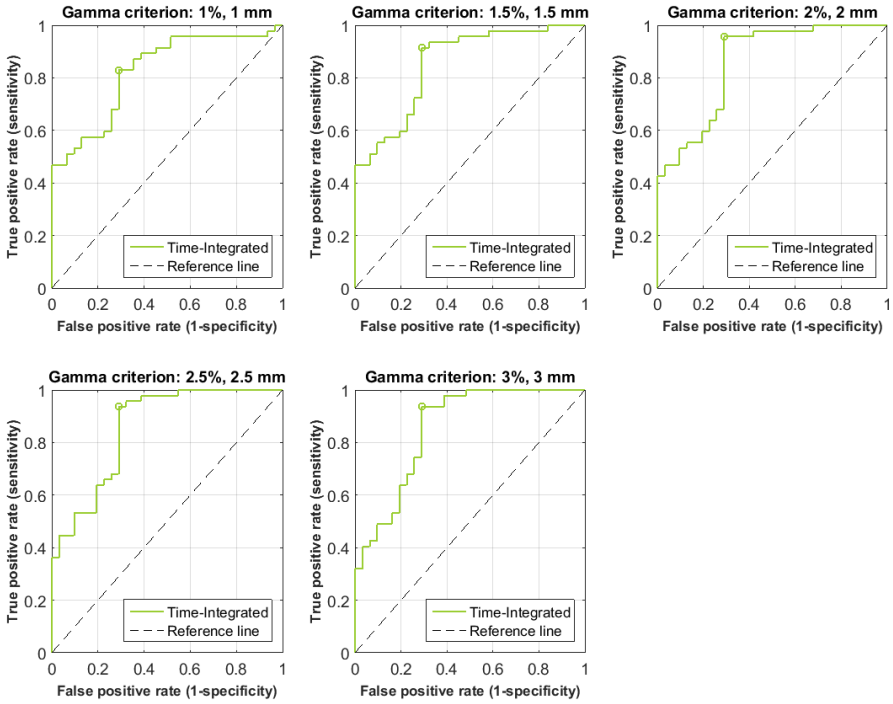

Figure 4.23 - ROC curves resultant from the tumor shift simulations for 3D time-integrated gamma analysis and for all the five gamma criteria used.

In table 4.2 the optimal thresholds are shown for each gamma analysis method and gamma criterion. This table suggests that, for instance, for 2D time-integrated gamma analysis when employing a [3%, 3 mm] gamma criterion, a gamma threshold of 0.647% should be used as decision criterion to consider that the measured dose is deviating significantly from the planned dose distribution. This table also shows that laxer gamma criteria require lower optimal thresholds in order to be capable of flagging small dose discrepancies.

Table 4.2- Optimal thresholds (%) obtained for 2D time-integrated, 2D time-resolved (% of failure inside the field mask) and 3D time-integrated (% of failure inside the GTV) gamma analyses corresponding to each gamma criterion for the tumor shift simulations.

	Gamma criteria				
Gamma analysis	1%, 1 mm	1.5%, 1.5 mm	2%, 2 mm	2.5%, 2.5 mm	3%, 3 mm
2D Time-integrated	10.5	7.07	3.58	1.50	0.647
2D Time-resolved	13.5	11.3	9.10	5.99	3.73
3D Time-integrated	52.1	32.0	19.2	11.8	8.68

The AUC values were determined for each ROC curve. In Figure 4.24 the AUC values are shown for the ROC curves obtained for the tumor shift simulations for 2D time-integrated, 2D time-resolved and 3D time-integrated gamma analyses. Although the differences are small, the time-resolved gamma analysis shows a better performance than 2D time-integrated for almost all gamma criteria used. Even so, 3D time-integrated is superior to 2D time-resolved gamma analysis in detecting tumor shifts.

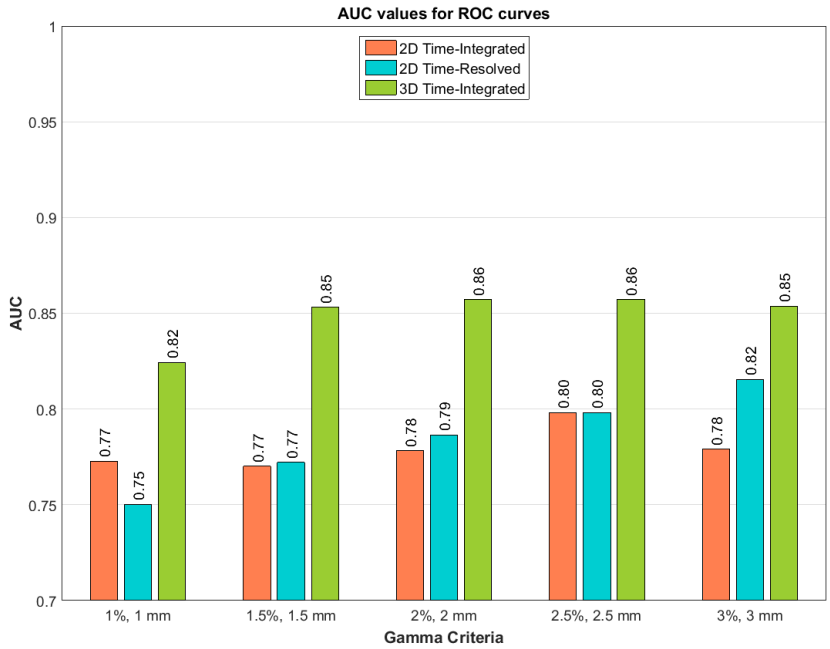

Figure 4.24 – AUC values for the ROC curves generated from the tumor shift simulations for 2D time-integrated, 2D time-resolved and 3D time-integrated gamma analyses.

4.3.2 Tumor regression

As was the case of tumor shift simulations, ROC curves were obtained for the tumor regression simulations for 2D time-integrated and 2D time-resolved gamma analysis methods as shown in Figure 4.25 and for 3D time-integrated as shown in Figure 4.26. The curves were generated for all the five gamma criteria and the circle represented in each ROC curve indicates the optimal threshold point for that gamma analysis method (Table 4.3).

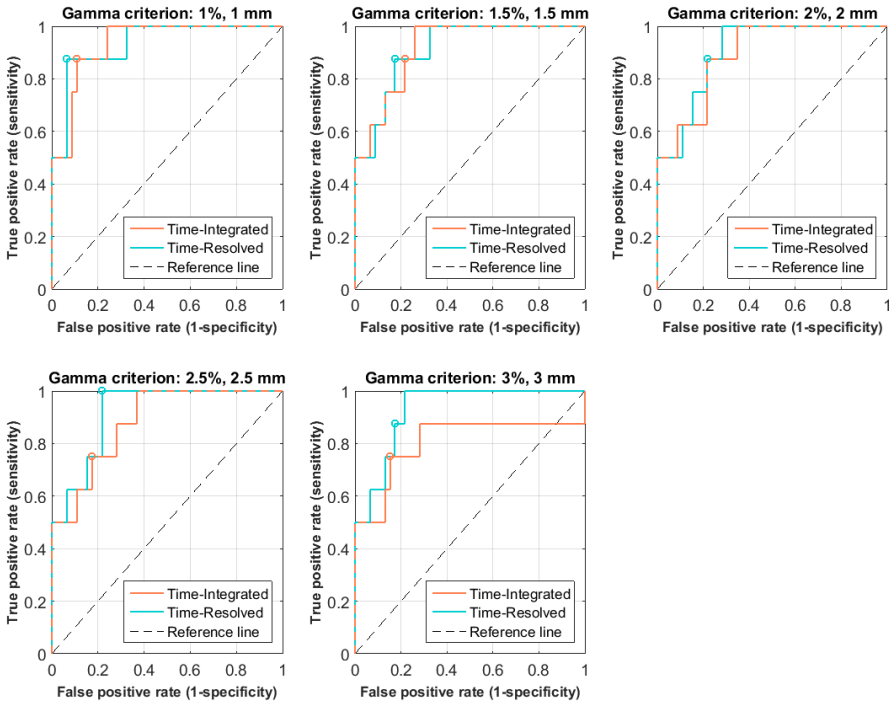

Figure 4.25 - ROC curves resultant from the tumor regression simulations for 2D time-integrated and 2D time-resolved gamma analyses and for all the five gamma criteria used.

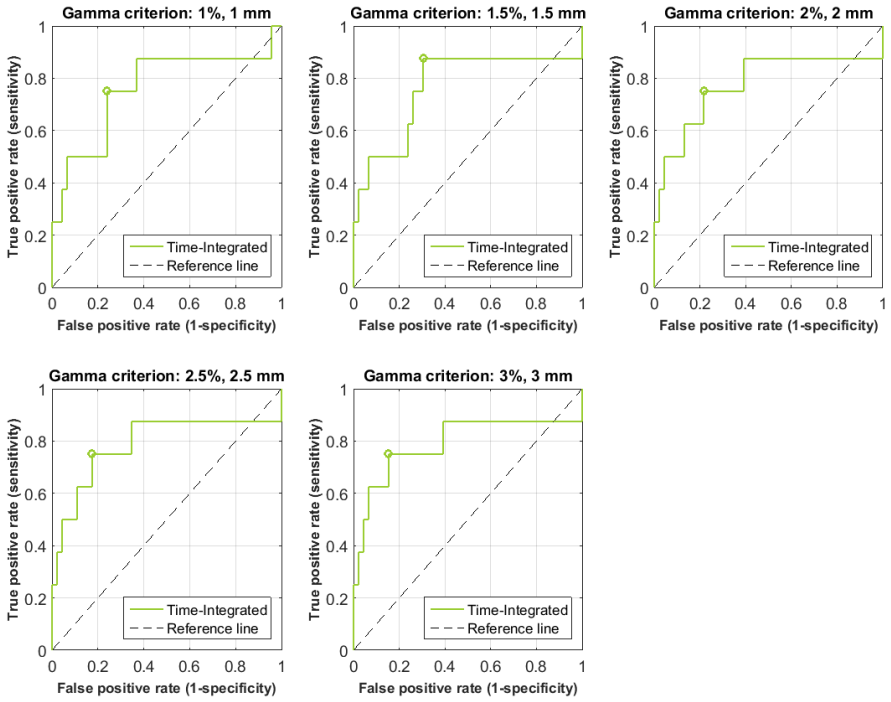

Figure 4.26 - ROC curves resultant from the tumor regression simulations for 3D time-integrated gamma analysis and for all the five gamma criteria used.

Table 4.3 - Optimal thresholds (%) obtained for 2D time-integrated, 2D time-resolved (% of failure inside the field mask) and 3D time-integrated (% of failure inside the GTV) gamma analyses correspondent to each gamma criterion for the tumor regression simulations.

	Gamma criteria				
Gamma analysis	1%, 1 mm	1.5%, 1.5 mm	2%, 2 mm	2.5%, 2.5 mm	3%, 3 mm
2D Time-integrated	11.6	3.73	1.85	1.13	0.539
2D Time-resolved	17.8	8.45	4.53	2.08	1.58
3D Time-integrated	46.0	20.6	12.1	5.23	1.63

As was the case of tumor shift simulations, the determined optimal thresholds were larger for 2D time-resolved than for 2D time-integrated gamma analysis. Even so, the 3D time-integrated gamma analysis shows the largest thresholds. Since the [3%, 3 mm] is the most lax gamma criterion it requires lower gamma thresholds in order to flag the dose discrepancies as previously demonstrated by Table 4.2.

The AUC values for the ROC curves obtained for the tumor regression simulations for the three gamma analysis methods are shown in Figure 4.27. The time-resolved gamma analysis is the method with the best performance for detecting tumor regression specially when using a [3%, 3 mm] gamma criterion (AUC = 0.93). Comparing to the tumor shift simulations, 2D time-integrated

and 2D time-resolved gamma analyses showed a better performance for detecting tumor regressions than tumor shifts. By contrast, 3D time-integrated gamma analysis yielded a better performance for detecting tumor shifts than tumor regressions (AUC = 0.85 and AUC = 0.81, respectively).

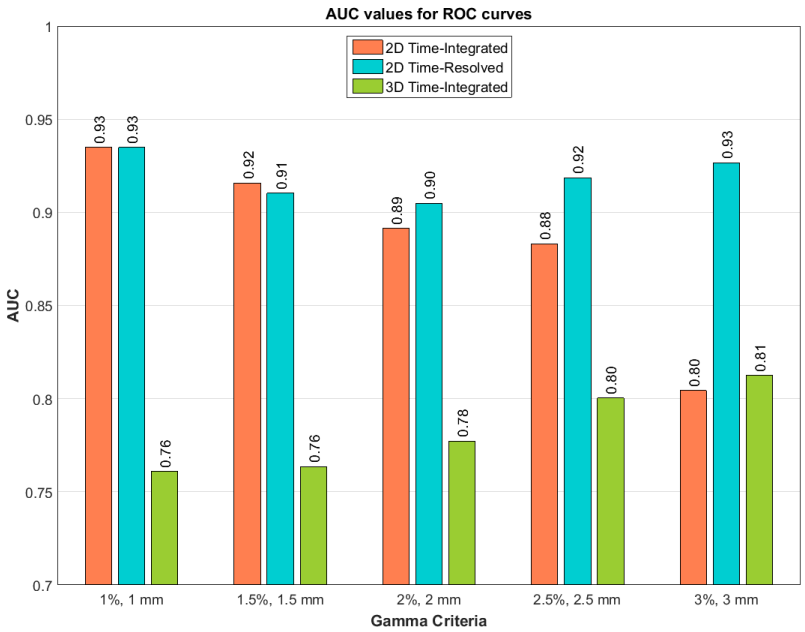

Figure 4.27 - AUC values for the ROC curves generated from the tumor regression simulations for 2D time-integrated, 2D time-resolved and 3D time-integrated gamma analyses.

4.4 Phantom simulations and measurements

For the phantom simulations a 3D dose distribution was calculated for the original simulated tumor position and for each tumor shift using the same unadapted treatment plan. Figure 4.28 shows the overlap of each CT image and corresponding 3D dose distribution for the original tumor position (shift = 0) and for each tumor shift along the negative direction of Y axis. This sequence of images shows the tumor leaving the highest dose region according to the tumor shift increase.

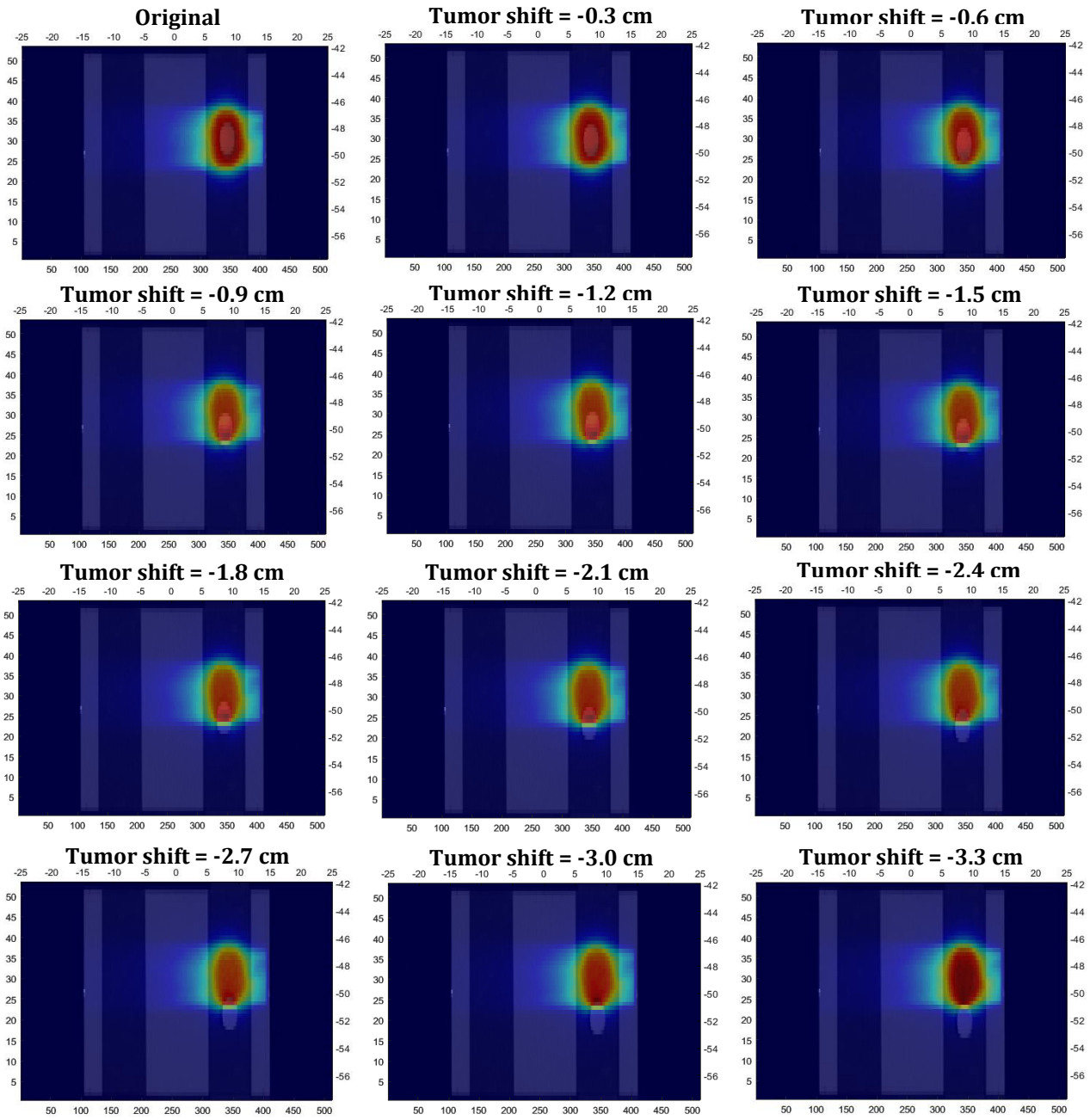

Figure 4.28 - CT image and respective 3D dose distribution correspondent to the original tumor position (top left) and each tumor shift along the negative direction of Y axis.

The mean dose values inside the film region of interest were determined as function of the tumor shift applied along the negative direction of Y axis for both the phantom simulations and measurements, as can be seen in Figure 4.29.

In both cases the mean dose starts decreasing sharply after a tumor shift of 1.5 cm. Although the curves show the same behavior, there are differences in the absolute dose values. These differences are due in part to errors during the measurements setup like sponge positioning errors. Even so, the results show that the measurements follow the same logic as the simulations, the mean dose starts decreasing after the same drop point (which corresponds to a tumor shift of 1.5 cm) and relates to the tumor shifts in the same way.

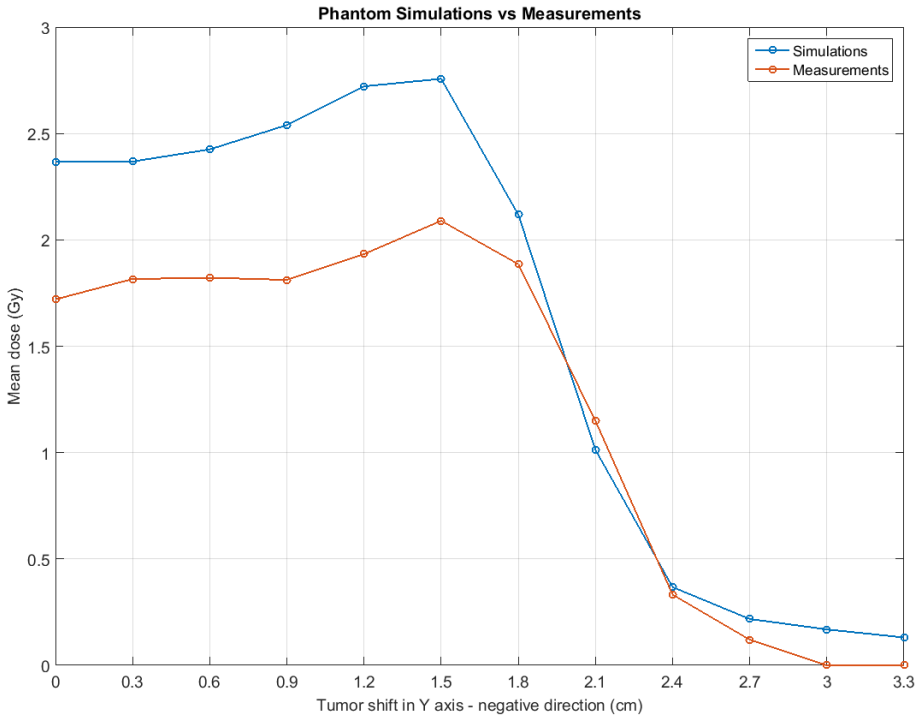

Figure 4.29 – Mean dose inside the region of interest of the film for each tumor shift along the negative direction of Y axis. The blue and red curves represent the phantom simulations and measurements, respectively.

4.4.1 Time-integrated and time-resolved gamma analyses

Table 4.4 summarizes the results of the 2D time-integrated and 2D time-resolved gamma analyses obtained from the EPID images collected during the phantom irradiations. The gamma analyses were performed for the five gamma criteria already mentioned in section 3.2.2 but only the results for the [3%, 3 mm] gamma criterion are shown in this table. Each row of the table represents the time-integrated and time-resolved gamma analyses for each tumor shift applied along the Y axis. The time-resolved gamma analyses are represented by their 110th time frame. The tumor is shifted towards the blue region. When the tumor is shifted, it occupies a region that was occupied by lung

tissue before. Since the HU values of the tumor tissue are higher than the HU values of the lung tissue, the dose in the new region where the shifted tumor is positioned is more attenuated at the level of the phantom resulting in lower dose (blue region) at the level of the EPID. The red region represents the region where the tumor used to be before shifting. This region is now occupied by lung tissue of the phantom which has lower HU values resulting in lower attenuation of the dose at the level of the phantom and therefore a higher dose (red region) at the level of the EPID.

The time-resolved gamma analysis is able to detect a tumor shift of -0.3 cm. However, the time-integrated gamma analysis almost does not reveal any dose discrepancy when this tumor shift is applied. The time-integrated gamma analysis is only able to detect tumor shifts larger or equal to -0.6 cm. For tumor shifts larger than -2.7 cm the blue region disappears due to the fact that the tumor is completely out of the radiation field.

Table 4.4 – 2D Time-integrated and 2D time-resolved gamma analyses (3%, 3 mm) for each tumor shift inside the left lung of the phantom.

Tumor shift	2D Time-integrated	2D Time-resolved
-0.3 cm	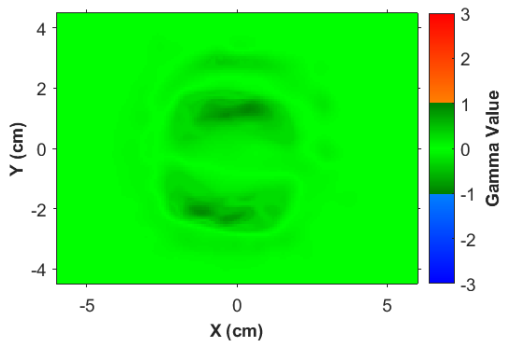	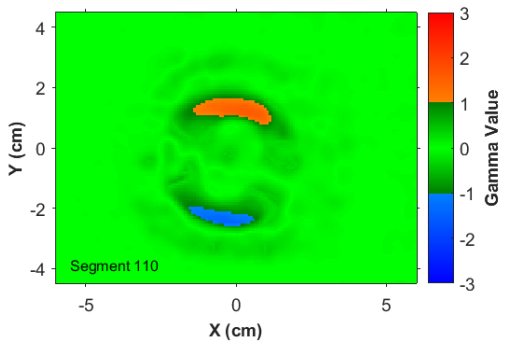
-0.6 cm	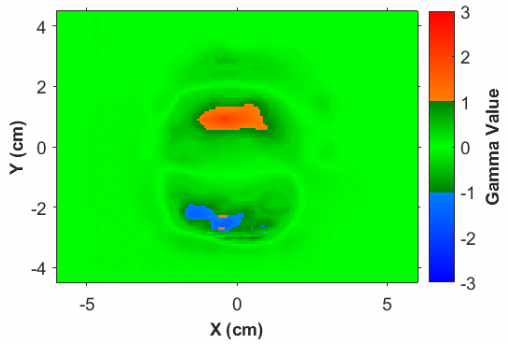	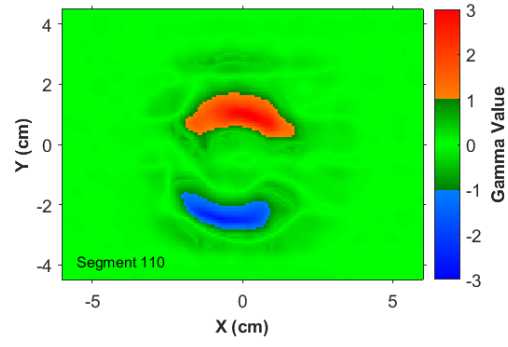

-0.9 cm	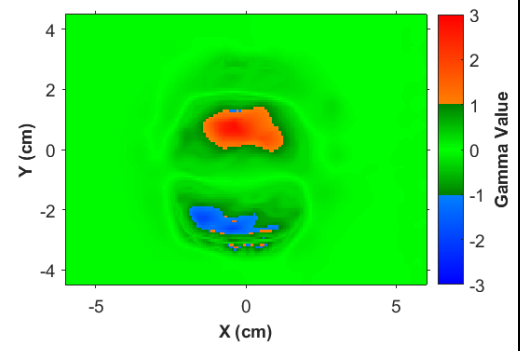	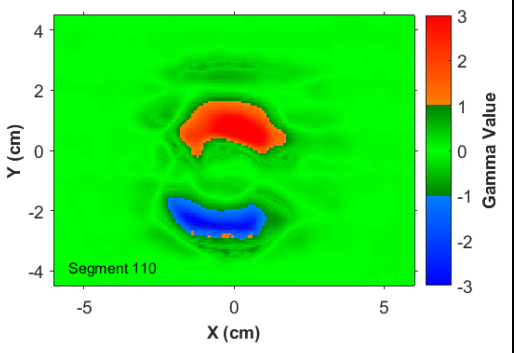
-1.2 cm	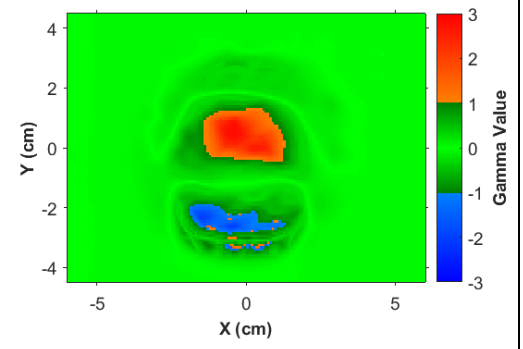	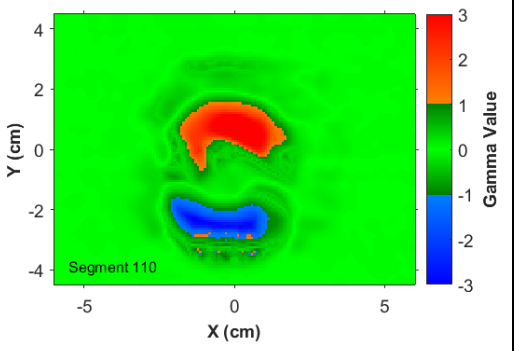
-1.5 cm	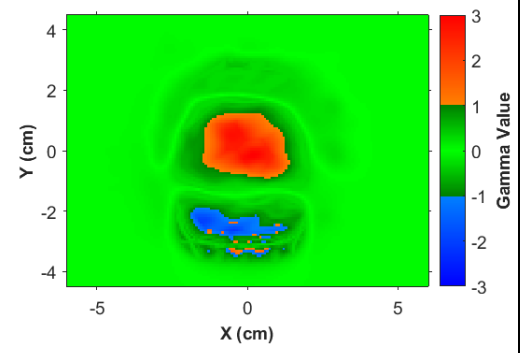	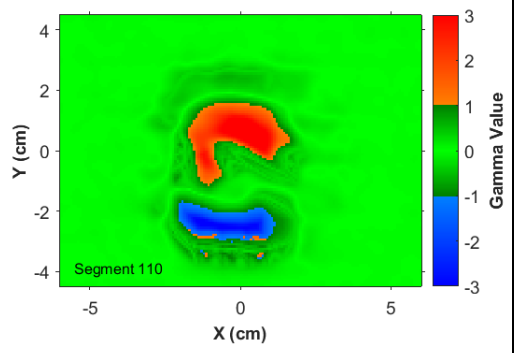
-1.8 cm	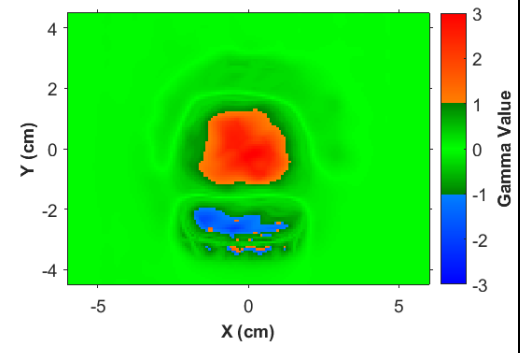	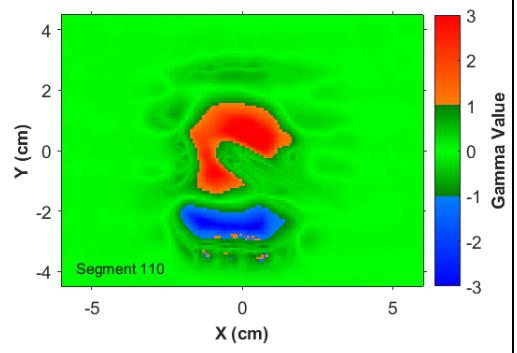

-2.1 cm	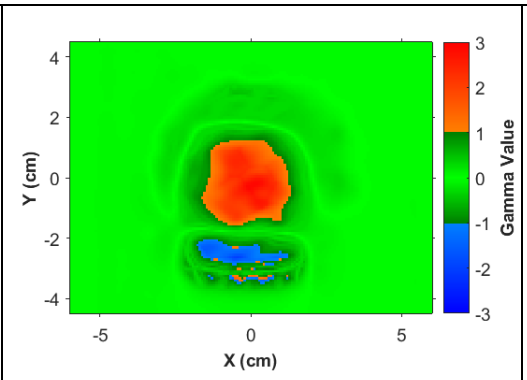	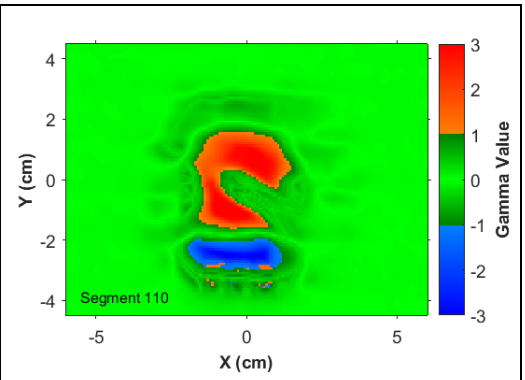
-2.4 cm	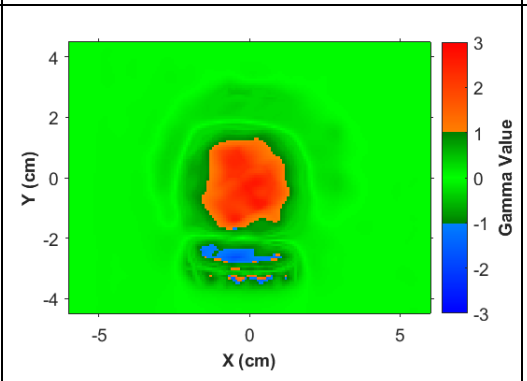	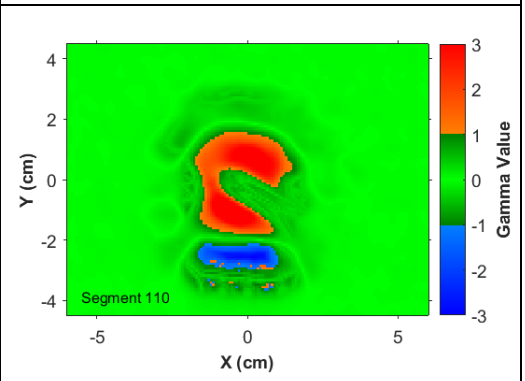
-2.7 cm	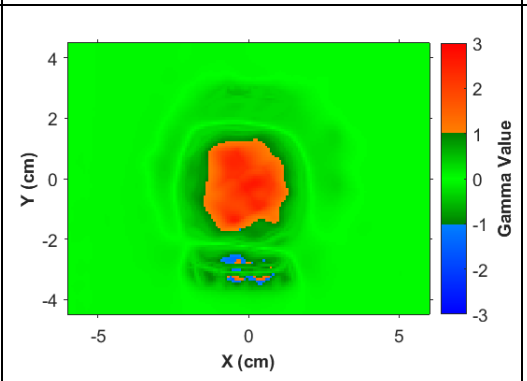	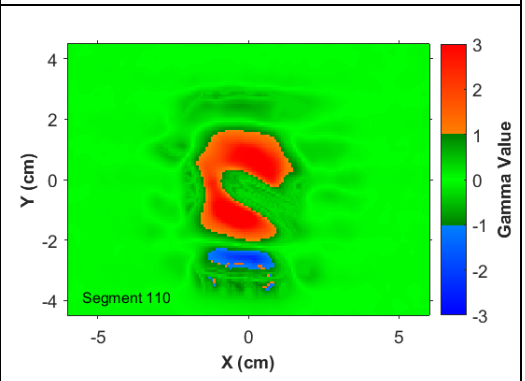
-3.0 cm	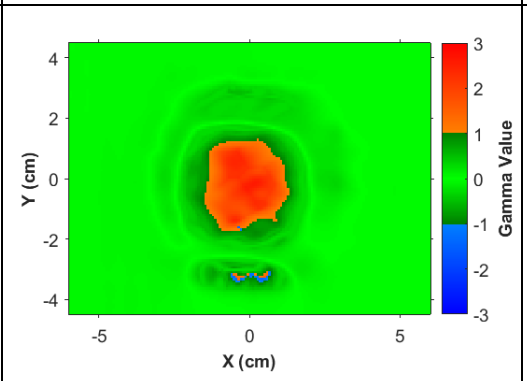	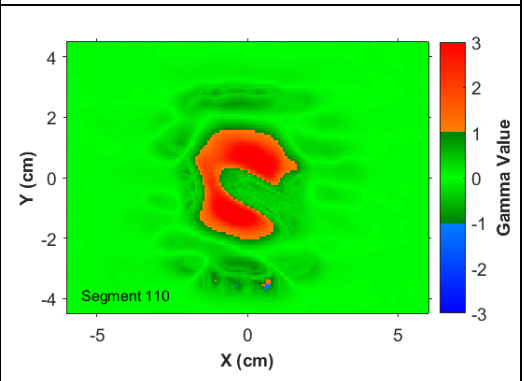

-3.3 cm	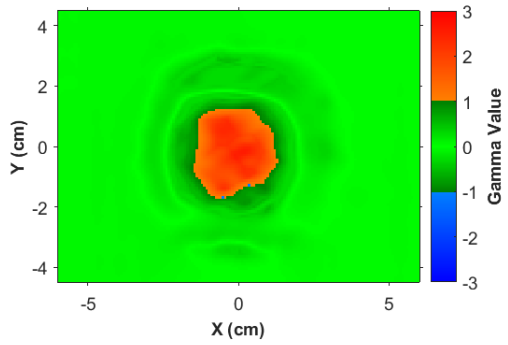	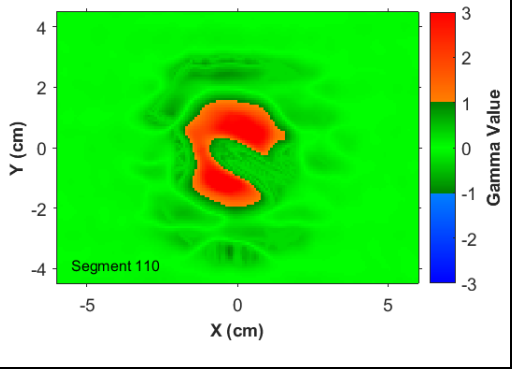

4.5 Supplementary study

4.5.1 Correlation between gamma failure and survival days

A correlation analysis between the gamma failure and the survival days of the 25 patients was performed for all the seven gamma criteria referred in section 3.2.6. However, in this section only the results for the [4%, 4 mm] gamma criterion are presented since these were the ones which showed the stronger correlations. Each point of the graphs represents the result relative to each patient and the straight line represents the linear fit of the data.

Figure 4.30 shows the correlation between the survival days and the gamma fail area per beam inside the radiation field mask obtained with 2D time-integrated gamma analysis (left side) and the correlation between the survival days and the gamma fail area per segment inside the radiation field mask obtained with 2D time-resolved gamma analysis (right side).

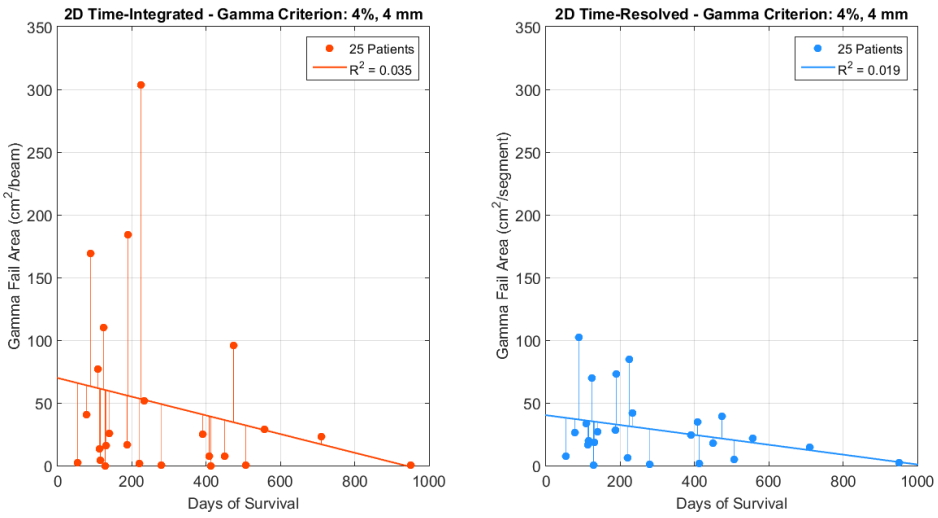

Figure 4.30 - Correlation between the days of survival and the absolute gamma fail area per beam inside the field mask obtained with 2D time-integrated gamma analysis (left) and between the days of survival and the gamma fail area per segment inside the field mask obtained with 2D time-resolved gamma analysis (right) for [4%, 4 mm] gamma criterion.

Both gamma analyses show a very weak or non-existing correlation with the days of survival (R^2 = 0.019 for time-resolved gamma analysis and R^2 = 0.035 for time-integrated gamma analysis). Even so, the time-resolved gamma analysis always shows more patients with gamma failure different from zero than the time-integrated gamma analysis. Despite the weak correlations, for both the cases the gamma failure decreases according to the increase of the survival days. This is an important finding that suggests that patients with lower gamma failure (less dose discrepancies) throughout the treatment fractions tend to survive more days after the first radiotherapy treatment.

4.5.2 Correlation between gamma failure and tumor volume

A correlation analysis between the gamma failure and the tumor volume of the 38 patients was performed for all 7 gamma criteria referred in section 3.2.6. However, in this section only the results for the [1%, 1 mm] gamma criterion are presented since these were the ones which showed the stronger correlations. Each point of the graphs represents the result relative to each patient and the straight line represents the linear fit of the data.

Figure 4.31 shows the correlation between the tumor volume and the absolute gamma fail area per beam inside the radiation field mask obtained with 2D time-integrated gamma analysis (left) and the correlation between the tumor volume and the absolute gamma fail area per segment inside the radiation field mask obtained with 2D time-resolved gamma analysis (right) for a [1%, 1 mm] gamma criterion. As expected, the results reveal that the gamma failure increases with the tumor volume suggesting that patients with larger tumors get higher gamma failure areas over the course of the radiotherapy treatment. Time-resolved gamma analysis showed a stronger correlation with the tumor volume (R^2 = 0.505) than time-integrated gamma analysis (R^2 = 0.296).

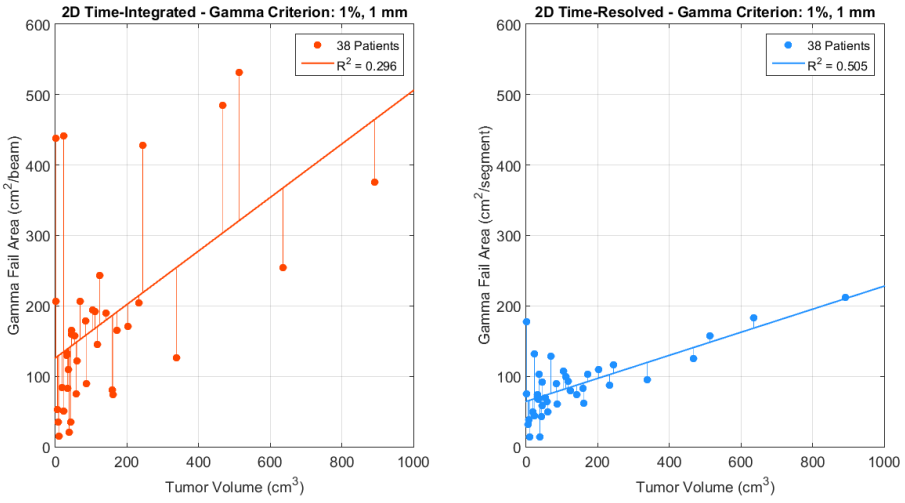

Figure 4.31 - Correlation between the tumor volume and the absolute gamma fail area per beam inside the radiation field mask obtained with 2D time-integrated gamma analysis (left) and between the days of survival and the gamma fail area per segment inside the radiation field mask obtained with 2D time-resolved gamma analysis (right) for [1%, 1 mm] gamma criterion.

5 Discussion

The patient simulations showed that time-resolved portal dosimetry is able to detect dose discrepancies caused by tumor shifts, tumor regressions and pleural effusion more accurately and earlier during treatment than time-integrated portal dosimetry (Figure 4.26, Figure 4.27 and Table 4.1). Moreover, the gamma analysis demonstrated to be a quantitative dose comparison method capable of identifying more deviations of the delivered dose from the planned dose than the DVH analysis which is the gold standard used by the physicians in clinical practice.

The DVH analysis demonstrated to be more sensitive to tumor shifts than to tumor regressions and pleural effusion (the percentage change of the $D_{95\%}$ metric inside the GTV was larger for the tumor shifts simulations than for the other geometrical changes). This could be explained by the fact that in the tumor shifts simulations the translation of the tumor relative to the central region of the radiation field is easier to detect when comparing, for instance, to a uniformly shrinkage of the tumor which remains in the central region of the field.

The correlation analyses demonstrated that there is a quantitative relationship between gamma fail rates and difference in $D_{95\%}$ metric for the 2D time-resolved, 2D and 3D time-integrated gamma fail rates when considering a single patient. This finding can allow establishing a relationship between $D_{95\%}$ change and gamma fail rate for individual patients. It means that for every patient simulation we can get the regression curve, and use it to derive $D_{95\%}$ changes from the measured gamma failure rates, and decide when to adapt the treatment. However, when taking into account the $D_{95\%}$ metric and gamma fail rates results from all six patients, the correlation is very weak. This result suggests that the correlation is valid for a single patient geometry but when considering multiple patient geometries there is no correlation between the DVH metric and the gamma fail rates as have been reported by several published studies. Persoon et al. (2015) and Podesta et al. (2015) also did not find a correlation in 46 patients, each showing a geometrical change [5]. This fact suggests that studying a larger patient population will not lead to a correlation.

The investigation of the sensitivity and specificity of the gamma analysis methods revealed that time-resolved gamma analysis yields a better performance than time-integrated gamma analysis for detecting tumor regression in the six patients studied. However, for capturing tumor shifts 3D time-integrated gamma analysis showed a better performance than 2D time-integrated and time-resolved gamma analyses. The performance of gamma analysis in flagging pleural effusion could not be investigated due to the fact that there were no positive DVHs, i.e., the difference in $D_{95\%}$ metric inside the GTV was never larger than 4% which is the MAASTRO clinical action level. This result suggests that DVH analysis is not suitable for detecting pleural effusion in lung cancer patients, at least not in the six patients studied here. It is also important to note that the results of this investigation depend on the clinical action level which is used as reference for considering a significant dose deviation of the delivered dose from the planned dose.

In this work it was also demonstrated that the portal dosimetry methods show different performances according to the geometrical change simulated within the patient. It becomes

therefore essential to look individually for each category of geometrical change and define a specific gamma analysis threshold for each one of those problems.

Moreover, it was also found that the [3%, 3 mm] gamma criterion was too lax to detect some of the dose discrepancies caused by the forced errors. Other studies have also shown that this gamma criterion is not suitable for gamma comparison in all cases and call into question its utility as an adequate metric in portal dosimetry [20, 48, 54]. In fact, despite being the most common gamma criterion it is unproven and arbitrary and should be changed according to the clinical needs [57]. Additional studies are necessary for choosing the optimal gamma criterion for both time-integrated and time resolved gamma analysis.

The phantom measurements showed that in reality the geometrical change that we were testing in the simulations starts being significant at the same point as in the measurements. For both cases the dose to the tumor drops when a shift equal or larger than -1.5 cm in Y axis is applied to the tumor. Moreover, the EPID images acquired during the phantom measurements revealed that time-resolved gamma analysis was able to detect more dose discrepancies caused by the tumor shifts and earlier than time-integrated gamma analysis. In fact, when applying a -0.3 cm shift to the tumor time-integrated analysis did not reveal any dose discrepancy while time-resolved gamma analysis showed some under-dosage and over-dosage regions resultant from the translation of the tumor.

The supplementary study which involved a cohort of 38 patients allowed confirming that despite the weak correlation, there is a quantitative relationship between the gamma failure and the tumor volume as well as between the gamma failure and the survival days of the patients. These results suggest that a patient with a larger tumor has a trend to get a higher gamma area failure between treatment fractions. In the same way, there is a trend showing that a patient who got higher gamma failure (more dose errors) throughout the treatment course tends to survive less days after the first treatment day. This important finding suggests that high gamma failures over the treatment course of the patient can impair his recovery resulting in less days of survival. It becomes therefore essential to verify the dose delivery during treatment in order to avoid dose discrepancies.

6 Conclusion and Future Work

This work demonstrated that time-resolved portal dosimetry is superior to time-integrated portal dosimetry in detecting anatomical changes in lung cancer patients caused by tumor shifts, tumor regressions and pleural effusion. The highly dynamic way of time-resolved portal dosimetry brings the advantage of measuring the dose during VMAT delivery from control point to control point thereby avoiding the geometrical shortcomings of the time-integrated portal dosimetry. Time-resolved portal dosimetry was able to identify dose differences more accurately, with a higher sensitivity and earlier during treatment.

The phantom measurements also confirmed the superiority of time-resolved portal dosimetry against 2D time-integrated portal dosimetry in flagging dose discrepancies caused by tumor shifts. Besides, it was shown that the measurements followed the same logic as the simulations: a shift of the tumor and replacing lung tissue by tumor tissue, results in similar effects in the simulations and the measurements. Thus, it was possible to mimic in reality the tumor shift simulations and demonstrate how they match.

As main conclusion, this work is indicative that 2D time-resolved portal dosimetry shows promising results in catching dose discrepancies for VMAT treatments. Further research is still needed including a larger patient cohort but maintaining the different categories of geometrical changes with different magnitudes. New methods should also be investigated especially 3D time-resolved portal dosimetry which allows a dose comparison per VMAT segment at the level of the patient. Other tumor sites than lung tumor should also be investigated with the same methodology.

Appendix

A. Film calibration and measurement film analysis

The film calibration was performed using ten pieces of GafChromic EBT3 films (International Specialty Product, NJ, US): one unirradiated and nine irradiated films. The films were irradiated at a Varian TrueBeam linear accelerator using a static 6 MV photon beam with a 10 cm x 10 cm field size. The films were irradiated with doses ranging from 0 Gy to 9 Gy in steps of 1 Gy.

About the experimental setup, each film was placed between 15 cm of water-equivalent RW3 slab phantoms (PTW–Freiburg, Germany): 10 cm at the bottom to provide for backscatter and 5 cm at the top to provide build-up. The size of each slab phantom is 30 cm x 30 cm x 1 cm. The films were positioned at the isocenter of the linear accelerator (Figure A.1).

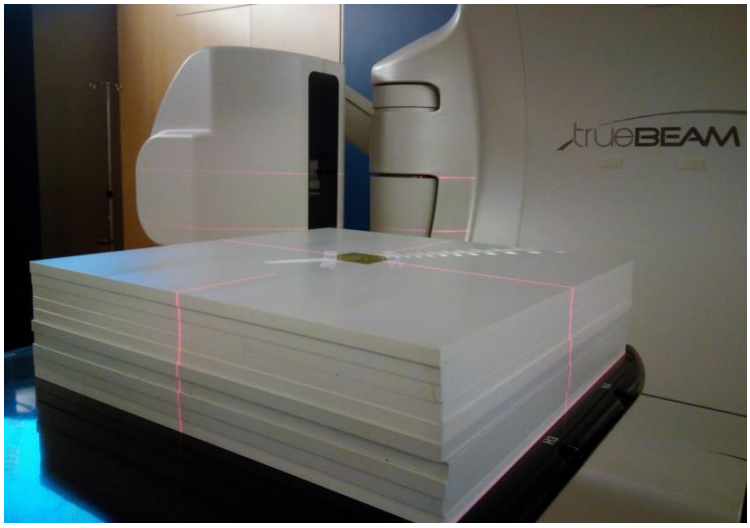

Figure A.1 – Representation of 10 cm of water equivalent slab phantoms with a film piece positioned at the top at the isocenter of the linac.

The films were placed between the solid water slab phantoms at the depth of 5 cm where 1 Gy equals to 100 MU. Since the calibration is performed at this depth and not at the maximum dose depth, the known dose is divided by PDD (Percentage Depth Dose)/100. According to MAASTRO clinical practice, the PDD for this measurement depth equals to 86% for a 6 MV photon beam with a 10 cm x 10 cm field size. Since the ionization in the slab phantoms is slightly lower than in water, a correction factor is applied. This correction factor is the ratio between the ionization in the water and the ionization in the slab phantoms. For a 6 MV photon beam with a 10 cm x 10 cm field size and a 5 cm measuring depth this correction factor equals 1.009 (Figure A.2).

In order to deliver the known doses from 0 Gy until 9 Gy in steps of 1 Gy, the machine outputs in monitor units applied for each film irradiation were calculated based on the following formula:

$$MU = h_{w/m} \cdot \frac{10^4 \cdot D}{PDD} = 1.009 \cdot \frac{10^4 \cdot D}{86}, \quad (A.1)$$

where MU indicates the monitor units, $h_{w/m}$ represents the correction factor, D represents the dose and PDD is the percentage depth dose.

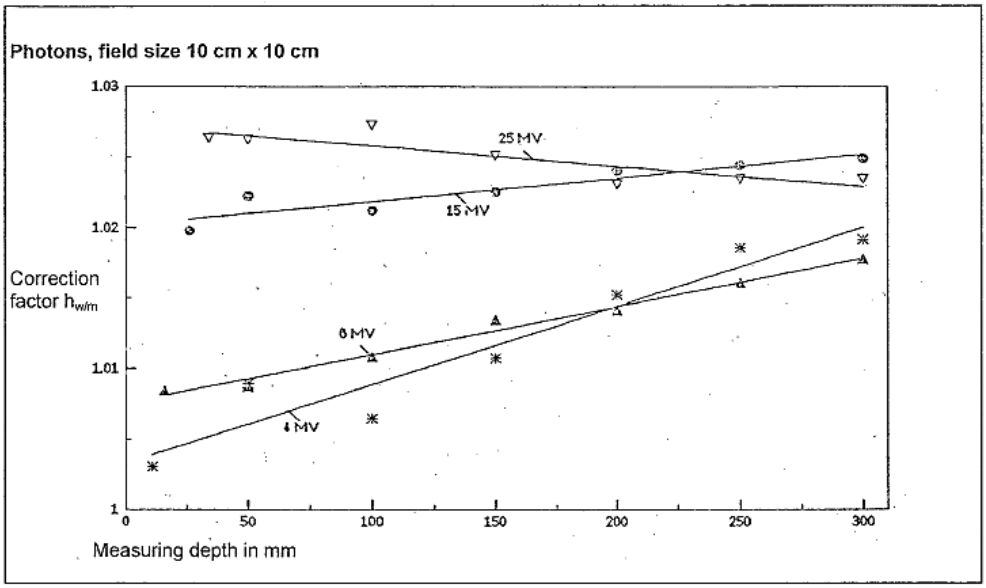

Figure A.2 – The correction factor $h_{w,m}$ as a function of depth for the field size 10 cm x 10 cm [58].

Table A.1 summarizes the machine outputs applied for each film irradiation and the respective dose values calculated according to the formula referred above.

Table A.1 – Machine outputs applied for each film irradiation and corresponding dose values.

Dose (Gy)	0	1	2	3	4	5	6	7	8	9
Machine Output (MU)	0	118	235	353	471	558	706	823	941	1059

After a period of six days post irradiation, the calibration and measurement films were scanned using an Epson Perfection V750 Pro flatbed scanner and Epson Scan software v3.83 (Seiko Epson Corporation, Nagano, Japan). Both calibration and measurement films were scanned separately in the center of the scanner with the same orientation. The scanned images were saved in RGB uncompressed tagged image file format (TIFF). These images were acquired at a resolution of 225 dpi in 48 bit (16 bit per color channel) with all colour corrections turned off. The scanner was turned on half an hour before image acquisition and six preview scans were taken to warm up the scanner lamp. The films were always handled with gloves and stored in a black envelope when not being handled.

After the scanning process each film was analyzed using the red channel due to its high contrast. The pixel values (PV) of each image were converted to optical density (OD) using the following formula:

$$\mathrm{OD} = -\log_{10}\left(\frac{\mathrm{PV}}{2^{16}}\right),$$

where OD represents the optical density, PV indicates the pixel value resulting from film digitization after irradiation and 16 indicates the number of bits per channel with which the images were acquired [59].

For the calibration analysis, a circular region of interest (0.5 cm radius) was defined in the central region of each calibration film piece. The average of the pixel values that fall into this radius was determined and converted to optical density using the formula referred above. Then the optical densities obtained for all calibration films were plotted as function of the known doses. To generate the calibration curve, the data points were fitted to the rational function OD(D):

$$\mathrm{OD}\,(\mathrm{D}) = \mathrm{a} + \frac{\mathrm{b}}{\mathrm{D} - \mathrm{c}},$$

where D represents the dose and a, b and c are the fit parameters [60]. The values that were determined for the fit parameters are shown in table A.2. Figure A.3 shows the calibration curve and the residual optical density.

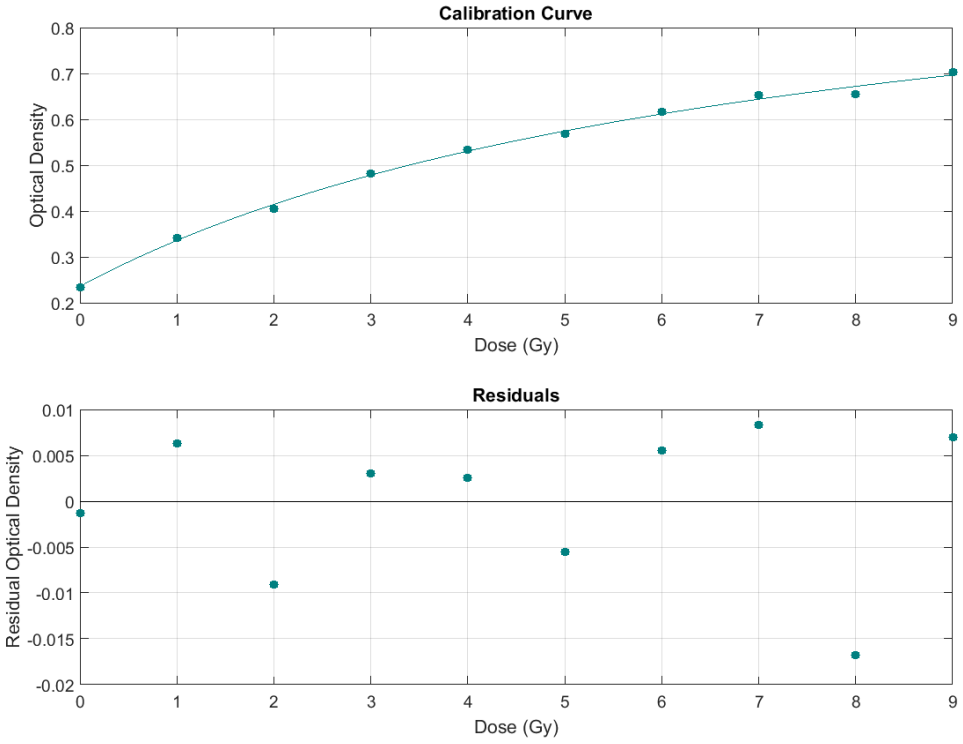

Figure A.3 – Film calibration curve (top) and residual optical density (bottom).

Table A.2 – Fit parameters of the calibration curve for red channel.

Fit Parameters		
a	**b**	**c**
1.073	-6.16	-7.357

For the measurement film analysis, a circular region of interest (0.5 cm radius) was also defined in the central region of each measurement film piece. The average of the pixel values that fall into this radius was determined and converted to optical density. Then, the optical density obtained for each measurement film was converted to dose based on the calibration curve function previously determined.

7 Bibliography

[1] Lang, S. et al. Pretreatment quality assurance of flattening filter free beams on 224 patients for intensity modulated plans: A multicentric study. *Medical Physics* **39,** 1351–1356 (2012).

[2] Podesta, M. et al. Time dependent pre-treatment EPID dosimetry for standard and FFF VMAT. *Physics in Medicine and Biology* **59,** 4749–4768 (2014).

[3] Woodruff, H. C., Fuangrod, T., Rowshanfarzad, P., McCurdy, B. M. C. & Greer, P. B. Gantry-angle resolved VMAT pretreatment verification using EPID image prediction. *Medical Physics* **40,** 081715 (2013).

[4] Vazquez Quino, L. A. et al. Patient specific pre-treatment QA verification using an EPID approach. *Technology in Cancer Research & Treatment* **13,** 1–10 (2014).

[5] Persoon, L. C. G. G., Podesta, M. et al. Is integrated transit planar portal dosimetry able to detect geometric changes in lung cancer patients treated with volumetric modulated arc therapy? *Acta Oncologica* **54,** 1501–1507 (2015).

[6] van Elmpt, W. et al. A literature review of electronic portal imaging for radiotherapy dosimetry. *Radiotherapy and Oncology* **88,** 289–309 (2008).

[7] Mans, A. et al. 3D Dosimetric verification of volumetric-modulated arc therapy by portal dosimetry. *Radiotherapy and Oncology* **94,** 181–187 (2010).

[8] Nijsten, S. M. J. J. G., Mijnheer, B. J., Dekker, A. L. A. J., Lambin, P. & Minken, A. W. H. Routine individualised patient dosimetry using electronic portal imaging devices. *Radiotherapy and Oncology* **83,** 65–75 (2007).

[9] Mans, A. et al. Catching errors with in vivo EPID dosimetry. *Medical Physics* **37**, 2638–2644 (2010).

[10] Ferlay, J., Parkin, D. M. & Steliarova-Foucher, E. Estimates of cancer incidence and mortality in Europe in 2008. *European Journal of Cancer* **46,** 765–781 (2010).

[11] Siegel, R. L., Miller, K. D. & Jemal, A. Cancer statistics, 2015. *CA: A Cancer Journal for Clinicians* **65,** 5–29 (2015).

[12] Cancer. *World Health Organization* (2016). at <http://www.who.int/mediacentre/factsheets/fs297/en/.>

[13] van Elmpt, W. 3D dose verification for advanced radiotherapy. PhD Thesis, Maastricht University (2009).

[14] Nijsten, S. Portal dosimetry in radiotherapy. PhD Thesis, Maastricht University (2009).

[15] Varian High Energy Linear Accelerator Comparison Chart. Radiology Oncology Systems (2016) at <http://www.oncologysystems.com/assets/001/6428.jpg>

[16] Prescribing, Recording, and Reporting Photon-Beam Intensity-Modulated Radiation Therapy (IMRT): Contents. *Journal of the ICRU* **10**, NP (2010).

[17] Rosenberg, I. Radiation Oncology Physics: A Handbook for Teachers and Students. *The British Journal of Radiology* **98,** 1020 (2008).

[18] Otto, K. Volumetric modulated arc therapy: IMRT in a single gantry arc. *Medical Physics* **35,** 310–317 (2008).

[19] Teoh, M., Clark, C. H., Wood, K., Whitaker, S. & Nisbet, A. Volumetric modulated arc therapy: a review of current literature and clinical use in practice. *The British Journal of Radiology* **84,** 967–996 (2011).

[20] Podesta, M., Persoon, L. C. G. G. & Verhaegen, F. A novel time dependent gamma evaluation function for dynamic 2D and 3D dose distributions. *Physics in Medicine and Biology* **59,** 5973–5985 (2014).

[21] VMAT - Plan Comparisons | Varian Medical Systems. Varian (2016). at <https://www.varian.com/pt-pt/oncology/treatment-techniques/external-beam-radiation/vmat?cat=plan-comparisons>

[22] Jaffray, D. A., Siewerdsen, J. H., Wong, J. W. & Martinez, A. A. Flat-panel cone-beam computed tomography for image-guided radiation therapy. *International Journal of Radiation Oncology, Biology, Physics.* **53**, 1337–1349 (2002).

[23] Nijsten, S. et al. A global calibration model for a-Si EPIDs used for transit dosimetry. *Medical Physics* **34,** 3872–3884 (2007).

[24] Low, D. A., Harms, W. B., Mutic, S. & Purdy, J. A. A technique for the quantitative evaluation of dose distributions. *Medical Physics* **25,** 656–661 (1998).

[25] Schyns, L. E. J. R. Time-resolved versus time-integrated portal dosimetry. The role of the isocenter position in volumetric modulate arc therapy. Master Thesis, Eindhoven University of Technology (2015).

[26] Low, D. A., Morele, D., Chow, P., Dou, T. H. & Ju, T. Does the γ dose distribution comparison technique default to the distance to agreement test in clinical dose distributions? *Medical Physics* **40,** 071722 (2013).

[27] Yan, D., Vicini, F., Wong, J. & Martinez, A. Adaptive radiation therapy. *Physics in Medicine and Biology* **42**, 123–132 (1997).

[28] Persoon, L. C. G. G. 3D dose verification for advanced radiotherapy. PhD Thesis, Maastricht University (2009).

[29] Persoon, L. C. G. G. et al. First clinical results of adaptive radiotherapy based on 3D portal dosimetry for lung cancer patients with atelectasis treated with volumetric-modulated arc therapy (VMAT). *Acta Oncologica* **52,** 1484–1489 (2013).

[30] Møller, D. S., Khalil, A. A., Knap, M. M. & Hoffmann, L. Adaptive radiotherapy of lung cancer patients with pleural effusion or atelectasis. *Radiotherapy and Oncology* 110, 517–522 (2014).

[31] McDermott, L. N., On radiotherapy dose verification with a flat-panel imager. PhD Thesis, University of Amsterdam (2007).

[32] Antonuk, L. E. et al. A real-time, flat-panel, amorphous silicon, digital x-ray imager. *Radiographics* **15,** 993–1000 (1995).

[33] Varian Medical Systems International Ag,. Time-resolved pre-treatment portal dosimetry systems, devices, and methods. (2016).

[34] *Portal Vision aS1000. The state of the art in electronic portal imaging*.. (Varian Medical Systems, 2006). at <http://www.behestandarman.com>

[35] van Elmpt, W. J. C., Nijsten, S. M. J. J. G., Mijnheer, B. J. & Minken, A. W. H. Experimental verification of a portal dose prediction model. *Medical Physics* **32,** 2805–2818 (2005).

[36] van Elmpt, W. J. C. et al. A Monte Carlo based three-dimensional dose reconstruction method derived from portal dose images. *Medical Physics* **33,** 2426–2434 (2006).

[37] Rozendaal, R. A., Mijnheer, B. J., van Herk, M. & Mans, A. In vivo portal dosimetry for head-and-neck VMAT and lung IMRT: linking γ-analysis with differences in dose-volume histograms of the PTV. *Radiotherapy and Oncology* **112**, 396–401 (2014).

[38] Mans, A. et al. 3D Dosimetric verification of volumetric-modulated arc therapy by portal dosimetry. *Radiotherapy and Oncology* **94**, 181–187 (2010).

[39] van Zijtveld, M., Dirkx, M. L. P., de Boer, H. C. J. & Heijmen, B. J. M. 3D dose reconstruction for clinical evaluation of IMRT pretreatment verification with an EPID. *Radiotherapy and Oncology* **82**, 201–207 (2007).

[40] van Elmpt, W., Nijsten, S., Mijnheer, B., Dekker, A. & Lambin, P. The next step in patient-specific QA: 3D dose verification of conformal and intensity-modulated RT based on EPID dosimetry and Monte Carlo dose calculations. *Radiotherapy and Oncology* **86**, 86–92 (2008).

[41] McDermott, L. N. et al. 3D in vivo dose verification of entire hypo-fractionated IMRT treatments using an EPID and cone-beam CT. *Radiotherapy and Oncology* **86**, 35–42 (2008).

[42] Fippel, M. Fast Monte Carlo dose calculation for photon beams based on the VMC electron algorithm. *Medical Physics* **26,** 1466–1475 (1999).

[43] van Elmpt, W. et al. 3D in vivo dosimetry using megavoltage cone-beam CT and EPID dosimetry. *International Journal of Radiation Oncology, Biology, Physics.* **73**, 1580–1587 (2009).

[44] Schyns, L. E. J. R., Persoon, L. C. G. G., Podesta, M., van Elmpt, W. J. C. & Verhaegen, F. Time-resolved versus time-integrated portal dosimetry: the role of an object's position with respect to the isocenter in volumetric modulated arc therapy. *Physics in Medicine and Biology* **61,** 3969–3984 (2016).

[45] Persoon, L. C. G. G., Podesta, M., Nijsten, S. M. J. J. G., Troost, E. G. C. & Verhaegen, F. Time-Resolved Versus Integrated Transit Planar Dosimetry for Volumetric Modulated Arc Therapy: Patient-Specific Dose Differences During Treatment, a Proof of Principle. *Technology in Cancer Research & Treatment* (2015).

[46] Persoon, L. C. G. G. et al. Interfractional trend analysis of dose differences based on 2D transit portal dosimetry. *Physics in Medicine and Biology* **57,** 6445–6458 (2012).

[47] van Elmpt, W., Petit, S., De Ruysscher, D., Lambin, P. & Dekker, A. 3D dose delivery verification using repeated cone-beam imaging and EPID dosimetry for stereotactic body radiotherapy of non-small cell lung cancer. *Radiotherapy and Oncology* **94**, 188–194 (2010).

[48] Nelms, B. E., Zhen, H. & Tomé, W. A. Per-beam, planar IMRT QA passing rates do not predict clinically relevant patient dose errors. *Medical Physics* **38**, 1037–1044 (2011).

[49] Heilemann, G., Poppe, B. & Laub, W. On the sensitivity of common gamma-index evaluation methods to MLC misalignments in Rapidarc quality assurance. *Medical Physics* **40**, 031702 (2013).

[50] Fredh, A., Scherman, J. B., Fog, L. S. & Munck af Rosenschöld, P. Patient QA systems for rotational radiation therapy: a comparative experimental study with intentional errors. *Medical Physics* **40,** 031716 (2013).

[51] Kumar, R. & Indrayan, A. Receiver operating characteristic (ROC) curve for medical researchers. *Indian Pediatrics* **48**, 277–287 (2011).

[52] CIRS. Dynamic Thorax Phantom. USA: CIRS, 2008.

[53] Bresciani, S. et al. Tomotherapy treatment plan quality assurance: the impact of applied criteria on passing rate in gamma index method. *Medical Physics* **40,** 121711 (2013).

[54] Kruse, J. J. On the insensitivity of single field planar dosimetry to IMRT inaccuracies. *Medical Physics* **37,** 2516–2524 (2010).

[55] Carrasco, P. et al. 3D DVH-based metric analysis versus per-beam planar analysis in IMRT pretreatment verification. *Medical Physics* **39**, 5040–5049 (2012).

[56] Stasi, M. et al. Pretreatment patient-specific IMRT quality assurance: A correlation study between gamma index and patient clinical dose volume histogram. *Medical Physics* **39**, 7626–7634 (2012).

[57] Low D. A. Gamma Dose Distribution Evaluation Tool. *Journal of Physics: Conference Series* **250,** 012071 (2010).

[58] Instruction manual RW3 Slab Phantom T29672 and T40006.1.001 D188.131.00/04 2007-07 Chr/zi/Sa.

[59] Hoof, S. J. van, Granton, P. V., Landry, G., Podesta, M. & Verhaegen, F. Evaluation of a novel triple-channel radiochromic film analysis procedure using EBT2. *Physics in Medicine and Biology* **57,** 4353 (2012).

[60] Lewis, D., Micke, A., Yu, X. & Chan, M. F. An efficient protocol for radiochromic film dosimetry combining calibration and measurement in a single scan. *Medical Physics* **39,** 6339–6350 (2012).